Master's thesis

NTNU
Norwegian University of Science and Technology
Faculty of Engineering
Department of Marine Technology

Olav Fiksdahl

Model-Based Optimization for Energy and Emission Management of a Marine Hybrid Electric Power System

Master's thesis in Marine Technology
Supervisor: Roger Skjetne
June 2020

NTNU
Norwegian University of Science and Technology

Olav Fiksdahl

Model-Based Optimization for Energy and Emission Management of a Marine Hybrid Electric Power System

Master's thesis in Marine Technology
Supervisor: Roger Skjetne
June 2020

Norwegian University of Science and Technology
Faculty of Engineering
Department of Marine Technology

NTNU
Norwegian University of
Science and Technology

NTNU Trondheim
Norwegian University of Science and Technology
Department of Marine Technology

MASTER OF TECHNOLOGY THESIS DEFINITION (30 SP)

Name of the candidate:	Fiksdahl, Olav
Field of study:	Marine control engineering
Thesis title (Norwegian):	Modellbasert optimalisering for energi- og utslippsstyring av et marint hybridelektrisk kraftsystem
Thesis title (English):	Model-based optimization for energy and emission management of a marine hybrid electric power system

Background
Hybrid electric ships have seen an increased popularity over the last years. They will be even more common in the years to come, as shipping must lower its emissions world-wide, to meet the climate goals of the Paris Agreement and to follow the requirements and regulations set by the International Maritime Organization (IMO). For smaller distances, battery-electric ships can be considered, as the battery packages will not need to be too big and there will be enough space for cargo. For larger ships, however, a hybrid electric solution is currently a better alternative. For hybrid-electric ships to be even more widely used by the industry, it is necessary to understand how to model the onboard power plant. This master thesis will therefore focus on the modeling and optimization of a marine hybrid-electric power system. It is considered important for the shipping industry to change into a greener direction, motivating the development of knowledge and competence-building towards such goals.

Work description
1. Perform a background and literature review to provide information and relevant references on:
   - The structure-preserving model (SPM), especially article by A. R. Dahl (2018) and references therein by Bergen & Hill and Hill & Bergen.
   - Model-predictive control (MPC); general theory and its application by A. R. Dahl (2018).
   - Typical configurations of marine hybrid-electric power systems.
   - Models and optimization strategies for marine hybrid-electric power systems; for instance PhD theses of Torstein Bø and Michel Miyazaki, corresponding papers, and MSc theses.

   Write a list with abbreviations and definitions of terms and symbols, relevant to the literature study and project report.
2. Define system structure for power management system (PMS), battery management system (BMS), and energy and emission management system (EEMS), including a description of the most relevant main modes and functions.
3. Define Battery-ESS (BESS; battery energy storage system) by its most important functions, inputs, outputs, and relevant constraints.
4. Extend the SPM with battery modules and converter models. Make changes to the code used in the article of A.R. Dahl (2018).
5. Formulate relevant control modes for the hybrid-electric system as respective optimization problems for minimizing energy and emissions. Propose solutions to the optimization problems using MPC with SPM as model. Consider configurations with or without a battery module on the power bus. Test both on an unrealistic deterministic load profile and a realistic load profile. Analyze and discuss the resulting performances with comparisons to other methods, if available.

Specifications

Every weekend throughout the project period, the candidate shall send a status email to the supervisor and co-advisors, providing two brief bulleted lists: 1) work done recent week, and 2) work planned to be done next week.

The scope of work may prove to be larger than initially anticipated. By the approval from the supervisor, described topics may be deleted or reduced in extent without consequences with regard to grading.

The candidate shall present personal contribution to the resolution of problems within the scope of work. Theories and conclusions should be based on mathematical derivations and logic reasoning identifying the various steps in the deduction.

The report shall be organized in a logical structure to give a clear exposition of background, problem, design, results, and critical assessments. The text should be brief and to the point, with a clear language. Rigorous mathematical deductions and illustrating figures are preferred over lengthy textual descriptions. The report shall have font size 11 pts., and it is not expected to be longer than 70 A4-pages, 100 B5-pages, from introduction to conclusion, unless otherwise agreed upon. It shall be written in English (preferably US) and contain the elements: Title page, abstract, acknowledgement, project definition, list of symbols and acronyms, table of contents, introduction (project motivation, objectives, scope and delimitations), background/literature review, problem formulation, method, results, conclusions with recommendations for further work, references, and optional appendices. Figures, tables, and equations shall be numerated. The original contribution of the candidate and material taken from other sources shall be clearly identified. Work from other sources shall be properly acknowledged using quotations and a Harvard citation style (e.g. *natbib* Latex package). The work is expected to be conducted in an honest and ethical manner, without any sort of plagiarism and misconduct, which is taken very seriously by the university and cause consequences. NTNU can use the results freely in research and teaching by proper referencing, unless otherwise agreed upon.

The thesis shall be submitted with an electronic copy to the main supervisor and department according to NTNU administrative procedures. The final revised version of this thesis description shall be included after the title page. Computer code, pictures, videos, dataseries, etc., shall be included electronically with the report.

Start date: 15 January, 2020 **Due date:** As specified by the administration.

Supervisor: Roger Skjetne
Co-advisor(s): Andreas Reason Dahl (KM)

Trondheim, 23.03.2020

Roger Skjetne

Digitally signed by Roger Skjetne
Date: 2020.03.23 13:25:59 +01'00'

Roger Skjetne
Supervisor

Abstract

The maritime industry accounts for approximately 3% of the global CO_2 emissions. With the rising concern for more environmentally friendly solutions and a desire to solve today's climate challenges, hybrid electric ships are essential for the maritime industry to reduce its emissions, and installation of batteries on ships is therefore an important measure for shipping to move in a greener direction.

This thesis presents a new model for hybrid electric power systems, which is called the structure-preserving model (SPM). The SPM is originally only valid for conventional power systems without battery, but one of the contributions of this thesis is to extend the SPM for hybrid electric power systems, where a battery model is developed. It is verified that the SPM is an accurate model for hybrid electric power systems through a verification study, and it is concluded that the SPM is well fit for control purposes, and that it can be used as a model to optimize the energy use in a hybrid electric power system. Optimization problems using model predictive control (MPC) are formulated for three different battery strategies, and the solutions to these problems are presented in a case study for a dynamically positioned vessel. The different battery strategies in this thesis are using the battery for peak-shaving, power smoothing and strategic loading, and in addition, a strategy without battery is used for comparison, representing a traditional power system. The results from the case study indicate that strategic loading is an efficient battery strategy. Compared to without using battery, strategic loading reduces the fuel consumption with 7% for a short simulation of 1000 seconds, and with 5.3% for a long simulation of 24 hours, based on a realistic vessel operation.

Even though not the main focus of this thesis, the results are also compared to another efficient strategy for reducing emissions, which is genset disconnection, meaning turning on and off generator sets depending on the load. Genset disconnection gives large fuel savings, and the results indicate that for the short simulation, the fuel consumption is reduced by 16.1% for genset disconnection without battery, and by 17.7% for genset disconnection combined with strategic loading. For the long simulation, the corresponding numbers are 38.1% and 38.5%, respectively. Consequently, combining genset disconnection and strategic loading is deemed an efficient strategy for hybrid electric ships. The simulations also show that transient effects can occur in the hybrid electric power system, either due to the battery power, which is assumed to be delivered instantly, or due to instabilities from the genset disconnection. When not performing genset disconnection, the frequency is within the steady-state limits set by class societies, but the simulations show that genset disconnection can make the frequency exceed these limits.

Sammendrag

Den maritime næringen står for omtrent 3% av de globale CO_2-utslippene. Med et økende fokus på mer miljøvennlige løsninger og et ønske om å løse dagens klimautfordringer, er hybridelektriske skip essensielle for at den maritime næringen skal klare å redusere utslippene sine. Det å installere batterier på skip er derfor et viktig tiltak for at skipsfarten skal bevege seg i en grønnere retning.

Denne avhandlingen presenterer en ny modell for hybridelektriske kraftsystemer, som kalles den strukturbevarende modellen (SPM). SPM-en gjelder opprinnelig kun for konvensjonelle kraftsystemer uten batteri, men et av bidragene i denne avhandlingen er å utvide SPM-en for hybridelektriske kraftsystemer, der en batterimodell er utviklet. Gjennom en verifikasjonsstudie bekreftes det at SPM-en er en nøyaktig modell for hybridelektriske kraftsystemer, og det konkluderes med at SPM-en er godt egnet til kontrollformål, og at den kan brukes som en modell for å optimalisere energibruken i et hybridelektrisk kraftsystem. Optimaliseringsproblemer som bruker modellprediktiv regulering (MPC) er formulert for tre forskjellige batteristrategier, og løsningene på disse problemene presenteres i en casestudie for et dynamisk posisjonert fartøy. De ulike batteristrategiene som brukes i denne avhandlingen er topputjevning (peak-shaving), kraftutjevning (power smoothing) og strategisk lasting (strategic loading), og i tillegg brukes en strategi uten batteri til sammenligning, som representerer et tradisjonelt kraftsystem. Resultatene fra casestudien indikerer at strategisk lasting er en effektiv batteristrategi. Sammenlignet med å ikke bruke batteri, reduserer strategisk lasting drivstofforbruket med 7% for en kort simulering på 1000 sekunder, og med 5,3% for en lang simulering på 24 timer, som er basert på en realistisk fartøysoperasjon.

Selv om det ikke er hovedfokuset i denne avhandlingen, sammenlignes også resultatene med en annen effektiv strategi for å redusere utslipp, såkalt gensettfrakobling, som betyr å slå av og på generatorsett avhengig av lasten. Gensettfrakobling gir store drivstoffbesparelser, og resultatene indikerer at for den korte simuleringen reduseres drivstofforbruket med 16,1% for gensettfrakobling uten batteri, og med 17,7% for gensettfrakobling kombinert med strategisk lasting. For den lange simuleringen er de tilsvarende tallene henholdsvis 38,1% og 38,5%. Følgelig anses det å kombinere gensettfrakobling og strategisk lasting som en effektiv strategi for hybridelektriske skip. Simuleringene viser også at transiente effekter kan oppstå i det hybridelektriske kraftsystemet, enten på grunn av batteriet, som antas å levere effekt øyeblikkelig, eller på grunn av ustabilitet knyttet til gensettfrakobling. Når gensettfrakobling ikke utføres, er frekvensen innenfor de stasjonære grensene satt av klasseselskap, men simuleringene viser at gensettfrakobling kan føre til at disse frekvensgrensene overskrides.

Preface

This master thesis is written on the Department of Marine Technology at the Norwegian University of Science and Technology (NTNU). The study has been performed during the spring of 2020, from January to June, and it is a continuation of the work done in the project thesis conducted autumn 2019.

I did not have any prior knowledge of hybrid electric ships, but I have since the beginning of my studies been very interested in the topic. I am grateful for having the opportunity to explore and learn more about it, and it has truly been very exciting to use my knowledge from Marine Cybernetics in a new way. It has been a hard process, but also a very rewarding one.

I want to thank my supervisor Roger Skjetne for great guiding through the master thesis. Also, I am very grateful for the help from my co-supervisor Andreas Reason Dahl, who has helped me with problems on the model and building up the understanding of marine power systems. He has always been available for questions about the model, as well as for meetings in Trondheim. In addition, I want to thank Daeseong Park for weekly meetings at the institute, which always have been very informative, and Namireddy Praveen Reddy for good help on the battery model. In addition, Mehdi Zadeh has been important in understanding more about hybrid electric ships.

Olav Fiksdahl, Trondheim, June 2020

Acknowledgements

I want to thank my supervisor Roger Skjetne for good guidance throughout the thesis, and for working in a very structured and organized way. I also want to thank my co-advisor Andreas Reason Dahl, who has always been available for questions about the model, and really motivated me to work on this thesis. Daeseong Park, Namireddy Praveen Reddy and Mehdi Zadeh have also been important for this thesis, and I am very grateful for their help. Finally, I want to thank my father, who is also an engineer, for reading through this thesis and giving me valuable feedback.

Thesis Definition

The thesis definition is taken from the *Master of Technology Thesis Definition* at the first pages, and it can be summarized by the following points:

1. Perform a background and literature review to provide information and relevant references on:
    - The structure-preserving model (SPM), especially article by Dahl et al. (2018) and references therein by Bergen and Hill (1981) and Hill and Bergen (1982).
    - Model predictive control (MPC); general theory and its application by Dahl et al. (2018).
    - Typical configurations of marine hybrid electric power systems. Models and optimization strategies for marine hybrid electric power systems; for instance PhD theses of Torstein Bø and Michel Miyazaki, corresponding papers, and MSc theses.
2. Define system structure for power management system (PMS), battery management system (BMS), and energy and emission management system (EEMS), including a description of the most relevant main modes and functions.
3. Define Battery-ESS (BESS; battery energy storage system) by its most important functions, inputs, outputs, and relevant constraints.
4. Extend the SPM with battery modules and converter models. Make changes to the code used in the article of Dahl et al. (2018).
5. Formulate relevant control modes for the hybrid electric system as respective optimization problems for minimizing energy and emissions. Propose solutions to the optimization problems using MPC with SPM as model. Consider configurations with or without a battery module on the power bus. Test both on an unrealistic deterministic load profile and a realistic load profile. Analyze and discuss the resulting performances with comparisons to other methods, if available.

Acronyms and Abbreviations

AC	=	Alternating current
AVR	=	Automatic Voltage Regulator
BESS	=	Battery Energy Storage System
BMS	=	Battery Management System
BSFC	=	Brake Specific Fuel Consumption (see SFC)
CO_2	=	Carbon dioxide
DC	=	Direct current
DNV GL	=	Det Norske Veritas and Germanischer Lloyd
DP	=	Dynamic Positioning
ECA	=	Emission Control Area
ECMS	=	Equivalent Cost Minimization Strategy
EKF	=	Extended Kalman Filter
EEMS	=	Energy and Emission Management System
EMS	=	Energy Management System
ESD	=	Energy Storage Device
ESS	=	Energy Storage System
FC	=	Fuel Consumption
Genset	=	Generator set
IMO	=	International Maritime Organization
LP	=	Linear Programming
MCR	=	Maximum Continuous Rating
MILP	=	Mixed Integer Linear Programming
MPC	=	Model Predictive Control
NLP	=	Nonlinear Programming
NO_x	=	Nitrogen oxide
PMS	=	Power Management System
PMP	=	Potryagin's Minimum Principle
PSV	=	Platform Supply Vessel
pu	=	Per unit
QP	=	Quadratic Programming
ROV	=	Remotely Operated Vehicle
SFC	=	Specific Fuel Consumption
SFOC	=	Specific Fuel Oil Consumption (see SFC)
SLD	=	Single-Line Diagram
SoC	=	State of Charge of a battery
SO_x	=	Sulphur oxide
SPM	=	Structure-Preserving Model
SQP	=	Sequential Quadratic Programming
SSV	=	Seismic Survey Vessel

Table of Contents

List of Tables

List of Figures

Chapter 1

Introduction

This chapter explains the background, motivation, objectives, scope and delimitations, contributions and structure of the thesis. The sections 1.1 and 1.2 include parts taken from my project thesis, see Fiksdahl (2019).

1.1 Background

Figure 1.1: MS Roald Amundsen. Photo: Karsten Bidstrup (2019).

Figure 1.1 shows MS Roald Amundsen, the world's first hybrid electric expedition ship, launched in 2019, which will reduce its fuel consumption and carbon dioxide (CO_2) emissions by 20% (Hurtigruten, 2019). It is also possible for the ship to sail in a fully electric operation for a shorter period of time.

MS Roald Amundsen has certainly shown that hybrid propulsion on large ships is possible. Hybrid electric ships will be even more common in the years to come, as shipping must lower its emissions world-wide, both to meet the climate goals of the Paris Agreement, but also to follow and comply with requirements and regulations set by the International Maritime Organization (IMO). For smaller distances, fully electric ships can be considered, as the battery packages will not be too big, and there will be enough space for cargo – but currently, for larger ships, a hybrid electric solution is a better alternative.

For hybrid electric ships to be even more widely used by the industry, it is necessary to understand how to model the onboard power plant. This master thesis will therefore focus on the modeling and optimization on a marine hybrid electric power system using a model called the structure-preserving model (SPM). It is considered important for the shipping industry to change into a greener direction, motivating the development of knowledge and competence-building towards such goals.

1.2 Thesis Motivation

The motivation of this thesis is to contribute to lowering emissions from shipping, in addition to learning more about green shipping. More than 90% of the trade worldwide is carried across the oceans by ships, and today, there are approximately 90 000 marine vessels operating on a global basis (Oceana, 2019). The Third IMO Greenhouse Gas Study estimated that for the period 2007-2012, shipping accounted for approximately 3.1% of the annual global CO_2 emissions (IMO, 2014).

In addition, 16 of the world's largest ships produce as much sulphur pollution as all the world's cars (Pearce, 2009; Akerbæk, 2018). Although emissions from ships are significant, shipping is nevertheless the most energy-efficient mode of mass transport, and efforts to effectively reduce emissions from ships are needed, as sea transport will continue to grow (IMO, 2019a).

The IMO has set regulations on both emissions of nitrogen oxide (NO_x) and sulphur oxide (SO_x), which can be found in Regulation 13 and 14, respectively, of

MARPOL Annex VI (IMO, 2008). There, it is stated that ships built after 1 January 2016 that operate in Emissions Control Areas (ECAs), located for instance in North America and in Northern Europe, have to limit their NO_x emissions to be between 2.0-3.4 g/kWh in comparison with ships built between 1 January 2000 and 1 January 2011, that are allowed to emit between 9.8-17.0 g/kWh, regardless of where they operate (IMO, 2019b).

This means a NO_x reduction of approximately 80% for new ships operating in ECAs. For the SO_x emissions, they have to be reduced from 3.5% m/m (meaning percentage by mass) to 0.5% m/m after 1 January 2020, and to 0.1% m/m in ECAs (IMO, 2019c). In other words, the sulphur content in the fuel from ships has to be reduced by around 85% globally.

Furthermore, the Norwegian government has set specific goals for reducing emissions from shipping, stating that emissions from shipping on Norwegian shelf must be reduced with 50% by 2030 (NTB, 2019). The government has also decided that all car ferries in Norway will be electric within 2025 (Dalaker, 2019).

With these facts in mind, it is highly motivating to be able to contribute to the development of hybrid electric power systems for ships. Another motivation is to extend the SPM for a marine hybrid electric power plant, and to verify that the SPM can be used as a control design model for hybrid ships.

1.3 Objectives

The objectives for this master thesis, and where in the thesis they are answered, are taken from the Thesis Definition, and they are as follows:

1. Perform a literature review on the structure-preserving model (SPM) and on model predictive control (MPC). The SPM will be explained in detail in Section 2.3, with an extension for batteries found in Section 2.10, and a review on MPC is found in Section 2.4. Investigate hybrid electric power systems on ships, and present typical configurations of these systems. Also, provide information on the models and optimization strategies for marine hybrid electric power systems. These points will be answered in an extensive literature review in Chapter 2, see especially Section 2.5 and Section 2.8.

2. Define system structure for power management system (PMS), battery management system (BMS), and energy and emission management system (EEMS), and include a description of the most relevant main modes and functions. This will be answered in Section 2.7, see more specifically Section 2.7.2 for the EEMS, Section 2.7.3 for the PMS, and Section 2.7.4 for the BMS.

3. Define battery energy storage system (BESS) by its most important functions, inputs, outputs, and relevant constraints. This point is also covered in Section 2.7, with a thorough explanation in Section 2.7.5, and a battery model presented in Section 2.9.

4. Extend the SPM with battery modules and converter models. The SPM with batteries is explained in Section 2.10, and it is developed further in the method in Chapter 4, with an explanation in Section 4.2.

5. Formulate relevant control strategies for the hybrid electric system as respective optimization problems for minimizing energy and emissions. These formulations are found in Section 4.4, where the strategies are explained in the literature review from Section 2.7.5. Further on, propose solutions to the optimization problems using MPC with SPM as model, considering configurations with and without a battery module, and testing both on an unrealistic deterministic load profile and a realistic load profile. The solutions of these problems will be shown in the results in Chapter 5, both with and without a battery, where the results for the deterministic load profile will be presented in Section 5.4, and the results for the realistic load profile will be shown in Section 5.5. Lastly, analyze and discuss the resulting performances with comparisons to other methods, if available. Another method will be genset disconnection, presented in Section 4.5, analyzed in Section 5.6 and further discussed in the discussion in Chapter 6.

1.4 Scope and Delimitations

The scope of this thesis is within modeling and optimization of a power system on a hybrid electric ship, and how to reduce the energy and emissions of the ship. For the modeling, a model called the SPM is used, and optimization with model predictive control will be performed, for two different load profiles, and for different battery strategies on the hybrid electric power system. The performance of the SPM as a power system model will also be compared to a verification model.

The model in this thesis, the SPM, is only valid for power systems with an alternating current (AC) grid, and therefore, a delimitation is that the model is not valid for direct current (DC) grid power systems. The SPM is also only valid for active loads, and does not take reactive loads into acccount. Another delimitation is that voltages on the electrical buses are assumed to be constant, and that the battery model does not include varying battery voltage or resistance.

1.5 Contributions

The main contributions of this thesis are to:

- Provide insight and understanding of hybrid electric ships and their power systems, through a thorough literature review.
- Model a power system on a hybrid electric ship with battery storage, using a new model called SPM, and provide insight of this model.
- Verify the SPM as a model for hybrid electric power systems.
- Develop a battery model for a hybrid electric ship.
- Extend the SPM for battery usage.
- Formulate optimization problems on a hybrid electric power system with batteries, using model predictive control.
- Compare different battery strategies for a hybrid electric ship, using the SPM as model, and estimate fuel consumption for the strategies.

1.6 Structure of the Thesis

The remaining parts of the master thesis are divided into six chapters, and a brief explanation of each chapter is presented below.

- **Chapter 2 - Literature Review**: Theory and literature about marine hybrid electric power systems, graph theory, the SPM, MPC, EEMS, PMS, BMS, and the battery as an energy storage device.
- **Chapter 3 - Problem Formulation**: Development of a research question and explanation of what this thesis tries to solve.
- **Chapter 4 - Method**: Contains the approach that is used, explaining the steps needed in order to build the model, and contains formulations for the optimization problems for the different battery strategies on the hybrid electric power system, using MPC.
- **Chapter 5 - Results from Case Study**: Presents the case study for a hybrid electric ship, verification of the SPM and results for the different battery strategies.
- **Chapter 6 - Discussion**: Discusses the results from the case study, performance of the SPM and improvements to this thesis.
- **Chapter 7 - Conclusion**: Contains concluding remarks of this thesis and recommendations for further work.

Chapter 2

Literature Review

As this master thesis is a continuation of the previously conducted project thesis by this author, relevant parts of Fiksdahl (2019) is included in this chapter, which will introduce the reader to relevant literature in the field of hybrid electric ships, giving theory about the SPM, MPC and batteries, for instance.

2.1 Important Electrical Concepts

To be able to get the most out of this thesis, an understanding of marine electric power systems is needed. This entire section explains some important electrical concepts for marine applications, and it is all taken from the lecture notes in the course TMR4290 - Marine Electric Power and Propulsion Systems, lectured at NTNU (Zadeh, 2019).

2.1.1 Difference between Alternating Current and Direct Current

An alternating current (AC) is a current which changes direction with a fixed frequency, usually between 57 and 63 Hz, while a direct current (DC) has a constant current. Power systems can be both AC and DC. An example of a DC component is a battery, since the current flows in only one direction, while current produced from a generator is AC. In AC grids, stability is important, since the frequency is desired to fluctuate as little as possible, and large oscillations will give an unstable system. Besides, there is a high risk of damaging the electrical devices if the frequency in an AC grid drastically falls or rises. Later in this thesis, an AC model, called SPM, will be presented.

2.1.2 Common Electrical Components

Electrical components used in a marine power system include prime movers (such as generator sets), switchboards, transformers, frequency converters, propulsion drives and loads. A generator set (from now on called a genset) normally consists of either a diesel engine or a gas turbine together with an electric generator that generates electrical energy and supplies the loads, where loads for instance can be propellers for the propulsion. Further on, the role of the switchboard is to direct and distribute the electricity from the energy sources, such as the gensets. A transformer is necessary in order to increase or decrease the AC voltages, and a frequency converter is needed for changing the AC frequency to the different devices. For a hybrid electric power system with an AC grid, a rectifier and inverter are needed between the AC grid and the battery, in order to convert the current from AC to DC (rectifier) and from DC to AC (inverter), as batteries are DC.

2.1.3 Single-Line Diagrams

A single-line diagram (SLD) is a simplified block diagram demonstrating the path of the power flow, and it is commonly used for marine power systems. An illustration of an SLD for a drilling rig, with gensets, switchboards, bus-tie breakers (used between the electrical buses), transformers, frequency converters, and propulsion units, among others, is shown in Figure 2.1.

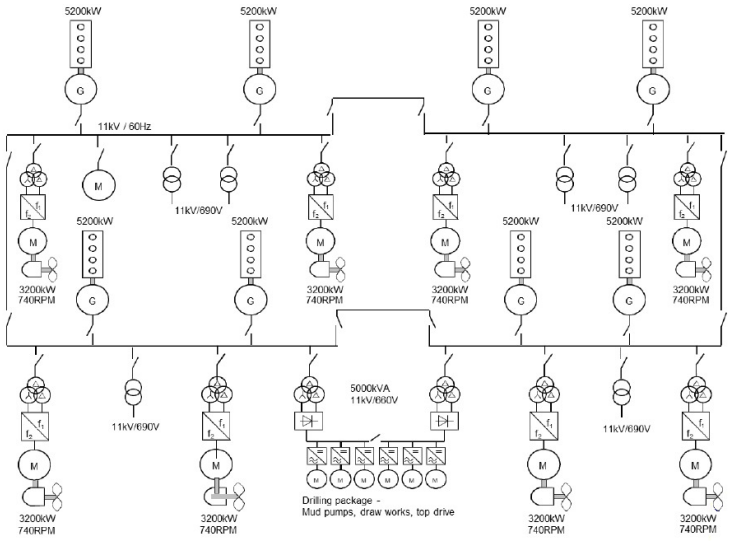

Figure 2.1: Example of an SLD, for the West Venture Platform. From lectures by Zadeh (2019).

2.2 Graph Theory and its Application in Power Systems

Many real-world situations can be described by graph theory, which can be explained as using a diagram consisting of a set of points together with lines joining certain pairs of these points (Bondy and Murty, 2008). One such example can be points representing people, with lines joining pairs of friends, as described by Bondy and Murty (2008), or it can be used to model real power systems, where the points are power consumers or power producers, as will be used in this master thesis.

According to Bondy and Murty (2008), a graph G is an ordered pair $(V(G), E(G))$ consisting of a set $V(G)$ of vertices and a set $E(G)$ of edges, where $E(G)$ is disjoint from $V(G)$. The vertices can be seen as points or nodes, and the edges as lines that connect the points. An incidence matrix is a notation for the network of edges and vertices, and it associates the edges and vertices to each other. As an example, Chartrand (1977) defines the incidence matrix $B = B(G) = [b_{ij}]$ to be the $p \times q$ matrix, where there are p vertices and q edges, in which $b_{ij} = 1$ if the vertex v_i is incident with the edge e_j, and $b_{ij} = 0$ otherwise.

An example of a graph with vertices $V(G) = \{v_1, v_2, v_3, v_4\}$ and edges $E(V) = \{e_1, e_2, e_3, e_4, e_5\}$ with the corresponding incidence matrix B is shown in Figure 2.2. From this figure, it can for instance be seen that edge e_1 connects the two vertices v_1 and v_2 by looking at the first column in B (remember that rows represent vertices and columns represent edges).

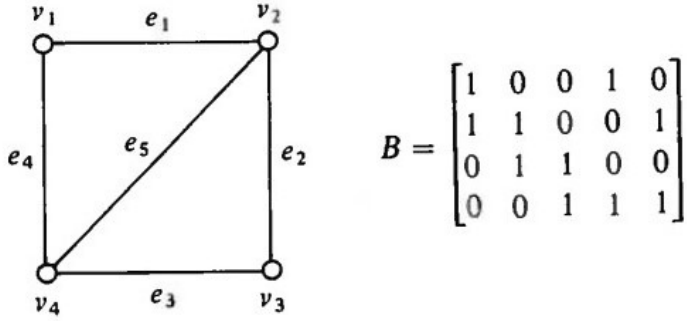

Figure 2.2: Example of a graph with its corresponding incidence matrix B. Courtesy: Chartrand (1977).

For many applications, such as for power system analysis, it is convenient to use a directed graph, since power is assumed to flow in a certain direction. A di-

rected graph is a graph in which each link has an assigned orientation (Bondy and Murty, 2008), and it can, according to Chartrand (1977), be formulated as a finite nonempty set V together with an irreflexive relation R on V (meaning that it does not relate any element to itself). The elements of V are still called vertices, and each ordered pair in R is referred to as a directed edge.

For power systems, the vertices can be modeled as nodes that are either power consumers or producers. A node that is a power consumer is a node that consumes or uses up power, and can for instance be a load, such as propulsion on a ship. Therefore, the power for a consumer is flowing *in to* the node. An example of a power producing node is a genset, with power flowing *out from* the node. The method of using power consumers and producers has for instance been adopted by Dahl et al. (2017), which used an incidence matrix to model the power flow between the nodes.

In order to set up such an incidence matrix for the power flow, a directed graph can be used, and the incidence matrix will consist of elements that are either -1, 0 or 1, depending on the direction of the power flow (Dahl et al., 2017). Using the definition by Desoer and Kuh (1969), the incidence matrix, for a graph with vertices i (called nodes) and edges k (called branches), will consist of elements a_{ik} which are

$$a_{ik} = \begin{cases} 1, & \text{if branch } k \text{ leaves node } i \\ -1, & \text{if branch } k \text{ enters node } i, \text{ and} \\ 0, & \text{if branch } k \text{ is not incident with node } i. \end{cases} \tag{2.1}$$

Dahl et al. (2017) studied a marine power plant consisting of two gensets (G_1 and G_2) and two loads (P_1 and P_2), where node 1 and 2 (n_1 and n_2) are load nodes (power consumers), and node 3 and 4 (n_3 and n_4) are genset nodes (power producers), as shown in Figure 2.3a. Lines 1, 2 and 3 are cables, called l_1, l_2 and l_3, that clearly show the direction of the power flow. The incidence matrix of the power system from Dahl et al. (2017) is shown in Figure 2.3b, using the definition from Equation (2.1), and it can be observed that n_1 is a pure consumer, n_2 is both a consumer and a producer, and n_3 and n_4 are pure producers. This agrees well with the definition of n_1 and n_2 being loads, and n_3 and n_4 being gensets, with a bus-tie breaker, represented by l_1, between the load nodes.

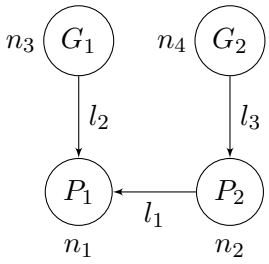

(a) Configuration of power system.

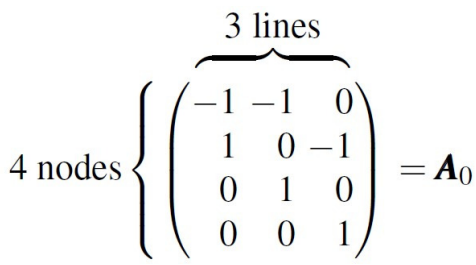

(b) Incidence matrix. Courtesy: Dahl et al. (2017)

Figure 2.3: Power system and corresponding incidence matrix from Dahl et al. (2017), with genset G, load P, line l and node n.

2.3 The Structure-Preserving Model

In Bergen and Hill (1981), a new model for studying power system stability, using Lyapunov functions, was proposed. The model was called a structure-preserving model, hereby denoted as SPM, and it was used as a tool for analyzing stability of power systems. The key feature of the SPM is, according to the authors, that the model assumes frequency-dependent load power, instead of the usual impedance loads, which will be used in a reduced network. In other words, the SPM does not rely on a reduced network, and the original network topology is explicitly represented (Bergen and Hill, 1981). An advantage of this is that the original network is preserved. In addition, the SPM will account for real power loads in the Lyapunov functions used in the stability analysis, and these Lyapunov functions will give a true representation of the stored energy in the system, according to Bergen and Hill (1981).

The SPM from Bergen and Hill (1981) assumes constant bus voltages, and as mentioned, it represents each load as a frequency-dependent power load. The article assumes that the real power drawn by the load at bus i, called P_{D_i}, can be written as

$$P_{D_i} = P^0_{D_i} + D_i\dot{\delta}_i,\ i = m+1, ..., m+n \tag{2.2}$$

where i denotes the index of the bus, m is the number of generators, n is the number of buses with loads, $P^0_{D_i}$ is the operating point, $D_i > 0$ is the generator damping, and $\dot{\delta}_i$ is the frequency. Equation (2.2) assumes that P_{D_i} is linear, by considering a constant voltage and small variations in the frequencies around the operating point.

Further on, Bergen and Hill (1981) mathematically formulate the SPM as

$$M_i\ddot{\delta}_i + D_i\dot{\delta} + \sum_{j=1,j\neq i}^{n} b_{ij}\sin(\delta_i - \delta_j) = P^0_{M_i} + P^0_{D_i},\ i = i, ..., n \tag{2.3}$$

where M_i is the generator inertia, b_{ij} is a constant for bus i and j, δ_i and δ_j are the bus angles, $P^0_{M_i}$ is the mechanical input power, and the other variables are as above.

Using an example of a power network with four buses (where two of them have generators attached), Bergen and Hill (1981) formulate the SPM on a state-space form, as

$$\dot{\boldsymbol{\alpha}} = \boldsymbol{T}_1\boldsymbol{\omega}_1 - \boldsymbol{T}_2\boldsymbol{D}_2^{-1}\boldsymbol{T}_2^{\top}\left[\boldsymbol{f}(\boldsymbol{\alpha}) - \boldsymbol{P}^0\right] \tag{2.4a}$$

$$\dot{\boldsymbol{\omega}}_1 = -\boldsymbol{M}_1^{-1}\boldsymbol{D}_1\boldsymbol{\omega}_1 - \boldsymbol{M}_1^{-1}\boldsymbol{T}_1^{\top}\left[\boldsymbol{f}(\boldsymbol{\alpha}) - \boldsymbol{P}^0\right] \tag{2.4b}$$

The description of the variables in Equation (2.4) is as the following (Bergen and Hill, 1981): $\boldsymbol{\alpha}$ contains the internodal angles (the angles between the nodes), defined by a transformation $\boldsymbol{\alpha} = \boldsymbol{T}\boldsymbol{\delta}$, with the matrix being $\boldsymbol{T} = [\boldsymbol{T}_1\ \boldsymbol{T}_2]$. $\boldsymbol{\omega}$ is the genset frequency, with subscript 1 referring to generator 1. As before, $\boldsymbol{D}$ is the generator damping, with subscripts assigned to each generator. Furthermore, $\boldsymbol{f}(\boldsymbol{\alpha})$ represents the load flow, and it is a vector containing the elements $f_i(\boldsymbol{\alpha}) = \sum_{k=1,k\neq i}^{n-1} b_{ik}\sin(\alpha_i - \alpha_k) + b_{in}\sin\alpha_i$, for $i = 1, ..., n-1$. Lastly, $\boldsymbol{P}^0$ is a vector containing elements P^0_i, which are defined as $P^0_i = P^0_{M_i} + P^0_{D_i}$.

Bergen and Hill (1981) also define the power flow p_k of each branch k, where it is assumed that k connects buses i and j. The power flow p_k is assumed to be a function of σ_k, i.e. $p_k = g_k(\sigma_k)$, with

$$g_k(\sigma_k) = b_k\sin(\sigma_k) \tag{2.5}$$

where $\sigma_k = \delta_i - \delta_j$ for the bus line k joining buses i and j, and $b_k = b_{ij}$ (Bergen and Hill, 1981).

The SPM from Bergen and Hill (1981) was further developed by the same authors to apply for power networks with linear frequency-dependent loads in Hill and Bergen (1982), and a stability analysis of both the local (dynamic) stability and asymptotic (transient) stability is performed. From Hill and Bergen (1982), a complete theoretical study of the stability is presented, and the advantage of the SPM is again repeated, in that Lyapunov functions allowing for real power loads

can be defined. However, the authors state that a major improvement of the SPM would be to allow for voltage-dependence of the loads. Still, the usual classical model also misrepresents voltage-dependencies by using impedance models calculated at the nominal bus voltages (Hill and Bergen, 1982).

The SPM equations developed by Bergen and Hill were developed for land-based power plants, but Dahl et al. (2017) used Bergen and Hill (1981) and Hill and Bergen (1982) and adapted the SPM to be valid for power plants onboard ships as well, by studying the use of the SPM on dynamic positioning (DP) vessels, with the DP system automatically maintaining the vessel's position and heading.

Dahl et al. (2017) describe the whole system by the following equations:

$$\boldsymbol{D}\dot{\boldsymbol{\delta}}_{n_0} = \boldsymbol{P} - \boldsymbol{B}_1\boldsymbol{f}(\boldsymbol{\delta}) + \boldsymbol{D}\boldsymbol{e}_{n_0}\omega_{net}, \qquad \text{W} \quad (2.6)$$

$$\dot{\boldsymbol{\delta}}_G = \boldsymbol{\omega}_G, \qquad \text{rad/s} \quad (2.7)$$

$$\boldsymbol{J}2\boldsymbol{p}^{-1}\dot{\boldsymbol{\omega}}_G = \boldsymbol{\tau} - 3\frac{1}{2}\boldsymbol{p}\,\mathrm{diag}(\boldsymbol{\omega}_G)^{-1}\boldsymbol{B}_2\boldsymbol{f}(\boldsymbol{\delta}), \qquad \text{Nm} \quad (2.8)$$

where $\boldsymbol{D} = \mathrm{diag}(D_1, ..., D_{n_0})$ is the diagonal matrix of damping constants, $\dot{\boldsymbol{\delta}}_{n_0}$ is the vector of n_0 load and terminal angles, $\boldsymbol{\delta}_G$ is the vector of m internal angles, $\boldsymbol{\delta} = [\boldsymbol{\delta}_{n_0}, \boldsymbol{\delta}_G]^\top$, $\boldsymbol{\omega}_G$ is the vector of m velocities, $\boldsymbol{P}$ is the vector of power injected at each node (which is negative for consumed power), $\boldsymbol{J} = \mathrm{diag}(J_{n_0+1}, ..., J_n)$ is the diagonal matrix of inertia constants, $\boldsymbol{p} = \mathrm{diag}(p_{n_0+1}, ..., p_n)$ is the diagonal matrix of pole numbers, $\boldsymbol{B_1} = [\boldsymbol{I}_{n_0}\ \boldsymbol{0}_{n_0\times m}]$ and $\boldsymbol{B_2} = [\boldsymbol{0}_{m\times n_0}\ \boldsymbol{I}_m]$ are matrices suitable to produce power flow vectors corresponding to the n_0 first and the m last nodes, respectively, e_0 is the vector of n_0 unity entries, $\boldsymbol{\tau}$ is the mechanical torque vector, and $\boldsymbol{f}(\boldsymbol{\delta})$ is the vector of power distributed to all network nodes (Dahl et al., 2017).

Finally, Dahl et al. (2017) summarize the state-space model of the SPM as

$$\dot{\boldsymbol{\alpha}} = \boldsymbol{T}_1\boldsymbol{D}^{-1}(\boldsymbol{P} - \boldsymbol{B}_1\boldsymbol{f}(\boldsymbol{\alpha})) + \boldsymbol{T}_2\boldsymbol{\omega}_G \quad (2.9)$$

$$\dot{\boldsymbol{\omega}} = \boldsymbol{M}^{-1}(\boldsymbol{\tau} - \boldsymbol{\omega}_{pu}^{-1}\boldsymbol{B}_2\boldsymbol{f}(\boldsymbol{\alpha})) \quad (2.10)$$

where $\boldsymbol{\alpha}$ is a vector of internodal angles, $\boldsymbol{D}$ is the damping matrix, $\boldsymbol{P}$ is the power injected at each node, $\boldsymbol{T}_1$ and $\boldsymbol{T}_2$ are transformations, $\boldsymbol{M}$ is the diagonal inertia matrix, $\boldsymbol{\omega}_{pu}$ is the diagonal matrix of per unit electrical angular velocities, $\boldsymbol{\omega}$ contains the angular velocities, and the rest of the variables are as before (Dahl et al., 2017).

Continuing, $\boldsymbol{f}(\boldsymbol{\alpha})$ from Equations (2.9) and (2.10) is the power flow defined by

$$\boldsymbol{f}(\boldsymbol{\alpha}) = \boldsymbol{A}\, \boldsymbol{g}(\boldsymbol{A}_{red}^{\top}\boldsymbol{\alpha}), \qquad \text{pu} \quad (2.11)$$

where $\boldsymbol{A}$ is the $n \times l$ incidence matrix with n vertices and l lines, and $\boldsymbol{A}_{red}$ is the reduced incidence matrix achieved by removing the row corresponding to the datum node (i.e. the n^{th} row from $\boldsymbol{A}$). As an example, Figure 2.3b is the incidence matrix $\boldsymbol{A}$ used by Dahl et al. (2017). Furthermore, $\boldsymbol{\alpha}$ is a vector of internodal angles, and $\boldsymbol{g}(.)$ is a vector-valued function which outputs the l line power flows, where the elements are

$$g_k = \frac{V_i V_j}{X_k} \sin(\sigma_k),\ k = 1, ..., l, \qquad \text{pu} \quad (2.12)$$

where V_i and V_j are the voltages of node i and j, X_k is the reactance of the line, and σ_k is the line angle difference (Dahl et al., 2017).

Further on, Dahl et al. (2017) assume that the bus voltages are constant, that the network frequency is equal to the genset frequency, that the load dynamics are applicable for large deviations in power, and that the transmission lines can be assumed to be lossless.

Using the SPM for marine vessels developed by Dahl et al. (2017), Dahl et al. (2018) applied the SPM for model predictive control (MPC), a control algorithm which will be discussed in Section 2.4. In Dahl et al. (2018), two gensets and two loads are used for the modeling, with the same setup from Figure 2.3a, with node 1 and 2 being loads (power consumers), and node 3 and 4 being gensets (power producers), and a midship cable with a bus-tie breaker between the loads. An illustration of the marine power plant used in the article of Dahl et al. (2018) is shown in Figure 2.3a.

By writing out Equations (2.9) and (2.10) from Dahl et al. (2017) on an explicit form, and using the power plant from Figure 2.3, with incidence matrix from Figure 2.3b, Dahl et al. (2018) express the SPM as

$$D_1\dot{\alpha}_1 = P_1 - \frac{V_1 V_2}{X_1}\sin(\alpha_1 - \alpha_2) - \frac{V_1 V_3}{X_2}\sin(\alpha_1 - \alpha_3), \qquad \text{pu} \quad (2.13a)$$

$$D_2\dot{\alpha}_2 = P_2 - \frac{V_2 V_1}{X_1}\sin(\alpha_2 - \alpha_1) - \frac{V_2 V_4}{X_3}\sin(\alpha_2 - \alpha_4), \qquad \text{pu} \quad (2.13b)$$

$$\dot{\alpha}_3 = (\omega_1 - \frac{M_1\omega_1 + M_2\omega_2}{M_1 + M_2})\omega^B, \qquad \text{rad/s} \quad (2.13c)$$

$$\dot{\alpha}_4 = (\omega_2 - \frac{M_1\omega_1 + M_2\omega_2}{M_1 + M_2})\omega^B, \qquad \text{rad/s} \quad (2.13d)$$

$$M_1\dot{\omega}_1 = \tau_1 - \frac{S^R}{S_1}\frac{1}{\omega_1}\frac{V_3V_1}{X_2}\sin(\alpha_3 - \alpha_1), \qquad \text{pu} \quad (2.13e)$$

$$M_2\dot{\omega}_2 = \tau_2 - \frac{S^R}{S_2}\frac{1}{\omega_2}\frac{V_4V_2}{X_3}\sin(\alpha_4 - \alpha_2), \qquad \text{pu} \quad (2.13f)$$

where, for node i, α_i is the node angle referred to the center of inertia of the system, V_i is the node voltage, P_i is the power injected (also referred to as the load), and D_i is a damping parameter for the load. Furthermore, for genset i, ω_i is the frequency of the genset, M_i is the generator inertia constant, τ_i is the torque from the prime mover, S_i is the machine-specific rated power, S^R is the plant voltampere base, and X_k is the reactance of line k (Dahl et al., 2018). Note that this is the *expanded model*, i.e. with Equations (2.9) and (2.10) written out, and that bus-tie breakers and power flows are defined in the power flow matrix from Equation (2.11), and visualized intuitively in Figure 2.3.

It should be noted by the reader that Equations (2.13a) and (2.13b) apply for the *load nodes* (P_1 and P_2 in Figure 2.3a), and that Equations (2.13c) to (2.13f) are valid for the *genset nodes* (G_1 and G_2 in Figure 2.3a). Therefore, Equations (2.13a) and (2.13b) are *plant* per unit (that is, for the whole power system), and Equations (2.13e) and (2.13f) are *machine* per unit (that is, only for the gensets).

To gain a better understanding of Equation (2.13), and understand what the different terms mean physically, each term will be explained briefly, using i, j and k as indices: $D_i\dot{\alpha}_i$ represents the genset damping, P_i is the load to node i, $\frac{V_iV_j}{X_k}\sin(\alpha_i - \alpha_j)$ is the power flow between two nodes i and j through a line k, as defined in Equation (2.12), which, divided by ω_i gives the engine torque (as torque is power divided by engine speed). Continuing, $\frac{M_i\omega_i + M_j\omega_j}{M_i + M_j}$ is a scaling factor for the center of inertia, $M_i\dot{\omega}_i$ is the genset inertia, and $\frac{S^R}{S_i}$ changes the term from plant per unit to machine per unit. ω^B is the velocity base, defined by

$$\omega^B = 2\pi f^R, \qquad \text{rad/s} \quad (2.14)$$

with f^R being the rated frequency of the system. Furthermore, the gensets are droop-controlled, so τ_i, the torque exercised by the genset, is according to Dahl et al. (2018) defined as

$$\tau_i = u_i - (\omega_i - \omega_{ref})\frac{1}{R}, \qquad \text{pu} \quad (2.15)$$

where u_i is the load setpoint to the genset, ω_{ref} is the speed reference, and R is the percentage droop of the generator. Later on, the load setpoint u_i will be used for optimization, as also was done by Dahl et al. (2018). The values for the parameters used by Dahl et al. (2018) in Equation (2.13) are listed in Table i in Appendix A.

The SPM explained in this section can be used for traditional power systems, but later on, the SPM will be expanded for *hybrid electric* power systems, using batteries as energy storage. Therefore, the SPM for hybrid electric power systems will be called *Battery SPM*, and model predictive control, using the Battery SPM as model, will be used for optimization.

2.4 Model Predictive Control

Model predictive control (MPC) is a type of closed-loop optimization, where the optimal solution is recomputed at every time step t to include feedback control, as opposed to conventional open-loop optimization problems, where there is no feedback in the solution and the solution that is computed at time $t = 0$ is used throughout the prediction horizon (Foss and Heirung, 2016).

According to Mayne et al. (2000), the MPC principle can be formulated as "a form of control in which the current control action is obtained by solving, at *each* sampling instant, a finite horizon open-loop optimal control problem, using the current state of the plant as the initial state". Further on, the authors assert that optimization with MPC will yield an optimal control sequence, where the first control in this sequence is applied to the plant.

In other words, with MPC, the model is optimized on a time horizon from $t = 0$ to $t = N$, and it essentially solves a similar optimization problem over and over again at each time step. It is said that MPC uses a *moving horizon* approach in which the prediction horizon changes from $t, ..., t + N$ to $t + 1, ..., t + N + 1$ from one time step to the next (Foss and Heirung, 2016; Imsland, 2019). A more thorough review of MPC can be found in the NTNU course TTK4135 - Optimization and Control, with lectures from Imsland (2019). To read more about the applications of MPC, such as past achievements of MPC and some of its current developments, Mayne (2014) has for instance discussed this.

The principle of MPC discussed in this section is shown in Figure 2.4.

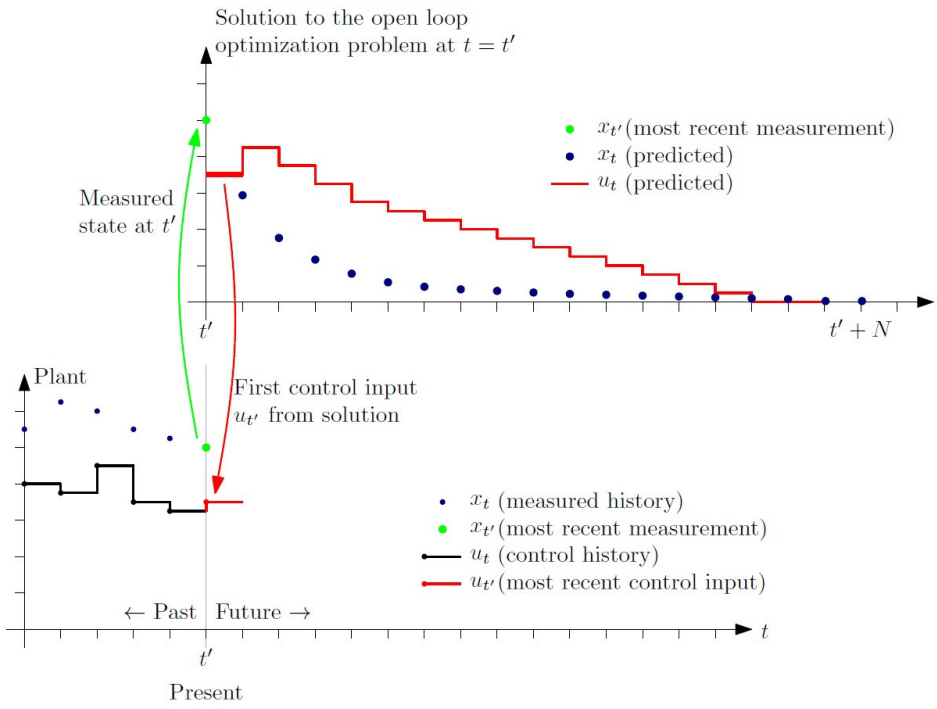

Figure 2.4: Illustration of the MPC principle. Courtesy: Foss and Heirung (2016).

An advantage of MPC is that it can be used to account for future disturbances in the system, since it couples open-loop optimization with feedback control. An algorithm of such an *output feedback MPC* uses available output data to estimate the state, and the algorithm of such an algorithm is shown in Figure 2.5, taken from Foss and Heirung (2016),

for $t = 0, 1, 2, \ldots$ **do**
  Get the current state x_t.
  Solve a dynamic optimization problem on the prediction horizon from t to $t + N$ with x_t as the initial condition.
  Apply the first control move u_t from the solution above.
end for

Figure 2.5: Algorithm for an output feedback MPC procedure. Courtesy: Foss and Heirung (2016).

2.4.1 Marine Applications of MPC

MPC has been used on marine vessels for design of power control. For instance, Bø and Johansen (2013) used MPC on a diesel-electric marine power plant. The authors suggested a controller that could handle a failure scenario, meet the safety requirements and lower the fuel consumption, by implementing constraints on the frequency of the diesel-electric power plant. A method for detecting that the plant is fault-tolerant was also presented.

Dahl et al. (2018) integrated MPC on a marine power plant for an AC system, using the SPM discussed in Section 2.3, by optimizing on the load setpoints to the gensets. Three objective functions were proposed to control the frequency, transient load and power flow. The article suggests that MPC based on SPM is viable for control of a marine power system, and that the controller's performance supersedes the benchmark controller (which has a constant load setpoint given to the gensets), especially for frequency regulation.

In addition, Stone et al. (2015) demonstrated the use of a constrained nonlinear MPC on a medium voltage DC test bed for a shipboard power system. Paran et al. (2015) used an MPC-based power management in the shipboard power system, applying MPC on a DC-based ship system, ensuring optimal load sharing among the generators while maintaining the DC bus voltage stability. A real-time MPC was presented by Park et al. (2015), employing MPC on a DC shipboard power system that consisted of several power sources and loads.

2.5 Typical Configurations of Marine Hybrid Electric Power Systems

A common configuration for a marine hybrid electric power system is shown in Figure 2.6, taken from Sørensen et al. (2017). The figure shows a power system with two gensets (consisting of a generator G and an engine E), one energy storage device (ESD), and three power consumers, which are two motors M and one load representing other loads.

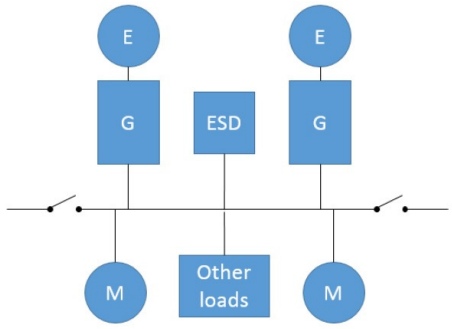

Figure 2.6: Example 1 of a marine hybrid electric power plant. Courtesy: Sørensen et al. (2017).

Common for all marine hybrid electric power systems is that they use energy storage in the form of an ESD, which is a device that can charge up and store energy and deliver it on demand (Sørensen et al., 2017). According to Hansen (2019) and Sørensen (2019), examples of ESDs are batteries, super-/ultracapacitors and flywheels. Batteries are the most common ESD in hybrid ships, as they significantly reduce fuel and maintenance costs and emissions (Reddy et al., 2019b). The use of batteries as an ESD for marine vessels has been investigated by Sørensen et al. (2017), for instance.

Another configuration for a marine hybrid electric power system is taken from Geertsma et al. (2017) and shown in Figure 2.7 below. It consists of three gensets, one ESD and one bus-tie breaker between the two buses, in addition to four power consumers, of which two are propulsion loads.

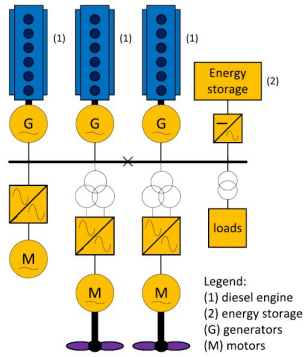

Figure 2.7: Example 2 of a marine hybrid electric power plant. Courtesy: Geertsma et al. (2017).

A typical configuration of a marine hybrid electric power system can also be as in Figure 2.8, taken from Kalikatzarakis et al. (2018). It is taken from a case study for a hybrid electric tugboat, with three gensets, two battery ESDs, and three power consumers, where two of them are propulsion and the other is remaining loads.

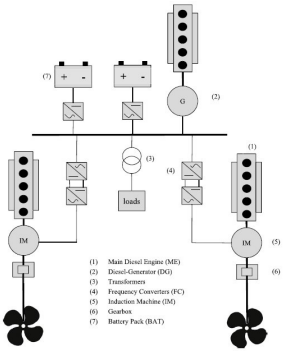

Figure 2.8: Example 3 of a marine hybrid electric power plant. Courtesy: Kalikatzarakis et al. (2018).

It should also be mentioned that an AC grid is a more conventional power system than DC, but the use of a DC grid configuration is becoming more common for hybrid electric ships, since batteries as an ESD are DC (Zadeh, 2019). An illustration of an AC grid and the proposed DC grid for a cutter dredger ship, taken from Kim et al. (2018), is shown in Figure 2.9. It can be seen that for the DC grid, no transformers are needed, and the number of frequency converters is reduced. However, AC grids are still widely used in the industry, and the model of the SPM in this thesis will for instance be based on a configuration with an AC grid.

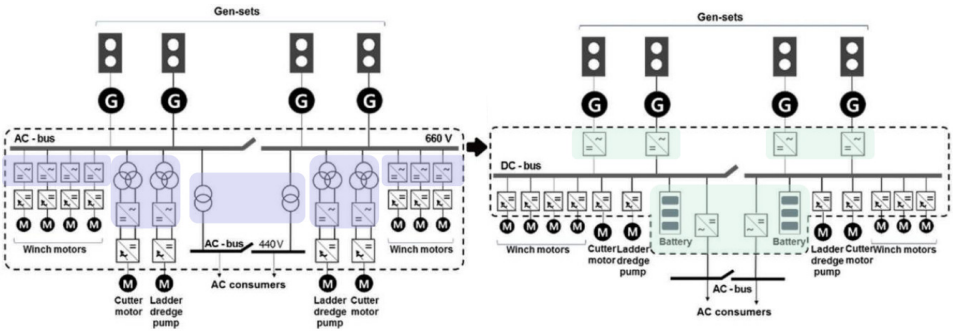

Figure 2.9: AC and DC bus power systems. Courtesy: Kim et al. (2018).

As a comparison with other marine power systems, a thorough overview of ships with both electric and diesel-electric propulsion, with details such as SLDs and

information about propulsion size, can be found in Siemens (2015). Furthermore, fuel cells can also be included as en energy source for marine hybrid power systems, as discussed by Ghimire et al. (2019) and Othman et al. (2019). However, this was not in focus of this section, which targeted hybrid electric power systems with batteries as ESD.

2.6 Typical Power Demands for Marine Vessels

Power demand for a ship depends on the type of vessel and type of operation that the vessel is going to encounter. Passenger vessels, such as cruise ships and ferries, typically have a demand for the propulsion power varying from a few MW for smaller ferries up to 30-40 MW for large cruise liners. For the latter, hotel loads can amount to a significant part of the total power installation, and it can be in the order of 10-15 MW for large cruise liners (Ådnanes, 2003).

For drilling units, production vessels and tankers, thruster-assisted positioning is often used for stationkeeping and DP operations, and thrusters normally constitute the main propulsion. Typically, these vessels have large power installed, ranging from around 25-55 MW (Ådnanes, 2003).

DP vessels usually have a total power demand of 8-30 MW, depending on the size of the vessel and the drilling/lifting capacity. For icebreakers, the power installed can be in the range of 5-55 MW, depending on the icebreaking capability (Ådnanes, 2003).

2.7 System Architecture of Control Layers

This section is written in collaboration with Kristoffer Lund, see Lund (2020).

An autonomous ship has several layers of autonomy functions. This section focuses on the system structure of the power system of an autonomous ship, and defines the system structure for the the energy and emission management system (EEMS), power management system (PMS), and the battery management system (BMS). The main functions of these systems and what is controlled by each of the control layers are also addressed in this section.

2.7.1 System Structure

Reddy et al. (2019b) define the system structure of control layers for a hybrid power and propulsion system of an autonomous ship. The system structure of the

control layers can be seen in Figure 2.10.

The control layers in Figure 2.10 are divided into three layers. The top level is the mission layer, where the vessel mission management system is located. The vessel mission management system supervises the vessel mission and objectives, and commands the lower level systems to act in accordance with these criteria. The next level is the online optimization layer. Here, the EEMS performs online optimization of the hybrid power and propulsion system.

The last level, the real-time control execution layer, consists of the PMS and the BMS. Both the PMS and the BMS provide safe operation of the hybrid power system. The PMS ensures that the power system delivers power according to the load requirement, and it prevents blackout if a fault occurs. The BMS ensures safe and reliable operation of the batteries (Reddy et al., 2019b). See also Figure 2.11 for the control and communication architecture of the control layers of an autonomous ship.

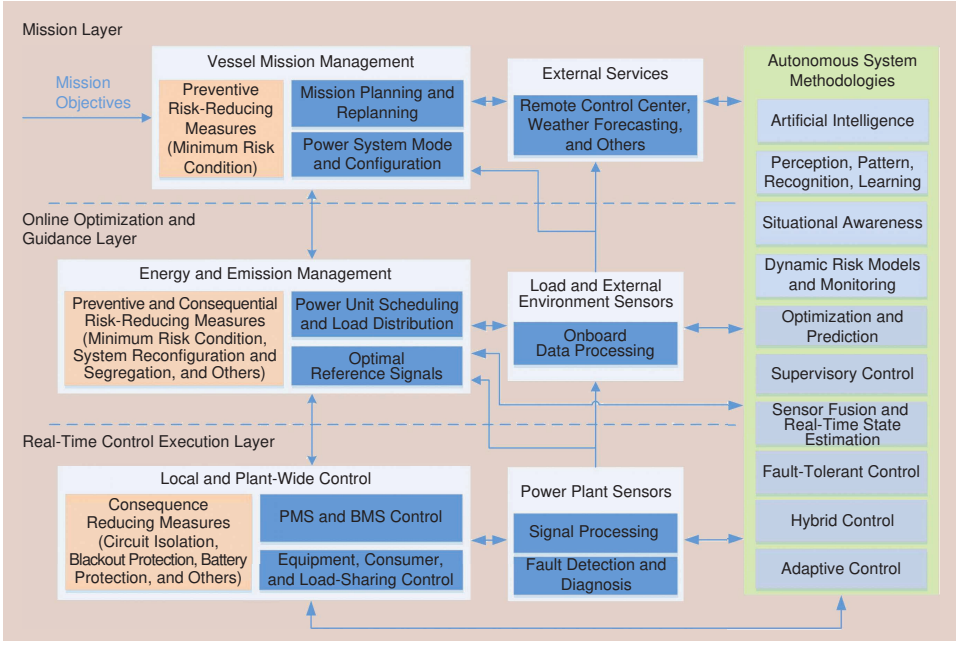

Figure 2.10: Control system layout of an autonomous ship and its power system. Courtesy: Roger Skjetne, NTNU AMOS. See also Reddy et al. (2019b).

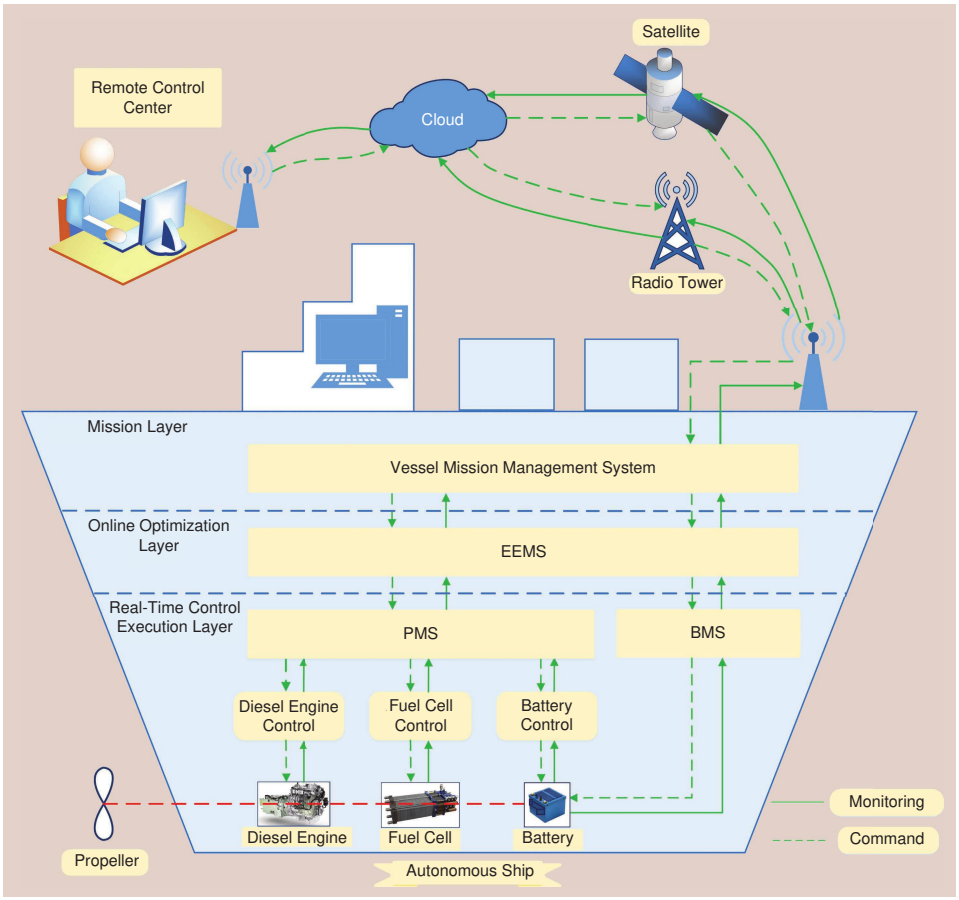

Figure 2.11: Control and communication architecture of an autonomous ship. Courtesy: Roger Skjetne, NTNU AMOS. See also Reddy et al. (2019b).

2.7.2 Energy and Emission Management System

An EEMS is defined by Reddy et al. (2019b) as a "high-level control system that commands the operation of a hybrid power plant to minimize energy usage and emissions while maintaining safety and resilience requirements and fulfilling the objectives of the vessel's mission". The EEMS distributes the required load power between several energy sources such that the energy sources are used in an optimal manner and the emissions from the power system are minimized. The optimal use of the different energy sources is determined by the EEMS by monitoring and controlling the energy flows in the power system, and a decision is made with respect to for instance minimizing the fuel consumption or other optimization objectives such as optimal load sharing or optimal connections/disconnections of power

producers. Within the EEMS lie many opportunities of implementing different optimization algorithms, utilizing the capabilities of each algorithm and considering different optimization objectives. The EEMS performs online optimization of the power system, meaning that the optimization problem contains no or limited knowledge of the future information about the states of the optimization variables. Due to this fact, the online optimization uses an instantaneous cost function for optimization (Reddy et al., 2019b), using instantaneous measurements of variables at the time instant the optimization is conducted. Therefore, an online optimization approach is suitable for optimizing the operation of a marine power system, as the loads experienced by the system are unpredictable and estimated at best. This means that an optimization which uses measurements from the power system throughout the optimization fits this purpose. Examples of such measurements are power loads and power outputs from the different energy sources.

In Figure 2.12, an illustration of the objectives of an EEMS is seen, ranging from minimizing fuel consumption to minimizing life-cycle operating costs.

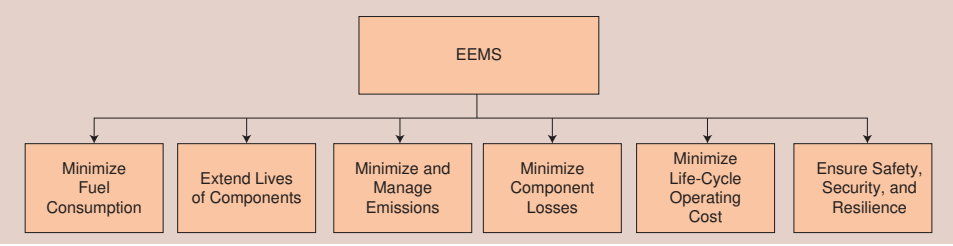

Figure 2.12: Objectives of an EEMS. Courtesy: Roger Skjetne, NTNU AMOS. See also Reddy et al. (2019b).

The EEMS uses three different control strategies, and a classification of these strategies can be seen in Figure 2.13. As can be seen from the figure, the EEMS is divided into a rule based, an optimization based and a learning based strategy. Both theses, Fiksdahl (2020) and Lund (2020), will focus on online optimization, using model predictive control (MPC) and mixed integer linear programming (MILP) optimization, respectively. Other online optimization methods include the equivalent cost minimization strategy (ECMS), Potryagin's minimum principle (PMP), linear programming (LP), quadratic programming (QP) and nonlinear programming (NLP).

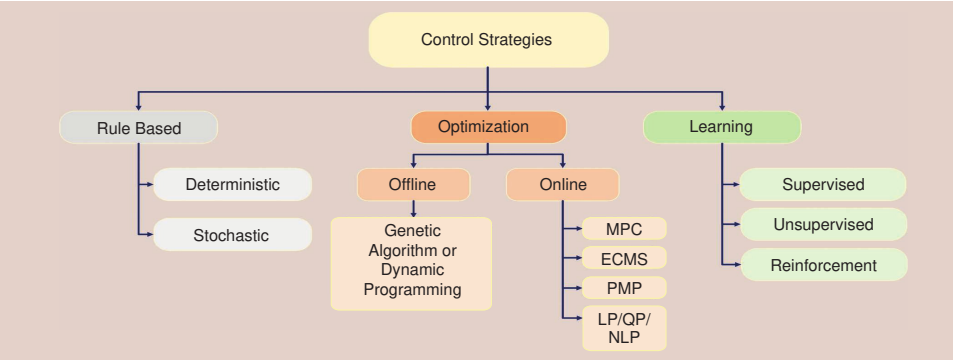

Figure 2.13: Classification of control strategies for the EEMS. Courtesy: Roger Skjetne, NTNU AMOS. See also Reddy et al. (2019b).

2.7.3 Power Management System

The purpose of a PMS is to ensure that there is enough power available in the power grid (Ådnanes, 2003). Given the operating condition, the PMS ensures that there are enough gensets running to provide power for the demanded load. Hence, the PMS has a very important job in the marine power plant; to ensure that faults are avoided, which in ultimate consequence can mean blackout. Also, if a blackout occurs, the PMS will restore power as soon as possible (Bø et al., 2015). The PMS is responsible for starting and connecting new gensets if needed, and can even perform disconnections of loads in dangerous situations, by for instance disconnecting power consumers of low importance, such as pumps or hotel loads. The PMS gives references to the main power sources and ESDs, and does this in real-time in order to ensure a safe and reliable operation of the power sources.

The most important functions of the PMS are (Skjetne, 2012):

- *Blackout restoration*: A function which, as its name implies, brings the power system back online if a blackout should occur.
- *Load shedding*: Means disconnecting non-essential power consumers from the power system, in the near event of a blackout. The load shedding function is an important part of the PMS when it comes to preventing blackouts.
- *Under- and over-voltage detection and handling:* Ensures that the voltage levels of the power system (component-wise and the power system as a whole) are kept within the appropriate, predetermined voltage levels. This is also an important feature in preventing blackouts from happening.

- *Under- and over-frequency detection and handling:* Takes the frequency of the power system into consideration, and ensures that these levels are kept within the allowed interval. As the under- and over-voltage detection, this function also prevents blackouts in the power system.
- *Active and reactive power load sharing:* Distributes the active and reactive power between power sources, where active power is the actual power dissipated in the circuit, and reactive power is the useless power, which moves back and forth between the load and the source. The active and reactive power load sharing is done by for instance *droop* control or *isochronous* control. In droop control, the power output of the generator reduces as the frequency increases, but in isochronous control, the gensets maintain a constant frequency regardless of the load.

2.7.4 Battery Management System

The BMS works in parallel with the PMS, as seen in Figures 2.10 and 2.11. The BMS ensures that the batteries operate in a safe and reliable manner, by avoiding over-current, over-voltage, and over-charging/-discharging of the battery, as this will accelerate the aging process and increases the risk of fire and explosion (Reddy et al., 2019b; Simonsen, 2019). The BMS works in real-time, and monitors the status of the battery and gives commands to the battery. According to Andrea (2010), a classic BMS needs to measure and monitor the following states of the battery: cell voltage, pack temperature and pack current. This is an absolute minimum in order to have a sufficient BMS.

Gulsvik (2017) has proposed a robust BMS for a remotely operated vehicle (ROV), and defines the BMS as a device or system whose purpose is to monitor, control, and/or optimize a battery, ensuring a safe and efficient operation of the battery.

2.7.5 Battery Energy Storage System

As mentioned earlier, batteries are the most common energy storage device (ESD) in all-electric and hybrid ships (Reddy et al., 2019b), and this section seeks to define the battery energy storage system (BESS), as specified in the thesis definition. The most important function of a battery is to consume or deliver power, thus manipulating the experienced load to the remaining power producers.

Common strategies for using the battery are, according to Sørensen et al. (2017) and Hansen (2019):

- *Enhanced dynamic performance*: The ESD can supply energy to the power plant during large load steps, so that the genset will be loaded gradually, which gives better performance and reduced risk of blackout. This strategy can for instance be used in "slower" energy sources like LNG and fuel cells, since it supplies the power instantly.

- *Peak-shaving*: The genset power supply is bounded between a lower and an upper limit, and the ESD supplies the power outside these bounds. This method can lead to both a reduction in fuel consumption and emissions, and it improves safety. When the load is below the lower limit, the battery is charged, and when it is above, the battery is discharged. See Figure 2.14a for a visual explanation of the peak-shaving principle.

- *Power smoothing*: This strategy is a form of peak-shaving, where fluctuations in the load are smoothed out. A band-pass filter can be used to control the battery load, where only the power variations in a given frequency range are counteracted by the battery, and the gensets consume the smoothed out load. This method has been used by Bø (2016), and Figure 2.14b illustrates power smoothing.

- *Spinning reserve*: An ESD works as a backup power to running generators. Class regulations from 2015 opened up for an ESD being used as a spinning reserve, where the ESD must be able to provide the necessary power to the plant for at least 30 minutes in case of a single fault (DNV GL, 2015).

- *Strategic loading*: Cyclic charging and discharging the ESD to strategically load the gensets to their optimal operating point, such that the total fuel consumption is reduced. Strategic loading has been studied in depth by Miyazaki (2017), and it is found to be an efficient strategy for reducing emissions.

- *Zero-emission operation*: Shutting down the generators and only use the ESD, which requires a large ESD installed on the vessel.

- *Enhanced ride through*: Use ESD as a short-time backup power in case of a failure.

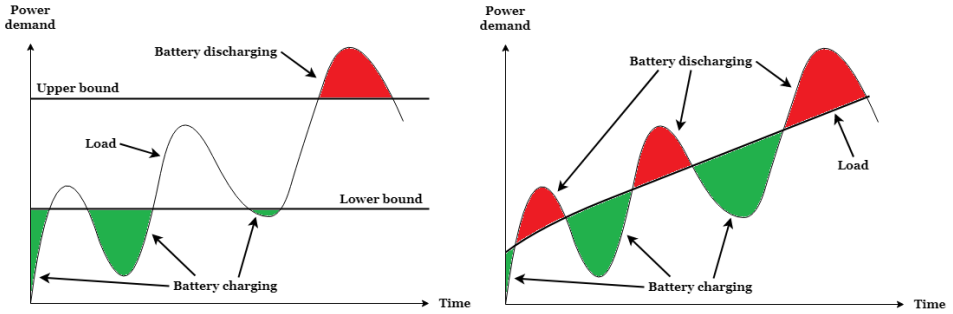

(a) Peak-shaving

(b) Power smoothing

Figure 2.14: Illustration of peak-shaving and power smoothing.

When using the battery, it is assumed that the sum of the genset and battery load is equal to the consumed power, according to

$$P_{gen} + P_{batt} = P_{load} \tag{2.16}$$

where P_{gen} is the generator power, P_{batt} is the battery power and P_{load} is the consumed power. In this way, the battery is used to change the genset load, and it can therefore, if used correctly, be efficient for reducing fuel consumption and emissions.

Typical constraints for the battery are temperature and state of charge (SoC), which should be kept within a lower and upper limit. Bø (2016) uses both SoC and temperature as battery constraints, but the temperature constraint can also be neglected. This was done in the work of Miyazaki (2017), which only included a constraint on the SoC. Another constraint in the battery can also be the battery power, with limits for the maximum charge and maximum discharge power, as stated by Dinh et al. (2018).

When it comes to inputs and outputs of the battery, Gulsvik (2017) has developed a thorough battery model, where the input is used to control the battery, and the output is used for measurements. In his battery model, the input was the battery current, and the output of the model was the voltage.

2.8 Models for Marine Hybrid Electric Power Plants

To model a marine hybrid electric power plant, a hybrid dynamic model, as well as a simplified steady-state space model, can be used, as proposed by Miyazaki

(2017). The hybrid dynamical model consists of both continuous-time and discrete-time dynamics. The continuous-time dynamics contain the gensets (such as the speed and power output), load demand and SoC of the battery, while the discrete-time dynamics consist of the ESD setpoint variation, which is an instantaneous change in the system (Miyazaki, 2017). The second model, the steady-state model, disregards the transient effects in the power plant, and genset dynamics and load dynamics are not taken into account. The models were validated in the Hybrid Machinery Lab at NTNU by Miyazaki (2017).

Bø (2016) mentions several simulators to model a marine power plant, in addition to establish and to qualitatively verify simulation models for power generators, storage, and consumers, such as gensets, batteries, and thrusters, respectively.

An example of a power flow model is presented by P. Kundur (1994). The power can be modeled as flowing between two nodes i and j through a line k, from node j to node i. Node j is therefore called the *sending* node, while node i is denoted the *receiving* node. The power that is transferred between nodes i and j, when the line k is AC and three-phase, is given as

$$P_{j,i} = -\frac{V_i V_j}{X_k} \sin(\delta_i - \delta_j), \qquad \text{W/phase} \quad (2.17)$$

where $P_{j,i}$ is the power, V_i and V_j are the phase voltage magnitudes for node i and j, X_k is the electrical reactance of the line, and δ_i and δ_j are the relative phase angles with regards to a common reference (P. Kundur, 1994). This power flow model is for instance used in the SPM presented in Section 2.3.

2.9 Battery Model for the Marine Hybrid Electric Power System

For marine hybrid electric power systems that use batteries, a suitable model is important. There are many possible ways to model a battery, such as using equivalent electric circuit models, by taking voltage and resistance into consideration, or to use Thevenin models. Both methods have been discussed by Gulsvik (2017), and Madani et al. (2019), in addition to Rahmoun and Biechl (2012), that discussed the use of an equivalent circuit model for lithium-ion batteries. This thesis will not use these models directly, as the voltage variation and resistance of the battery are

not of importance, but it is something that can be looked at for future work.

The battery model in this thesis presents a simplified model that uses a Coulomb counting method. This was also used in Gulsvik (2017), in addition to other papers, such as in Madani et al. (2019) and Gonzalez-Castellanos et al. (2019). It is based on the SoC of the battery, which is the level of charge of an electric battery relative to its capacity, where 0% means an empty battery and 100% means a full battery. The Coulomb counting can be formulated as

$$SoC(t) = SoC_0 + \frac{1}{3600 \cdot C} \int_0^t i(t)dt \tag{2.18}$$

where $SoC(t)$ is the state of charge of the battery at a given time t, SoC_0 is the initial SoC of the battery, and C is the capacity of the battery. The division with 3600 is done to convert into SI units, since C is given in Ah. Lastly, $i(t)$ is the battery current, which is calculated by

$$i(t) = \frac{P_{batt}(t)}{V_{batt}} \tag{2.19}$$

where P_{batt} is the necessary battery power calculated by the EEMS, and V_{batt} is the battery voltage.

To make the simulations more realistic, losses in the battery can be taken into consideration. This has for instance been done in Miyazaki et al. (2016a), where the modeling of the SoC included battery efficiencies of charging and discharging. In this thesis, the efficiencies for charging and discharging are denoted η_C and η_D, and they are assumed to be constant. However, the charging and discharging efficiencies of the battery vary, and they depend on both the SoC and the charging and discharging power. The battery efficiency is higher for lower battery current, and the efficiency also increases for a higher SoC, as shown by Gonzalez-Castellanos et al. (2019).

Implementing battery efficiency in Equation (2.18) gives the following equation for battery charging:

$$SoC(t) = SoC_0 + \frac{\eta_C}{3600 \cdot C} \int_0^t i(t)dt \tag{2.20}$$

where η_C is the charging efficiency, and the battery current $i(t) > 0$, making the SoC increase when charging the battery.

Accordingly, also using Equation (2.18), the corresponding equation for battery discharging, with efficiency taken into account, becomes

$$SoC(t) = SoC_0 + \frac{1}{3600 \cdot C \cdot \eta_D} \int_0^t i(t)dt \tag{2.21}$$

where η_D is the discharging efficiency, and the battery current $i(t) < 0$, making the SoC decrease when discharging the battery.

The SoC can be written on state-space form by differentiating Equation (2.18) with respect to the time, and inserting Equation (2.19), resulting in

$$\dot{z} = \frac{i(t)}{3600 \cdot C} = \frac{P_{batt}(t)}{3600 \cdot C \cdot V_{batt}} = k_z \cdot P_{batt}(t) \tag{2.22}$$

where z is introduced to represent the SoC of the battery (notation from Gulsvik (2017)), and the constant $k_z = \frac{1}{3600 \cdot C \cdot V_{batt}}$. With efficiencies taken into consideration, the constant will become $k_z = \frac{\eta_C}{3600 \cdot C \cdot V_{batt}}$ for charging and $k_z = \frac{1}{3600 \cdot \eta_D \cdot C \cdot V_{batt}}$ for discharging. Putting SoC on a state-space form as in Equation (2.22) has for instance been done in Moura et al. (2011) and in Dinh et al. (2018), and it will be used for the simulations.

2.9.1 Typical Values for SoC

Dinh et al. (2018) model a battery for a hybrid electric vessel with an SoC between 10-90% and an initial SoC of 85%, while Borhan et al. (2012) use SoC values for a battery on a hybrid electric vehicle in the range of 20-90%, and initial SoC between 59-70%. In addition, Borhan et al. (2012) set the target SoC at 70%, meaning that this is the desired SoC of the battery in the simulations. Furthermore, in Miyazaki et al. (2016a), the authors study models for hybrid marine power plants, where the SoC is within 20-80% and the initial SoC is 80%.

2.9.2 Typical Values for Battery Efficiency

As mentioned, the battery can be assumed to have losses in the charging and discharging. The efficiency of a battery for a marine vessel with hybrid propulsion normally lies between 85-92%, according to Dedes et al. (2012). Miyazaki et al. (2016a) define the battery efficiency η as the product between the discharging and charging efficiency of the battery, and they say that typical values for a lithium ESD on a marine power plant is between 90-95%.

2.9.3 Typical Battery Size for Marine Applications

Battery sizing is an important topic for hybrid electric ships, but it will not be the focus in this thesis. As a comparison from the literature, Dinh et al. (2018) discuss an optimal EMS for a hybrid electric dynamic positioning vessel, and use a battery with a power level of 480 V and 500 Ah for a 553 kW engine, when the power grid is AC.

Another example of battery size on a marine vessel is from Ghimire et al. (2019), where the authors propose a battery of 1 kV and 300 kWh and a fuel cell of 300 kW for four propulsion motors, where two of the motors have a capacity of 500 kW each and the remaining two have 2000 kW capacity each. Furthermore, Bassam et al. (2016) suggest a lithium-ion battery pack with a 500 Ah capacity and an output voltage of 600 V for a ferry with hybrid propulsion, with a passenger capacity of 975 people and a car capacity of 200 cars.

When it comes to the battery power, Skjong et al. (2017) utilize a battery with a limit on the discharge and charge power between -1 MW and 1 MW for a platform supply vessel (PSV) with 7 MW as max genset power, and the same battery power limits for a seismic survey vessel (SSV) with a total genset capacity of around 10 MW. For the battery capacity, Skjong et al. (2017) choose 1 MWh as the maximum battery capacity for both the PSV and SSV. Later on, these values will be used for setting constraints on the battery.

2.9.4 Typical Efficiencies of Converter and Transformer

Converters and transformers are necessary for hybrid electric power systems with an AC grid, as can be seen in Figure 2.9, for instance. There are losses in both the transformer and frequency converter that should be accounted for, even though the losses connected to them are small. The efficiency of a transformer is normally between 0.99-0.995, and the efficiency of the converter is between 0.98-0.99, according to Ådnanes (2003). The same numbers for the efficiency are also mentioned by Zadeh (2019).

When it comes to the entire power system, the overall efficiency of a diesel-electric system is normally between 0.88-0.92 at full load (Ådnanes, 2003). However, the efficiency depends on the loading, as discussed in Electronic Design (2013) and shown for a converter in Figure 2.15, with the efficiency being nearly constant from 40% of maximum to full load, and decaying for loads below 40%. In this thesis, the efficiencies are assumed to be constant for all loads, which is a simplification that will be discussed later.

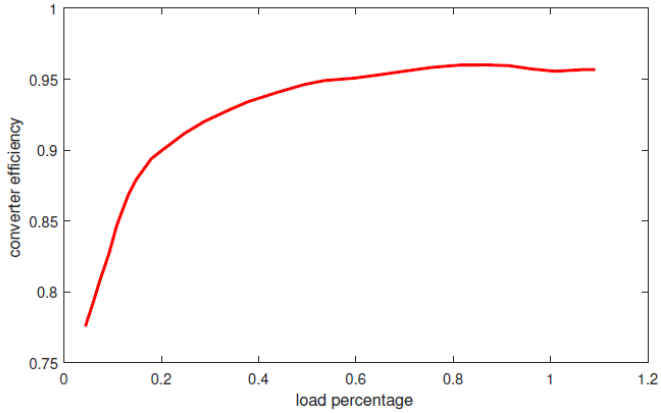

Figure 2.15: Converter efficiency against load percentage. Courtesy: Wu (2018).

2.10 Battery SPM

The SPM was introduced and explained in Section 2.3, and as mentioned, it can be extended for a hybrid electric power system, with use of battery as energy storage. This was part of my previous work in the project thesis, see Fiksdahl (2019) for more information.

The model for the battery implements the SoC equations from Equations (2.20) and (2.21), in addition to converting the battery current to power, as described by Equation (2.19). The SoC is put on state-space form using Equation (2.22).

In addition, the load to the gensets are changed by the EEMS, and therefore, a term $P_{batt,i}$, accounting for the battery power, should be added to or subtracted from the loads P_1 and P_2, depending on charging or discharging of the battery. Then, using the SPM from Equation (2.13) and the power system from Dahl et al. (2018), the Battery SPM can be defined as

$$D_1\dot{\alpha}_1 = P_1 + P_{batt,1} - \frac{V_1V_2}{X_1}\sin(\alpha_1 - \alpha_2) - \frac{V_1V_3}{X_2}\sin(\alpha_1 - \alpha_3), \quad \text{pu} \quad (2.23a)$$

$$D_2\dot{\alpha}_2 = P_2 + P_{batt,2} - \frac{V_2V_1}{X_1}\sin(\alpha_2 - \alpha_1) - \frac{V_2V_4}{X_3}\sin(\alpha_2 - \alpha_4), \quad \text{pu} \quad (2.23b)$$

$$\dot{\alpha}_3 = (\omega_1 - \frac{M_1\omega_1 + M_2\omega_2}{M_1 + M_2})\omega^B, \quad \text{rad/s} \quad (2.23c)$$

$$\dot{\alpha}_4 = (\omega_2 - \frac{M_1\omega_1 + M_2\omega_2}{M_1 + M_2})\omega^B, \qquad \text{rad/s} \quad (2.23d)$$

$$M_1\dot{\omega}_1 = \tau_1 - \frac{S^R}{S_1}\frac{1}{\omega_1}\frac{V_3V_1}{X_2}\sin(\alpha_3 - \alpha_1), \qquad \text{pu} \quad (2.23e)$$

$$M_2\dot{\omega}_2 = \tau_2 - \frac{S^R}{S_2}\frac{1}{\omega_2}\frac{V_4V_2}{X_3}\sin(\alpha_4 - \alpha_2), \qquad \text{pu} \quad (2.23f)$$

$$\dot{z}_i = k_{z,i} \cdot P_{batt,i}, \qquad - \quad (2.23g)$$

where the variables are defined as in Equation (2.13), except that $P_{batt,i}$ is the battery power to each node i, with $P_{batt,i} > 0$ meaning charging and $P_{batt,i} < 0$ meaning discharging of the battery, z_i is the SoC of battery i, and $k_{z,i}$ is a constant defined in Equation (2.22), with the SoC obviously increasing for charging and decreasing for discharging. It should be mentioned that the Coulomb counting model of the SoC in Equation (2.23g) is sensible to drift-off problems, since an error will be accumulated in the integration, so it can be a difficult approach to use in practice.

$P_{batt,i}$ is determined by the EEMS, which typically is used with one of the strategies from Section 2.7.5, like peak-shaving or power smoothing. Therefore, how $P_{batt,i}$ is defined depends on the ESD strategy. $P_{batt,i}$ for three different ESD strategies will be mathematically formulated in Chapter 4.

2.11 Specific Fuel Consumption

The specific fuel consumption is a measure of the amount of fuel that is consumed by an engine per unit of the power output, and it is given as g/kWh. In the literature, brake specific fuel consumption (BSFC), speficic fuel oil consumption (SFOC) and specific fuel consumption (SFC) are used to denote the fuel consumption, and in this thesis, they will all be denoted as SFC.

The total fuel consumption m_{fuel} of an engine is given by

$$m_{fuel} = \int_0^\tau P_{gen} \cdot SFC(P_{gen})dt, \qquad \text{g} \quad (2.24)$$

where $SFC(P_{gen})$ is the specific fuel consumption in g/kWh as a function of $P_{gen} = P_{gen}(t)$, which is the power generated in kW, as a function of time t, integrated over a time period from $t = 0$ to $t = \tau$.

2.11.1 SFC Curves

Four curves for the specific fuel consumption are shown in Figure 2.16, where the trend from the SFC curves is that the lowest fuel consumption is between medium high and high engine loads that not approach the maximum capacity. Typically, the gensets are most efficient in the range between 60% and 80% of the maximum capacity of the engine (Zadeh, 2019), which fits well with the SFC curves in Figure 2.16.

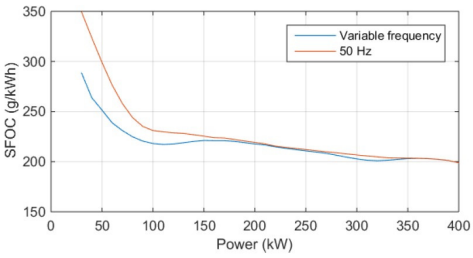

(a) SFC curve as a function of power. Courtesy: Sørensen et al. (2017).

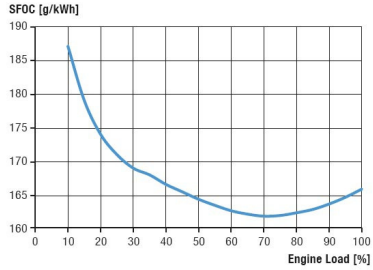

(b) SFC curve as a function of engine load. Courtesy: V. Shipping (2017).

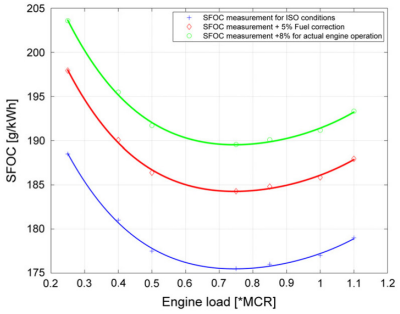

(c) SFC curve as a function of engine load. Courtesy: Dedes et al. (2012).

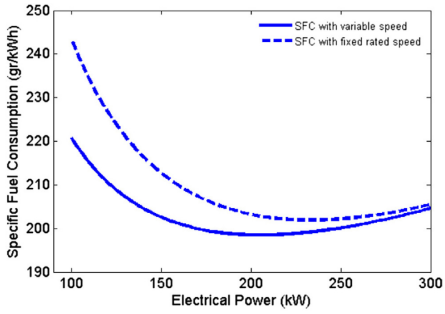

(d) SFC curve as a function of power. Courtesy: Zahedi et al. (2014).

Figure 2.16: Typical specific fuel consumption (SFC) curves.

An SFC curve can also be projected with both engine speed and power, as has been done at the Hybrid Power Systems Laboratory at Department of Marine Technology at NTNU in Trondheim (Miyazaki et al., 2016a). This is shown in Figure 2.17.

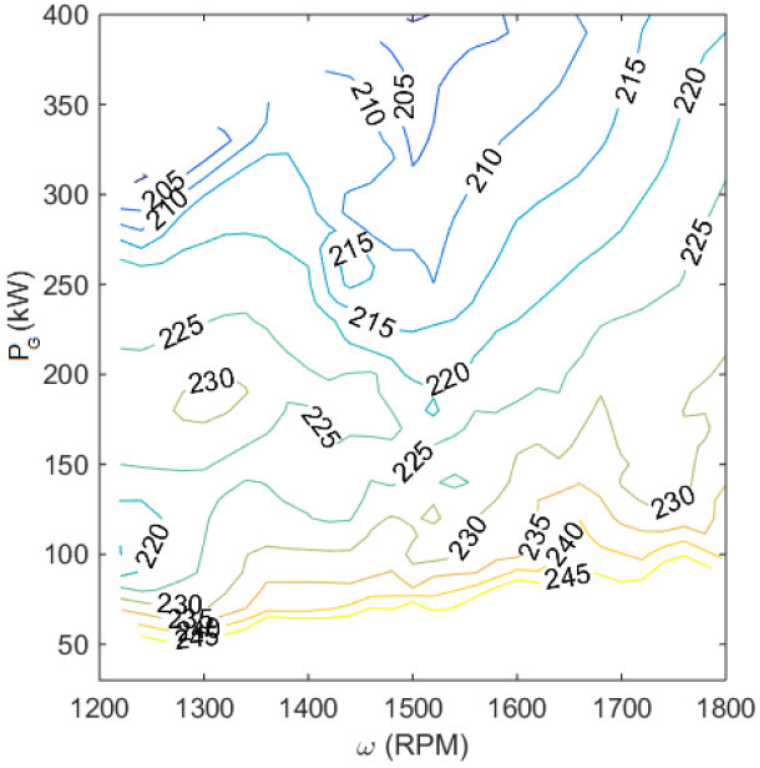

Figure 2.17: SFC curve as a function of engine speed and power, from NTNU Hybrid Lab. Courtesy: Miyazaki et al. (2016a).

Chapter 3

Problem Formulation

The problem formulation of this thesis can be stated by the following research question: "*What battery strategy is the most efficient on a hybrid electric ship, according to the SPM?*".

The SPM and the battery strategies have already been presented in Chapter 2 (see Sections 2.3 and 2.10 for the SPM and Section 2.7.5 for the battery strategies), and the battery strategies that will be used in this thesis are peak-shaving, power smoothing and strategic loading, which will be formulated in detail in the next chapter.

In other words, this thesis is trying to solve the research question using the SPM as model for the hybrid electric power system, where the SPM has to be developed for battery usage. The operation of the hybrid electric power system will be optimized using MPC and SPM as model, and the battery strategies are compared to each other and to a strategy without battery storage. The performance of each case will be compared using fuel consumption as a comparison, where a fuel consumption model has to be developed. In addition, genset frequency, genset power flow, load setpoint for the gensets, battery power and battery SoC will be compared between the strategies.

The work description also specifies that the resulting performances should be compared to other methods, if available. Such a method will be disconnecting gensets in order to save fuel, so-called genset disconnection, which will be explained more in detail in the next chapter.

Chapter 4

Method

This chapter will explain the method and setup of the SPM as a model for hybrid electric power systems, and it will show how the verification model Simscape is constructed. Then, the optimization problems for different battery strategies will be formulated, using MPC and SPM as model, as specified in the work description, and the method for another strategy, genset disconnection, will be presented.

4.1 Power System Configuration

The hybrid electric power system used in this thesis has four gensets and four loads, with two batteries, one on each bus, which is a realistic setup (see Section 2.5 and Figure 2.6, for instance). The configuration is shown in Figure 4.1, where $n_1, ..., n_8$ are nodes, $l_1, ..., l_7$ are lines, $P_1, ..., P_4$ are loads, $G_1, ..., G_4$ are gensets, B_1 and B_2 are batteries, b_1 is a binary variable denoting the power flow through the bus-tie breaker, and $y_1, ..., y_4$ are binary variables representing the power flow from the gensets. $P_{batt,1}$ and $P_{batt,2}$ are battery power from battery 1 to n_1 and n_2, and $P_{batt,3}$ and $P_{batt,4}$ from battery 2 to n_3 and n_4. The battery powers are bidirectional, as the battery is used for both charging and discharging (intuitively, an arrow entering the battery means charging, and an arrow leaving means discharging).

Note that the batteries are *not* modeled as separate nodes in the SPM, but they are rather seen as external loads. Therefore, they do not enter the incidence matrix for the SPM, but they instead ”manipulate” the loads P_i in the SPM equation, by adding or subtracting battery power to the bus. In Figure 4.1, l_1 and l_3 symbolize the buses, where each battery is connected, and l_2 is the bus-tie breaker.

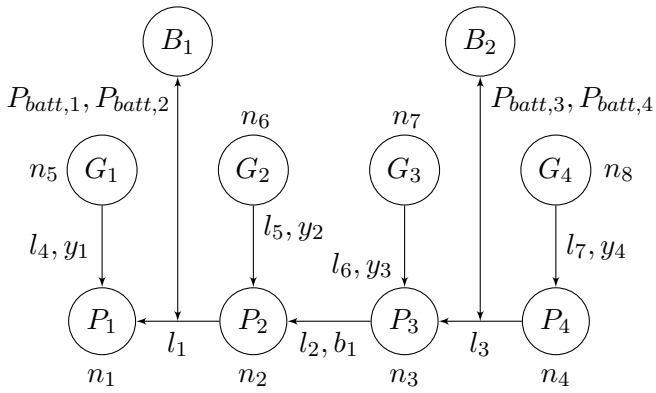

Figure 4.1: Configuration of the marine power plant used in thesis.

4.2 Battery SPM for the Hybrid Electric Power System

From the configuration in Figure 4.1, the incidence matrix $\boldsymbol{A}$ for the power system, with 8 nodes and 7 lines, as seen in the figure, is the (8×7) matrix defined as

$$\boldsymbol{A} = \begin{bmatrix} -1 & 0 & 0 & -1 & 0 & 0 & 0 \\ 1 & -b_1 & 0 & 0 & -y_2 & 0 & 0 \\ 0 & b_1 & -1 & 0 & 0 & -y_3 & 0 \\ 0 & 0 & 1 & 0 & 0 & 0 & -y_4 \\ 0 & 0 & 0 & y_1 & 0 & 0 & 0 \\ 0 & 0 & 0 & 0 & y_2 & 0 & 0 \\ 0 & 0 & 0 & 0 & 0 & y_3 & 0 \\ 0 & 0 & 0 & 0 & 0 & 0 & y_4 \end{bmatrix} \tag{4.1}$$

using the graph theory presented in Section 2.2 on the configuration in Figure 4.1 (remember that rows symbolize nodes, and columns represent the lines). In Equation (4.1), b_i is for the bus-tie and y_i is for the gensets, as illustrated in Figure 4.1. Both b_i and y_i are binary variables, either 0 or 1, with 0 meaning no power flow through the line, and 1 means power flowing. Therefore, $b_i = 0$ signifies open bus-tie breaker (no power through bus-tie), $b_i = 1$ is a closed bus-tie breaker (power flowing through bus-tie), $y_i = 0$ means that genset i is disconnected/turned off, and $y_i = 1$ when genset i is turned on/producing power.

Later on, some of the y_i values will be set to 0 for a limited amount of time, when genset disconnection is performed, but to begin with, all gensets are connected/turned on, meaning $y_1 = y_2 = y_3 = y_4 = 1$. Throughout this thesis, the bus-tie breaker will be assumed to be closed, i.e. power is flowing through the bus-tie, so $b_1 = 1$ can be assumed from now on.

Using the incidence matrix from Equation (4.1) with the binary variables b_1, y_1, y_2, y_3 and y_4 included, the corresponding Battery SPM, with two batteries, becomes

$$D_1\dot{\alpha}_1 = P_1 + P_{batt,1} - \frac{V_1V_2}{X_1}\sin(\alpha_1-\alpha_2) - y_1\frac{V_1V_5}{X_4}\sin(\alpha_1-\alpha_5), \quad \text{pu} \quad (4.2a)$$

$$D_2\dot{\alpha}_2 = P_2+P_{batt,2}-\frac{V_2V_1}{X_1}\sin(\alpha_2-\alpha_1)-y_2\frac{V_2V_6}{X_5}\sin(\alpha_2-\alpha_6)-b_1\frac{V_2V_3}{X_2}\sin(\alpha_2-\alpha_3), \quad \text{pu} \quad (4.2b)$$

$$D_3\dot{\alpha}_3 = P_3+P_{batt,3}-b_1\frac{V_3V_2}{X_2}\sin(\alpha_3-\alpha_2)-y_3\frac{V_3V_7}{X_6}\sin(\alpha_3-\alpha_7)-\frac{V_3V_4}{X_3}\sin(\alpha_3-\alpha_4), \quad \text{pu} \quad (4.2c)$$

$$D_4\dot{\alpha}_4 = P_4 + P_{batt,4} - \frac{V_4V_3}{X_3}\sin(\alpha_4-\alpha_3) - y_4\frac{V_4V_8}{X_7}\sin(\alpha_4-\alpha_8), \quad \text{pu} \quad (4.2d)$$

$$\dot{\alpha}_5 = (\omega_1 - \frac{M_1\omega_1+M_2\omega_2+M_3\omega_3+M_4\omega_4}{M_1+M_2+M_3+M_4})\omega^B, \quad \text{rad/s} \quad (4.2e)$$

$$\dot{\alpha}_6 = (\omega_2 - \frac{M_1\omega_1+M_2\omega_2+M_3\omega_3+M_4\omega_4}{M_1+M_2+M_3+M_4})\omega^B, \quad \text{rad/s} \quad (4.2f)$$

$$\dot{\alpha}_7 = (\omega_3 - \frac{M_1\omega_1+M_2\omega_2+M_3\omega_3+M_4\omega_4}{M_1+M_2+M_3+M_4})\omega^B, \quad \text{rad/s} \quad (4.2g)$$

$$\dot{\alpha}_8 = (\omega_4 - \frac{M_1\omega_1+M_2\omega_2+M_3\omega_3+M_4\omega_4}{M_1+M_2+M_3+M_4})\omega^B, \quad \text{rad/s} \quad (4.2h)$$

$$M_1\dot{\omega}_1 = \tau_1 - y_1\frac{S^R}{S_1}\frac{1}{\omega_1}\frac{V_5V_1}{X_4}\sin(\alpha_5-\alpha_1), \quad \text{pu} \quad (4.2i)$$

$$M_2\dot{\omega}_2 = \tau_2 - y_2\frac{S^R}{S_2}\frac{1}{\omega_2}\frac{V_6V_2}{X_5}\sin(\alpha_6-\alpha_2), \quad \text{pu} \quad (4.2j)$$

$$M_3\dot{\omega}_3 = \tau_3 - y_3\frac{S^R}{S_3}\frac{1}{\omega_3}\frac{V_7V_3}{X_6}\sin(\alpha_7-\alpha_3), \quad \text{pu} \quad (4.2k)$$

$$M_4\dot{\omega}_4 = \tau_4 - y_4\frac{S^R}{S_4}\frac{1}{\omega_4}\frac{V_8V_4}{X_7}\sin(\alpha_8-\alpha_4), \quad \text{pu} \quad (4.2l)$$

$$\dot{z}_i = k_{z,i}\cdot P_{batt,i} \quad (4.2m)$$

with the variables defined as in Equations (2.13) and (2.23). As before, some of these equations are valid for the load nodes, while others are valid for the genset nodes. Here, Equation (4.2a) to Equation (4.2d) apply for the load nodes, while Equation (4.2e) to Equation (4.2l) apply for the genset nodes, and Equation (4.2m) is for the battery.

4.3 Modeling and Simulation of the Hybrid Electric Power System

Simscape (MATLAB, 2019) was used to simulate the hybrid electric power system, which also has been done by Dahl et al. (2018). The entire power system can be found in Appendix B, and each component will be explained briefly here.

4.3.1 Diesel Genset

The diesel genset is taken from the Simscape toolbox, and shown in Figure 4.2. It will not be discussed in detail here, but more information can be found on MathWorks (2020). The input to the genset is u, which is the load setpoint to the genset, and the output is the genset frequency ω in radians, multiplied with four, since each generator in the model has four poles.

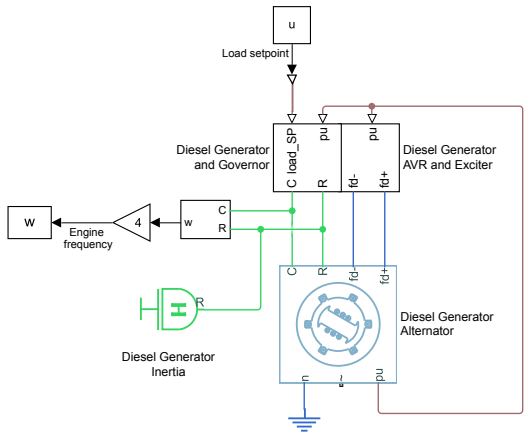

Figure 4.2: Genset model.

4.3.2 Load Profile

The load input is shown in Figure 4.3, where the user can choose between two load profiles using a switch; either a realistic or a deterministic load profile, as specified in the work description. The data from the two load profiles are stored in the load profile blocks.

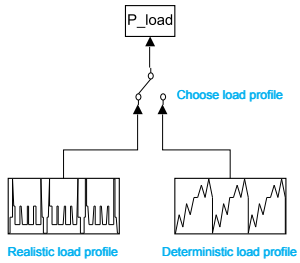

Figure 4.3: Load profile.

4.3.3 Battery Model

The battery model is built with help from Namireddy Praveen Reddy, who has written the articles Reddy et al. (2019a) and Reddy et al. (2019b), among others. The model is shown in Figure 4.4, and it implements the SoC equations from Equations (2.20) and (2.21), with battery efficiencies included.

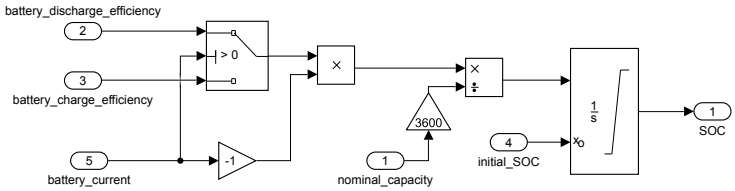

Figure 4.4: Battery model.

4.3.4 Converter and Transformer Model

Since the SPM is an AC model, and the battery is DC, converters and transformers are needed. The model for the converter and transformer takes efficiencies into account, shown in Figure 4.5, where the model implements Equation (2.19), with converter and transformer efficiencies included.

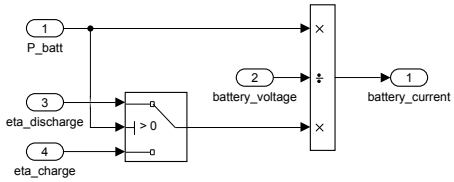

Figure 4.5: Converter and transformer model.

4.3.5 Fuel Consumption Model

The fuel consumption is calculated according to Equation (2.24). The SFC curve is made using the SFC curves from Section 2.11.1, along with curve-fitting to make them polynomial. The fuel consumption model is shown in Figure 4.6, where the fuel consumption is divided by 1000 to convert it to kg.

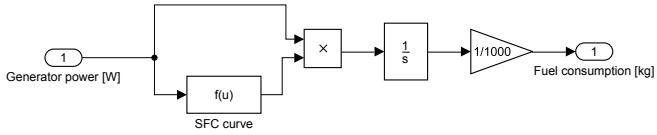

Figure 4.6: Fuel consumption model.

4.4 Optimization Strategies

There will be conducted three different optimization strategies on the hybrid electric power system, which will be using the battery for **peak-shaving**, **power smoothing** and **strategic loading**, explained in Section 2.7.5. In addition to this, and as specified in the work description, a case ***without*** **battery** will be used as a comparison. The SPM is solved solved using SQP, sequential quadratic programming, see Nocedal and Wright (2006) for more information.

The cases will be presented in the following order:

- **No battery usage**
- **Peak-shaving**
- **Power smoothing**
- **Strategic loading**

4.4.1 Cost Function

The cost function J, which should be minimized, is based on Dahl et al. (2018), and it is used in all the cases, to make comparison between the cases easier. J is formulated as

$$\begin{aligned} J = &\sum_{j=1}^{N} (\boldsymbol{x}_j - \boldsymbol{x}_{ref})^\top \boldsymbol{Q} (\boldsymbol{x}_j - \boldsymbol{x}_{ref}) \\ &+ \sum_{j=1}^{N} (\boldsymbol{u}_j - \boldsymbol{u}_{j-1})^\top \boldsymbol{R} (\boldsymbol{u}_j - \boldsymbol{u}_{j-1}) \\ &+ \sum_{j=1}^{N} (\boldsymbol{u}_j - \boldsymbol{u}_{ref})^\top \boldsymbol{S} (\boldsymbol{u}_j - \boldsymbol{u}_{ref}) \end{aligned} \tag{4.3}$$

where $\boldsymbol{x}_j = [\alpha_{j,1}, ..., \alpha_{j,n}, \omega_{j,1}, ..., \omega_{j,m}]^\top$, for n nodes and m gensets, is the state vector in the SPM at time step j, $\boldsymbol{x}_{ref} = [0, ..., 0, \omega_{ref,1}, ..., \omega_{ref,m}]^\top$ contains the reference frequency of the gensets, $\boldsymbol{u}_j = [u_{j,1}, ..., u_{j,m}]^\top$ is the control input, which is the load setpoint to the gensets, and $\boldsymbol{u}_{ref} = [u_{ref,1}, ..., u_{ref,m}]^\top$ contains the desired load setpoints of the gensets. In the summation signs, N denotes the time horizon in the MPC.

For the configuration in this thesis, with eight nodes in total (where four of them are loads and four are gensets), the vectors in Equation (4.3) become:

$$\boldsymbol{x}_j = [\alpha_{j,1}, \alpha_{j,2}, \alpha_{j,3}, \alpha_{j,4}, \alpha_{j,5}, \alpha_{j,6}, \alpha_{j,7}, \alpha_{j,8}, \omega_{j,1}, \omega_{j,2}, \omega_{j,3}, \omega_{j,4}]^\top,$$

$$\boldsymbol{x}_{ref} = [0, 0, 0, 0, 0, 0, 0, 0, \omega_{ref}, \omega_{ref}, \omega_{ref}, \omega_{ref}]^\top,$$

$$\boldsymbol{u}_j = [u_{j,1}, u_{j,2}, u_{j,3}, u_{j,4}]^\top, \text{and}$$

$$\boldsymbol{u}_{ref} = [u_{ref}, u_{ref}, u_{ref}, u_{ref}]^\top.$$

$\boldsymbol{Q}$, $\boldsymbol{R}$ and $\boldsymbol{S}$ in Equation (4.3) are weight matrices, which are tuned depending on what kind of control is wanted. The first term in J penalizes deviation from the engine frequency, the second term penalizes setpoint changes in the gensets, and the third term penalizes deviation from a desired load setpoint. Higher values in the weight matrices mean a bigger penalty on the corresponding state. For instance will high values in the $\boldsymbol{Q}$ matrix give less deviation from the reference frequency, high values in the $\boldsymbol{R}$ matrix give less changes in the setpoint, and high values in $\boldsymbol{S}$ will give less deviation from the desired setpoint.

4.4.2 No Battery Usage

This section presents the method for a power system without a battery.

Logic for No Battery Usage

When there is no battery in the power system, $P_{batt} = 0$ in Equation (2.16). Therefore, the genset load P_{gen} is equal to P_{load}, as shown in Figure 4.7.

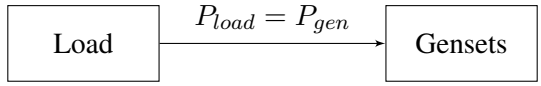

Figure 4.7: Block diagram of no battery usage.

Formulation for No Battery Usage

For the case without battery storage, the goal of the MPC optimization problem is to optimize the load setpoints u_i to the gensets, for a given load. The optimization problem is solved at every control step, and the formulation is

$$\begin{aligned} &\min_{\boldsymbol{u}_1,...,\boldsymbol{u}_N} J(\boldsymbol{x}_0, \boldsymbol{u}_0, \boldsymbol{P}_0, ..., \boldsymbol{P}_N, \boldsymbol{u}_1, ..., \boldsymbol{u}_N) \\ &\text{subject to Battery SMP from Equation (4.2)} \\ &\qquad 0.2y_i \leq u_{j,i} \leq y_i, \\ &\qquad y_i \in \{0, 1\} \\ &\qquad (\sum_{i=1}^{m} u_i \cdot y_i \cdot P_{gen,i})_j \geq P_{load,j} \\ &\qquad j = 1, ..., N \text{ time steps} \\ &\qquad i = 1, ..., m \text{ gensets} \end{aligned} \tag{4.4}$$

where there is no battery power in the Battery SPM from Equation (4.2), i.e. $P_{batt,i} = 0$, for node i.

From Equation (4.4), $J(.)$ is the cost function from Equation (4.3), that is minimized by the control input $\boldsymbol{u}_j = [u_{j,1}, ..., u_{j,m}]^\top$ at the time steps $j = 1, ..., N$ and for gensets $1, ..., m$, where N is the time horizon for the MPC. Furthermore, $\boldsymbol{x}_0 = [\alpha_{0,1}, ..., \alpha_{0,n}, \omega_{0,1}, ..., \omega_{0,m}]^\top$, for n nodes and m gensets, $\boldsymbol{u}_0 = [u_{0,1}, ..., u_{0,m}]^\top$ and $\boldsymbol{P}_0 = [P_{0,1}, ..., P_{0,m}]^\top$ are the initial state, control and load vectors, and $\boldsymbol{P}_j = [P_{j,1}, ..., P_{j,m}]^\top$ is the expected load at time step $j = 1, ..., N$. As earlier, y_i is a binary variable, introduced to ensure that gensets that are *disconnected*/turned

off will have a setpoint of 0, and that the setpoint of a *connected* genset lies between 0.2 and 1. $P_{gen,i}$ is the rated power of genset i, and P_{load} is the total load from the load profile. The constraint where $P_{gen,i}$ and P_{load} appear, ensures that there always will be enough delivered power from the gensets for a given load condition.

As Dahl et al. (2018) explain, the node angles α_i are not directly measurable, and the node angles in the initial state vector $\boldsymbol{x}_0$ have to be estimated. Therefore, an estimate $\hat{\boldsymbol{x}}_0 = [\hat{\alpha}_{0,1}, ..., \hat{\alpha}_{0,n}, \omega_{0,1}, ..., \omega_{0,m}]^\top$ will be used, where $\hat{\alpha}_{0,i}$ are estimated angles. A solution is obtained by using relative angles, by setting the last node angle to zero, i.e. setting $\hat{\alpha}_{0,n} = 0$ as a reference, and solving the remaining angles from line power measurements.

Furthermore, Dahl et al. (2018) also assume that the load characteristics $\boldsymbol{P}_j$ at time steps $j = 1, ..., N$ are known ahead, since this is realistic for vessels where heavy electric consumers notify the control system ahead of large load changes.

The lower bound for $\boldsymbol{u}_j$ for a connected genset was originally set to 0 by Dahl et al. (2018), but it is in this thesis chosen to be 0.2. This is because there is a time limit for low-load operations, as operating on low loads over a longer period of time is unhealthy for the engine. In particular, it leads to a lower efficiency and increased hazardous emissions from the gensets (Thorat and Skjetne, 2018). As an example, both Wärtsilä (2018) and Hyundai Heavy Industries (2019) recommend not operating the engine below 20% load, and only do so for a maximum of 100 hours, hence u_{min} for a connected genset was chosen to be 0.2.

4.4.3 Peak-Shaving

As mentioned in Section 2.7.5, peak-shaving is using the ESD to smooth out power fluctuations, and it reduces oscillations. It is not the most efficient strategy to reduce the fuel consumption, but it can give less transient behavior and thus give less sooting, which is beneficial.

Peak-Shaving Logic

The peak-shaving strategy used in this thesis is rule-based, with a set lower and upper bound for peak-shaving, called P_{peak}^{min} and P_{peak}^{max}, as shown earlier in Figure 2.14a, where they are called *lower bound* and *upper bound*, respectively. The peak-shaving logic is shown in Figure 4.8 below, where the peak-shaved battery power P_{batt} is subtracted from the load and given to the gensets as

$$P_{gen} = P_{load} - P_{batt}, \tag{4.5}$$

which is consistent with Equation (2.16) and the theory in Chapter 2.

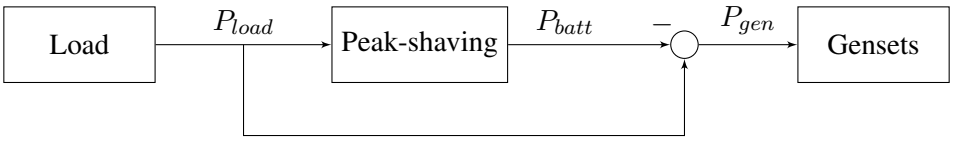

Figure 4.8: Block diagram of peak-shaving.

Peak-Shaving Formulation

For the peak-shaving, the MPC optimization problem also optimizes the load setpoints to the gensets, and it is formulated as

$$\begin{aligned}
&\min_{\boldsymbol{u}_1,...,\boldsymbol{u}_N} J(\boldsymbol{x}_0, \boldsymbol{u}_0, \boldsymbol{P}_0, ..., \boldsymbol{P}_N, \boldsymbol{u}_1, ..., \boldsymbol{u}_N) \\
&\text{subject to Battery SMP from Equation (4.2)} \\
&\qquad 0.2y_i \leq u_{j,i} \leq y_i, \\
&\qquad y_i \in \{0, 1\} \\
&\qquad (\sum_{i=1}^{m} u_i \cdot y_i \cdot P_{gen,i})_j \geq P_{load,j} \\
&\qquad j = 1, ..., N \text{ time steps} \\
&\qquad i = 1, ..., m \text{ gensets}
\end{aligned} \tag{4.6}$$

where the variables in Equation (4.6) are defined in Equation (4.4). The peak-shaving battery power $P_{batt,i}$ from the Battery SPM in Equation (4.2) is formulated as, for node i,

$$P_{batt,i} = \begin{cases} -\frac{P_{gen,i}}{P_{gen,tot}} u_{batt}, & \text{if } z^{min} \leq z \leq z^{max} \\ 0, & \text{otherwise} \end{cases} \tag{4.7}$$

where $P_{gen,i}$ is the rated power of genset i, $P_{gen,tot}$ is the total rated power of all gensets, with $\frac{P_{gen,i}}{P_{gen,tot}}$ representing a scaling factor to each node, in case the gensets have different size, and z is the SoC of the battery, bounded between z^{min} and z^{max}. The battery sizes are assumed to be equal, so the SoC values will be the same for all the batteries, therefore using z and not z_i as notation for the SoC. The reason why the negative sign is included in Equation (4.7), is to ensure that $P_{batt,i}$ is positive for charging and negative for discharging, as it is defined in the Battery SPM. The variable u_{batt} is the total peak-shaved battery power given as

$$u_{batt} = \begin{cases} P_{load} - P_{peak}^{max}, & \text{if } P_{load} > P_{peak}^{max} \\ 0, & \text{if } P_{peak}^{min} \leq P_{load} \leq P_{peak}^{max} \\ P_{load} - P_{peak}^{min}, & \text{if } P_{load} < P_{peak}^{min} \end{cases} \tag{4.8}$$

where P_{peak}^{min} and P_{peak}^{max} are defined as the peak-shaving limits in the EEMS, and P_{load} is the total load from the load profile. As mentioned, u_{batt} is scaled to the corresponding genset in Equation (4.7).

From Equations (4.7) and (4.8), it is easy to recognize the peak-shaving logic, which uses the battery for charging above a set higher limit, and discharging for a set lower limit, as long as the battery is within specified SoC limits.

4.4.4 Power Smoothing

The power smoothing strategy has earlier been illustrated in Figure 2.14b. In this thesis, it is optimization-based, and uses MPC, inspired of the method used in Bø (2016). Temperature in the battery is ignored, as done by Miyazaki (2017). A filter is used to give a reference to the battery, and the difference between the original value and the filtered value will be the value that the ESD should supply or absorb. This method is also similar to the one used in Yao et al. (2014), which performed optimization of peak-shaving with filtering for hybrid electric vehicles.

Power Smoothing Logic

The power smoothing algorithm is shown below in Figure 4.9.

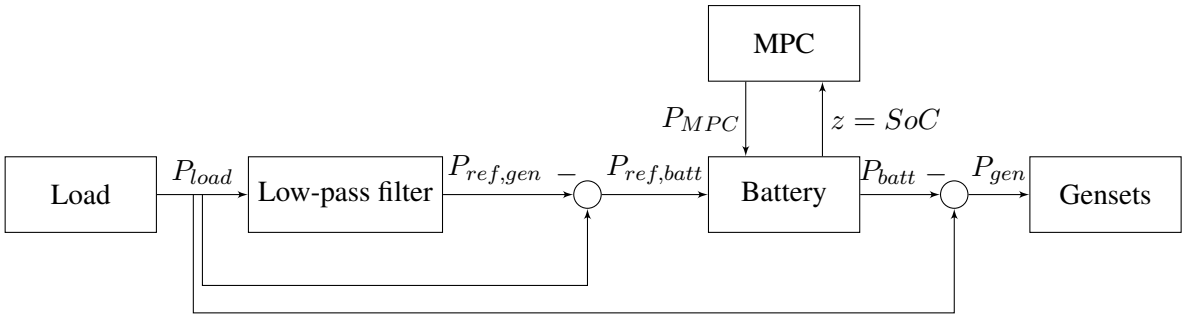

Figure 4.9: Block diagram of power smoothing.

The low-pass filter takes the load, P_{load}, as input, while the output from the filter is $P_{ref,gen}$, which is the smoothed out load reference to the gensets. The transfer function for the low-pass filter, $H_{low}(s)$, is defined as

$$H_{low}(s) = \frac{P_{ref,gen}(s)}{P_{load}(s)} = \frac{1}{1 + T_{low}s} \tag{4.9}$$

where T_{low} is the time constant of the low-pass filter.

As can be seen from Figure 4.9, the battery reference power $P_{ref,batt}$ is the difference between P_{load} and $P_{ref,gen}$. Further on, the MPC takes the SoC from the SPM as input, and gives out an optimal power from the MPC, called P_{MPC} (which Bø (2016) calls a mean charging power), where P_{MPC} is used to control the SoC of the battery. The battery power is controlled by the sum of the battery reference from the low-pass filter and the power from the MPC as

$$P_{batt} = P_{ref,batt} + P_{MPC} \tag{4.10}$$

As before, the battery power is subtracted from the genset load, similar to the definition in Equation (4.5).

Power Smoothing Formulation

For the power smoothing, the MPC optimization problem now optimizes on both the load setpoints to the gensets, u_i, as well as P_{MPC}, and it is formulated as

$$\begin{aligned}
\min_{\boldsymbol{u}_1, P_{MPC,1}, ..., \boldsymbol{u}_N, P_{MPC,N}} \quad & J(\boldsymbol{x}_0, \boldsymbol{u}_0, \boldsymbol{P}_0, ..., \boldsymbol{P}_N, \boldsymbol{u}_1, ..., \boldsymbol{u}_N) \\
\text{subject to Battery SMP from Equation (4.2)} \\
& 0.2 y_i \leq u_{j,i} \leq y_i, \\
& y_i \in \{0, 1\} \\
& (\sum_{i=1}^{m} u_i \cdot y_i \cdot P_{gen,i})_j \geq P_{load,j} \\
& P_{MPC}^{min} \leq P_{MPC,j} \leq P_{MPC}^{max} \\
& z^{min} \leq z_j \leq z^{max} \\
& j = 1, ..., N \text{ time steps} \\
& i = 1, ..., m \text{ gensets}
\end{aligned} \tag{4.11}$$

where the variables are defined in Equation (4.4), except that this formulation implements SoC control, and therefore includes P_{MPC} from the MPC and the SoC z (which is equal for the batteries, since they are assumed to have equal size), constrained between minimum and maximum values P_{MPC}^{min}, z^{min}, P_{MPC}^{max} and z^{max}. In addition, the state vector now also consists of z, the SoC, where $\boldsymbol{x}_0 = [\alpha_{0,1}, ..., \alpha_{0,n}, \omega_{0,1}, ..., \omega_{0,m}, z_0]^\top$, and therefore, the cost function J from Equation (4.3) now penalizes deviation from an SoC reference z_{ref}.

The power smoothing battery power $P_{batt,i}$ from the Battery SPM in Equation (4.2) is scaled, such that, for genset i,

$$P_{batt,i} = \frac{P_{gen,i}}{P_{gen,tot}} (P_{ref,batt} + P_{MPC}) \tag{4.12}$$

The constraints on the SoC, z^{min} and z^{max}, are used to avoid accelerated aging of the battery, which for lithium batteries occurs at low and high SoC, as Bø (2016) points it out.

4.4.5 Strategic Loading

Strategic loading is an efficient ESD strategy of reducing the fuel consumption, introduced in Section 2.7.5. The method was presented by Miyazaki et al. (2016b) and also used by Wu (2018) in her master thesis. Miyazaki (2017) has developed both a hybrid dynamical and a steady-state model for strategic loading, which yielded the same results for fixed-speed engines. This thesis uses the steady-state model, as the engines are AC, i.e. fixed-speed, which was also the one used by Wu (2018). For more information about hybrid dynamical systems, which are systems that contain both continuous and discrete dynamic behavior, see Goebel et al. (2012).

Derivation of the Strategic Loading Concept

The following derivation, from Miyazaki et al. (2016b), shows how the strategic loading works, and how the fuel consumption can be calculated by using the weighted average of the battery charging and discharging power, under certain assumptions.

First, it is assumed that the sum of the battery and generator power equal the load, according to Equation (2.16). Using the battery to either consume or provide power, it is possible to change the load applied to the gensets.

Assuming that the operation has a long duration, it is expected that the SoC of the battery does not change after many charge/discharge cycles, and it is required that

$$E_C = E_D \tag{4.13a}$$

where E_C and E_D are defined as

$$E_C = \int_0^{\tau_C} P_{batt,C}(t) \cdot \eta_C(t) dt \tag{4.13b}$$

$$E_D = \int_0^{\tau_D} \frac{P_{batt,D}(t)}{\eta_D(t)} dt \tag{4.13c}$$

with $P_{batt,C}(t)$ and $P_{batt,D}(t)$ being

$$P_{batt,C}(t) = P_{gen,C}(t) - P_{load}(t) \tag{4.13d}$$

$$P_{batt,D}(t) = P_{load}(t) - P_{gen,D}(t) \tag{4.13e}$$

E_C is the energy charged and stored by the battery, and E_D is the energy discharged by it. τ_C is the charging time, τ_D the discharging time, $P_{batt,C}$ and $P_{batt,D}$ are the battery charging and discharging power, and η_C and η_D are the charging and discharging efficiencies, which are values between 0 and 1. P_{load} is the load power demand, $P_{gen,C}$ is the power produced by the generator while the battery is charging, and $P_{gen,D}$ is the generator power during battery discharge. Note that the notation in Equation (4.13) is slightly different than the one used by Miyazaki et al. (2016b) (which for instance denote $P_{batt,C}$ and $P_{batt,D}$ as Δ_C and Δ_D). The notation was changed in order to make the notation consistent throughout the thesis.

Assuming that the variables $P_{gen,C}$, $P_{gen,D}$, P_{load}, $P_{batt,C}$ and $P_{batt,D}$ are constant during one charge/discharge cycle, Equation (4.13a) can, by inserting Equation (4.13b) and Equation (4.13c), be simplified as

$$P_{batt,C} \cdot \tau_C \cdot \eta_C = \frac{P_{batt,D} \cdot \tau_D}{\eta_D} \tag{4.14}$$

The average fuel consumption ($\overline{F}$) is given by

$$\overline{F} = \frac{\int_0^{\tau_C+\tau_D} P_{gen} \cdot SFC(P_{gen})dt}{\tau_C + \tau_D} \tag{4.15}$$

which can be divided into two parts as

$$\overline{F} = \frac{\int_0^{\tau_C} P_{gen,C} \cdot SFC(P_{gen,C})dt}{\tau_C + \tau_D} + \frac{\int_{\tau_C}^{\tau_C+\tau_D} P_{gen,D} \cdot SFC(P_{gen,D})dt}{\tau_C + \tau_D} \tag{4.16}$$

As previously, SFC denotes the instantaneous specific fuel consumption, as a function of the genset power.

If it is assumed that $P_{gen,C}$ and $P_{gen,D}$ are constant during one charge/discharge cycle, and substituting Equation (4.13) into Equation (4.16), as well as using the fuel consumption FC instead of SFC, the result is

$$\overline{F} = \frac{FC(P_{gen,C}) \cdot P_{batt,D} + FC(P_{gen,D}) \cdot P_{batt,C} \cdot \eta_C \cdot \eta_D}{P_{batt,D} + P_{batt,C} \cdot \eta_C \cdot \eta_D} \tag{4.17}$$

Equation (4.17) shows that the final FC is calculated by the weighted average of the points $FC(P_{gen,C})$ and $FC(P_{gen,D})$, and that it is possible to look for optimal pairs of $P_{batt,C}$ and $P_{batt,D}$ that lead to an optimal average fuel consumption $\overline{F}$ under a certain load.

The optimization problem for strategic loading is formulated as

$$\begin{aligned} \min_{P_{batt,C}, P_{batt,D}} \quad & \overline{F} \\ \text{subject to } & 0 < P_{batt,C} \leq P_{batt,C}^{max} \\ & 0 < P_{batt,D} \leq P_{batt,D}^{max} \\ & P_{batt,C} = P_{gen,C} - P_{load} \\ & P_{batt,D} = P_{load} - P_{gen,D} \end{aligned} \tag{4.18}$$

with $P_{batt,C}^{max}$ and $P_{batt,D}^{max}$ being the maximum charge and discharge power of the battery.

As Miyazaki (2017) points out, strategic loading is most efficient at lower loads, because of the shape of the typical FC curve. A typical FC curve is shown in Figure 4.10, where the curvature is concave for lower loads (approximately below 50% of maximum load). This allows for fuel savings when using the battery, since the optimal fuel consumption (marked as a red F) is lower than without a battery (in the figure, P_1 and P_2 correspond to $P_{gen,D}$ and $P_{gen,C}$, respectively, and P_L corresponds to P_{load}. Also, the left Δ is $P_{batt,D}$, and the right Δ is $P_{batt,C}$).

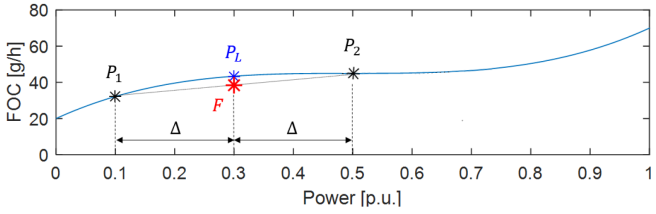

Figure 4.10: Geometrical representation of strategic loading. Courtesy: Miyazaki (2017).

The optimal pairs $P_{batt,C}$ and $P_{batt,D}$ were found using `fmincon` in MATLAB and the interior-point method, and the result was validated with a linear interpolation model, as done in Miyazaki (2017), that ensured that the optimization found the optimal point, and not a local solution.

Strategic Loading Logic

The strategic loading used in this thesis is shown in Figure 4.11.

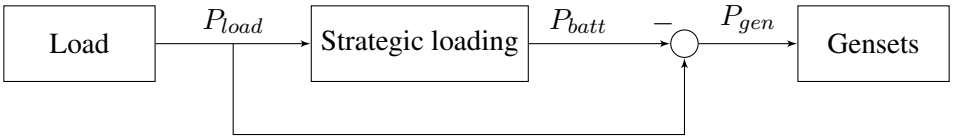

Figure 4.11: Block diagram of strategic loading.

Strategic Loading Formulation

For the strategic loading, the MPC optimization problem is formulated as

$$\begin{aligned}
&\min_{\boldsymbol{u}_1,...,\boldsymbol{u}_N} J(\boldsymbol{x}_0, \boldsymbol{u}_0, \boldsymbol{P}_0, ..., \boldsymbol{P}_N, \boldsymbol{u}_1, ..., \boldsymbol{u}_N) \\
&\text{subject to Battery SMP from Equation (4.2)} \\
&\qquad 0.2y_i \leq u_{j,i} \leq y_i, \\
&\qquad y_i \in \{0, 1\} \\
&\qquad (\sum_{i=1}^{m} u_i \cdot y_i \cdot P_{gen,i})_j \geq P_{load,j} \\
&\qquad \text{Strategic loading from Equation (4.18)} \\
&\qquad j = 1, ..., N \text{ time steps} \\
&\qquad i = 1, ..., m \text{ gensets}
\end{aligned} \tag{4.19}$$

where the variables are defined in Equation (4.4), and strategic loading is put in as a constraint. The battery power $P_{batt,i}$ from the Battery SPM in Equation (4.2) is calculated from the strategic loading in Equation (4.18), which, for genset i, is formulated as

$$P_{batt,i} = \begin{cases} \frac{P_{gen,i}}{P_{gen,tot}} \cdot P_{batt,C}, & \text{if } \textbf{mode} = \text{"charge"} \\ -\frac{P_{gen,i}}{P_{gen,tot}} \cdot P_{batt,D}, & \text{if } \textbf{mode} = \text{"discharge"} \end{cases} \tag{4.20}$$

where the introduced variable **mode** denotes charging or discharging of the battery (also done by Skjong et al. (2017)), since the strategic loading performs cyclic charge and discharge. The variable is defined by

$$\textbf{mode} = \begin{cases} \text{"charge"}, & \text{if } z \leq z^{min} \\ \text{"discharge"}, & \text{if } z \geq z^{max} \end{cases} \tag{4.21}$$

It can be seen clearly from Equation (4.21) that the battery starts charging if it reaches the minimum SoC (z^{min}), and it is charged until the maximum SoC (z^{max}) is reached, before it starts discharging the battery until z^{min} is reached, and the

battery starts charging again. These charge/discharge cycles go on and on in the strategic loading algorithm. As before, note that the battery discharge power in Equation (4.20) is negative, and the battery charge power is positive, as $P_{batt,i}$ is positive for charging and negative for discharging in the Battery SPM.

4.5 Genset Disconnection

Genset disconnection, or genset scheduling, means disconnection of some of the engines depending on the load, and it is efficient for saving fuel and emissions, as demonstrated by Miyazaki (2017), for instance. Genset disconnection has also been performed by Wu (2018), Skjong et al. (2017), Thorat and Skjetne (2018) and Hovland (2019) (which calls the genset scheduling for unit commitment). Thorat and Skjetne (2018) perform the genset scheduling using MILP optimization, and they implement redundancy in the algorithm. In this thesis however, the vessel is assumed to always have two gensets connected when the vessel is in DP operation, as a redundancy requirement. This is also done by Wu (2018), that states that during DP operation, it is not possible to deliver load using only a single genset.

The genset disconnection algorithm in this thesis is inspired by the *rule-based logic algorithm* from Skjong et al. (2017). The algorithm in the article turns off gensets depending on the load, so that the gensets that are on can operate at 80% load, which is assumed to be the most efficient for the fuel consumption.

The rule-based algorithm for genset disconnection, similar to the one from Skjong et al. (2017), is in this thesis formulated as:

$$
\begin{aligned}
&\textbf{if } P_{load} < 0.8 \cdot P_{gen,1} \\
&\qquad y_1 = 1, \\
&\qquad y_2 = y_3 = y_4 = 0 \\
&\textbf{else if } P_{load} < 0.8 \cdot (P_{gen,1} + P_{gen,2}) \\
&\qquad y_1 = y_2 = 1, \\
&\qquad y_3 = y_4 = 0 \\
&\textbf{else if } P_{load} < 0.8 \cdot (P_{gen,1} + P_{gen,2} + P_{gen,3}) \\
&\qquad y_1 = y_2 = y_3 = 1, \\
&\qquad y_4 = 0 \\
&\textbf{else} \\
&\qquad y_1 = y_2 = y_3 = y_4 = 1 \\
&\textbf{end}
\end{aligned}
\tag{4.22}
$$

with P_{load} as before, and where y_1, y_2, y_3 and y_4 are the binary variables from the incidence matrix in Equation (4.1), with 1 for a connected genset, and 0 for a disconnected genset, which decide the power flow in the Battery SPM from Equation (4.2). $P_{gen,1}$, $P_{gen,2}$ and $P_{gen,3}$ are the rated power of genset 1, 2 and 3, and the multiplication with 0.8 is made, as 80% of the maximum continuous rating (MCR), which is 80% of the maximum power output of the genset, is assumed to be the most fuel efficient for the gensets (as discussed from the SFC curves in Section 2.11).

From the algorithm in Equation (4.22), it can be seen that genset 1 is the only connected genset for loads below 80% of $P_{gen,1}$, that genset 1 and 2 are connected if they do not exceed 80% MCR, that genset 1, 2 and 3 are connected if the load is below the sum of their optimal loading, and that all gensets are connected if the load exceeds this limit. The reason why genset 1 is connected first, and genset 4 last, is because genset 1 has the smallest rated power, and genset 4 the largest one (as will be seen in the next chapter), and it is desirable to minimize the generator power (Skjong et al., 2017).

Later on, genset disconnection will be performed as a strategy to reduce the fuel consumption, and it can be combined with the battery strategies presented in this chapter. Note that if genset disconnection is *not* performed, all gensets are connected at all times, and intuitively, $y_1 = y_2 = y_3 = y_4 = 1$ throughout the entire simulation, not changing the incidence matrix in Equation (4.1).

Chapter 5

Results from Case Study

In this chapter, the results for the four cases in Section 4.4 (which were **without battery**, and with the battery performing **peak-shaving**, **power smoothing** and **strategic loading**), will be presented. As specified in the thesis definition, the cases will be tested for two different load profiles.

5.1 Model Configuration

The power system is the one from Figure 4.1, and it consists of four gensets, where the genset ratings are shown in Table 5.1. Note that in the table, $P_{gen,i}$ is the variable S_i in the SPM, and S^R in the SPM is equal to $P_{gen,tot}$.

Table 5.1: Rated power of the gensets.

Description	Parameter	Value	Unit
Genset 1	$P_{gen,1}$	4.9	[MW]
Genset 2	$P_{gen,2}$	5.0	[MW]
Genset 3	$P_{gen,3}$	5.1	[MW]
Genset 4	$P_{gen,4}$	5.2	[MW]
Total	$P_{gen,tot}$	20.2	[MW]

The total genset power, from Table 5.1, is 20.2 MW, which is consistent with a DP vessel, which has a typical power demand between 8-30 MW, as discussed in Section 2.6. All the gensets in Table 5.1 are chosen to be diesel gensets, but gas

turbines could also have been used. These are however not as common as diesel gensets, and gas turbines are suitable for higher power levels or in light high-speed vessels (Ådnanes, 2003). Gas turbines are also a bit slower than diesel gensets, as was studied in Dahl et al. (2018).

For the optimization of the power system, the parameters are shown in Table 5.2. As mentioned before, the voltage is assumed to be constant, set to 1 per unit (Dahl et al., 2018).

Table 5.2: Parameters for the optimization model.

Description	Parameter	Value	Unit
Rated frequency	f^R	60	[Hz]
Load damping	D_i	0.0001	[s/rad]
Rated voltage	V_i	1	[pu]
Line reactance	X_1	0.0188	[pu]
	X_2	0.0188	[pu]
	X_3	0.0188	[pu]
	X_4	4.1224	[pu]
	X_5	4.0400	[pu]
	X_6	3.9608	[pu]
	X_7	3.8846	[pu]
Mechanical starting time	M_i	7.05	[s]
Droop percentage	R	5	[%]
Frequency reference	ω_{ref}	1	[pu]
Load setpoint reference	u_{ref}	0.8	[pu]
MPC prediction horizon	N	4	steps
MPC step length	t_s	1	[s]

5.1.1 Peak-Shaving Model

The parameters used in the peak-shaving are shown in Table 5.3. When there are two values in the table, the first one refers to the value for the deterministic load profile, while the second one refers to the realistic one (i.e., P_{peak}^{min} is 0.1 for the deterministic load profile and 0.15 for the realistic profile).

Table 5.3: Parameters for peak-shaving.

Description	Parameter	Value	Unit
Minimum SoC	z^{min}	20	[%]
Maximum SoC	z^{max}	80	[%]
Lower peak limit	P_{peak}^{min}	0.1 / 0.15	[pu]
Upper peak limit	P_{peak}^{max}	0.8 / 0.75	[pu]
Weight matrices	$\boldsymbol{Q}$	diag(0,...,0,10,10,10,10)	[-]
	$\boldsymbol{R}$	diag(0.1,...,0.1)	[-]
	$\boldsymbol{S}$	diag(0.01,...,0.01)	[-]

5.1.2 Power Smoothing Model

Table 5.4 shows the parameters used in the power smoothing. Again, if there are two values in the table, the first one applies to the deterministic load profile and the second for the realistic one. Also, note that the weight matrix $\boldsymbol{Q}$ has a weight of 100 on the SoC state, which now is included in the state vector.

Table 5.4: Parameters for power smoothing.

Description	Parameter	Value	Unit
Minimum SoC	z^{min}	20	[%]
Maximum SoC	z^{max}	80	[%]
Reference SoC	z_{ref}	50	[%]
Lower MPC power	P_{MPC}^{min}	-2	[MW]
Upper MPC power	P_{MPC}^{max}	2	[MW]
Time constant, low-pass filter	T_{low}	20 / 250	[s]
Weight matrices	$\boldsymbol{Q}$	diag(0,...,0,10,10,10,10,100)	[-]
	$\boldsymbol{R}$	diag(0.1,...,0.1)	[-]
	$\boldsymbol{S}$	diag(0.01,...,0.01)	[-]

5.1.3 Strategic Loading Model

For strategic loading, the parameters used are found in Table 5.5. As before, when there are two values, the first is for the deterministic load profile, and the second is for the realistic profile.

Table 5.5: Parameters for strategic loading.

Description	Parameter	Value	Unit
Minimum SoC	z^{min}	40 / 30	[%]
Maximum SoC	z^{max}	60 / 70	[%]
Maximum battery charge	$P^{max}_{batt,C}$	2	[MW]
Maximum battery discharge	$P^{max}_{batt,D}$	2	[MW]
Weight matrices	$\boldsymbol{Q}$	diag(0,...,0,10,10,10,10)	[-]
	$\boldsymbol{R}$	diag(0.1,...,0.1)	[-]
	$\boldsymbol{S}$	diag(0.01,...,0.01)	[-]

5.1.4 Battery Model

The parameters that are chosen for the battery model are shown in Table 5.6. The initial SoC value from the table, z_0, is taken from the literature review in Section 2.9.1, the charging and discharging efficiencies for the battery, η_C and η_D, are taken from the literature presented in Section 2.9.2, and the values for the battery capacity and voltage, C and V_{batt}, are taken from Section 2.9.3 as well as from common voltage levels from Ådnanes (2003). In addition, the efficiencies for the transformer and converter are included in the battery model, as it is needed to change from DC of the battery to AC on the grid. Their values, η_{trans} and η_{conv}, are taken from the literature review in Section 2.9.4.

Table 5.6: Parameters for the battery model.

Description	Parameter	Value	Unit
Initial SoC	z_0	0.5	[-]
Charging efficiency	η_C	0.9	[-]
Discharging efficiency	η_D	0.9	[-]
Battery capacity	C	1400	[Ah]
Battery voltage	V_{batt}	690	[V]
Transformer efficiency	η_{trans}	0.99	[-]
Converter efficiency	η_{conv}	0.98	[-]
Maximum battery discharge	P^{max}_{batt}	2	[MW]
Maximum battery charge	P^{min}_{batt}	-2	[MW]

The battery charge and discharge power was taken from Skjong et al. (2017), as explained in Section 2.9.3, and scaled up to the generator power used in this thesis.

As mentioned, Skjong et al. (2017) used a battery power of ± 1 MW on gensets of 10 MW. With a total genset power of 20.2 MW in this thesis, the battery power was set to ± 2 MW.

5.2 Load Profiles

The two different load profiles are shown in Figure 5.1, with a simulation time of 1000 seconds for the deterministic load profile, and 24 hours for the realistic one. In this context, a *deterministic* load profile means a simplified load profile with a short simulation time, and a *realistic* load profile means a load profile with a long simulation time, that a real vessel can be assumed to operate in.

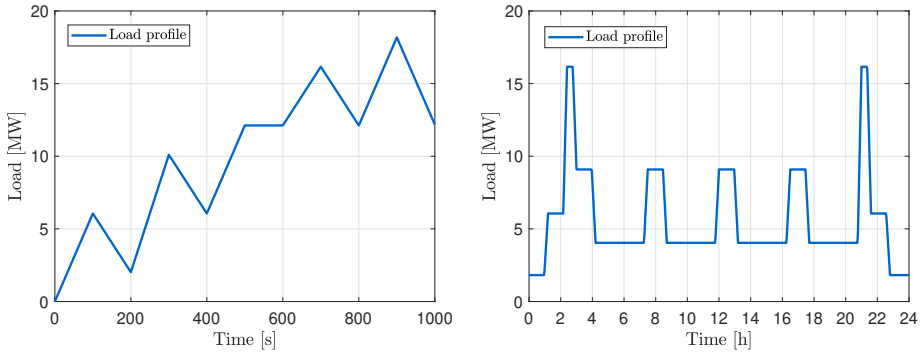

(a) Deterministic load profile.

(b) Realistic load profile.

Figure 5.1: Load profiles.

The deterministic load profile in Figure 5.1a is inspired by the load profile that Hovland (2019) used, and the realistic load profile from Figure 5.1b is similar to the one used by Wu (2018), where different operational profiles of offshore construction vessels were compared. For the realistic profile, it is assumed that the vessel has five different operating conditions, which are in port, transit low, transit high, DP low and DP high. When the vessel is in port, the main power consumer is low voltage hotel load and loading and offloading equipment (Wu, 2018), and the power demand is low. In transit, most of the power demand comes from the propulsion, and the vessel does not necessarily have long distances of transit from shore to offshore installation. In DP mode, the vessel is kept stable at a fixed point, using the vessel's propellers and thrusters. The power demand depends on the weather, since the DP is counteracting forces from wind, waves and current. Simonsen (2019) defines transit low as the vessel sailing between

port and offshore locations at fuel economic sailing, so-called slow steaming, at a significantly lower speed than the maximum speed. Transit high is performed only in special cases, where the vessel operates at higher speed, and therefore has a much higher power demand, with less duration. In DP low, the vessel is in stand-by and awaiting signal to approach the offshore installation, operating outside a 500 m safety zone, while in DP high, the vessel is within the safety zone and in DP operation (Simonsen, 2019). The operations discussed above, their duration and power demand are shown in Table 5.7, taken from Wu (2018). The values from the table were used to make the realistic load profile in Figure 5.1b.

Table 5.7: Realistic load profile. Courtesy: Wu (2018).

Operation	Duration [% of total duration]	Power demand [% of total MCR]
In port	10	9
Transit low	10	30
Transit high	5	80
DP low	55	20
DP high	20	45

The realistic load profile from Figure 5.1b assumes a constant load during each operation, even though load variations probably will occur. Wu (2018) also used the average load, and neglected load variations, since the strategic loading algorithm considers stationary conditions, and since the fuel consumption curves are obtained under static load.

5.3 Verification Study of the SPM

The SPM has to be verified as a frequency model, and it has to be shown that the SPM can be used to model a hybrid electric power system. This was part of the work in my project thesis, see Fiksdahl (2019) for more details. In the following, Simscape (MATLAB, 2019) will be used as a verification model for the SPM.

Figure 5.2 shows the average genset frequency from the SPM and Simscape for the *deterministic* load profile, for the cases presented in Section 4.4, that are without battery and with the battery performing peak-shaving, power smoothing and strategic loading.

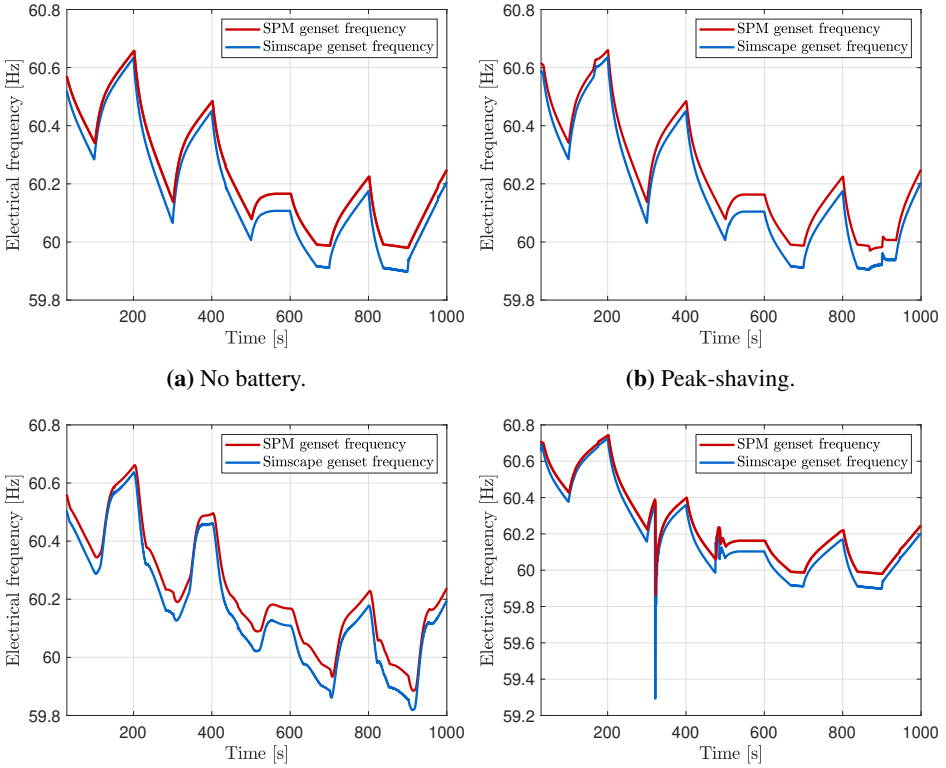

(a) No battery.

(b) Peak-shaving.

(c) Power smoothing.

(d) Strategic loading.

Figure 5.2: SPM and Simscape genset frequencies for the deterministic load profile. Note that Figure 5.2d has different scaling on the y-axis.

In Figure 5.2, it is seen that the SPM estimates frequencies that are slightly higher than the Simscape frequencies, but overall, the SPM frequencies calculate satisfactory frequencies, that are the close to the Simscape verification model. The SPM frequencies also fluctuate less than the Simscape, which for instance can be seen in Figure 5.2d (at around 300 seconds, when the strategic loading changes from discharge to charge mode on the battery), where the frequency drops much less in the SPM than in Simscape. This motivates using the SPM as a control design model, since it is not desired for a controller to act on all the disturbances, as this will increase the wear and tear of the controller.

Those were the verification results for the *first* load profile. Now, the *second* load profile is tested with the SPM, and again, Simscape is used as a verification model. Figure 5.3 shows the genset frequencies from the SPM and Simscape for the *realistic* load profile.

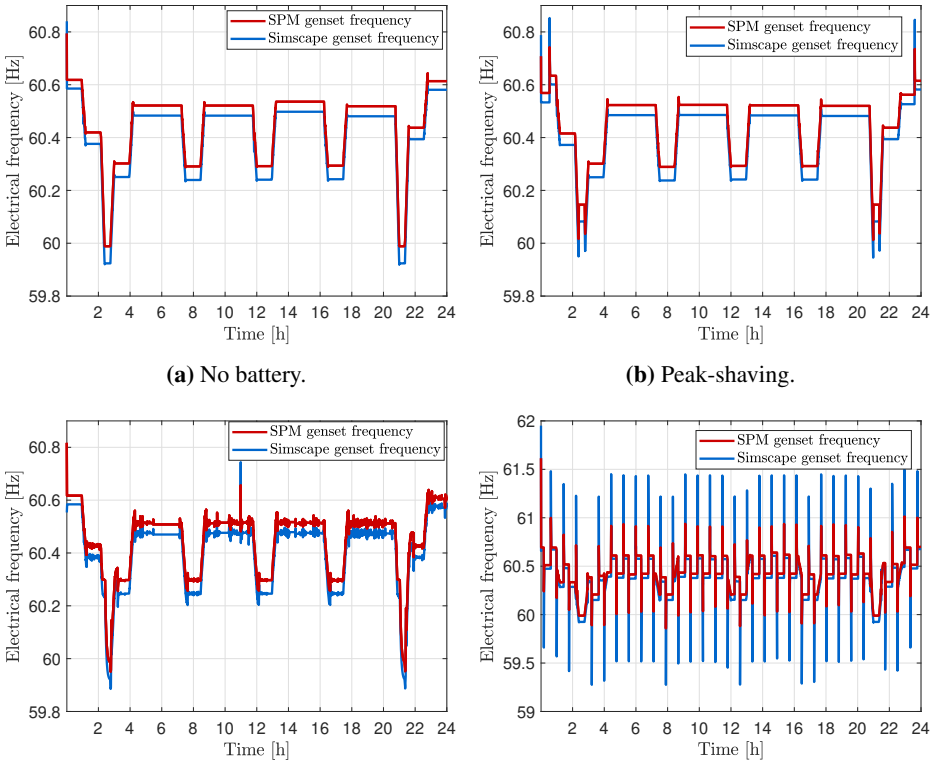

(a) No battery.

(b) Peak-shaving.

(c) Power smoothing.

(d) Strategic loading.

Figure 5.3: SPM and Simscape genset frequencies for the realistic load profile. Note that Figure 5.3d has different scaling on the y-axis.

As can be seen from Figure 5.3, the SPM again estimates slightly higher frequencies than Simscape, which also was the case for the deterministic load profile. There are more transient effects now in the realistic load profile, and again, the SPM does not capture all the fluctuations. This is seen in the spikes in Figure 5.3b and Figure 5.3c, and especially true for the strategic loading in Figure 5.3d, where the SPM frequency fluctuates much less than the Simscape frequency. In this plot, the transient effects happen when the charge/discharge mode in the strategic loading is switched (as the battery is cyclically charged and discharged), and the genset load and frequency therefore is changed depending on these cycles.

In order to make the SPM frequencies even closer to the Simscape frequencies, the SPM frequencies can be reduced by for instance multiplying with a constant factor (bigger than 1) in the load in the SPM equations (because a higher load gives lower frequency, with droop control).

Another way of reducing the SPM frequencies is by including an extra damping term in the SPM, for instance by taking losses like windage into account, which will lower the SPM frequency (by adding a term $D_{W,i}\omega_i$ on the left-hand side of the genset equations in the SPM, where $D_{W,i}$ is the windage loss for genset i, and ω_i is the genset frequency). None of these strategies were however performed, as the SPM is sufficiently close to the verification model Simscape.

The plots in Figures 5.2 and 5.3 will in the next sections be compared to each other, with the same axis scaling on the plots. The purpose of this section was to verify the SPM as a frequency model for AC power systems. As seen from Figures 5.2 and 5.3 and already discussed here and in Fiksdahl (2019), the SPM is considered a good frequency model. It is concluded that the SPM is well fit for optimization and control purposes on power systems, as the error between the SPM and the verification is small. Thus, the optimization, which will be presented in the next sections, uses the SPM as a model to optimize the operation of the hybrid electric power system.

5.4 Optimization for the Deterministic Load Profile

This section presents and analyzes the results from the MPC optimization on the hybrid electric power system, for the deterministic load profile from Figure 5.1a, and using SPM as model, where the Battery SPM from Equation (4.2) has been solved.

The optimization problems are explained in Chapter 4, where the MPC optimization problem for the power system without battery storage is formulated in Equation (4.4), the peak-shaving MPC is found in Equation (4.6), the power smoothing MPC in Equation (4.11) and the strategic loading MPC in Equation (4.19). All the strategies are optimizing on the load setpoints to the gensets, u_i, as stated in the MPC formulations.

The results for the deterministic load profile are shown in Figure 5.4.

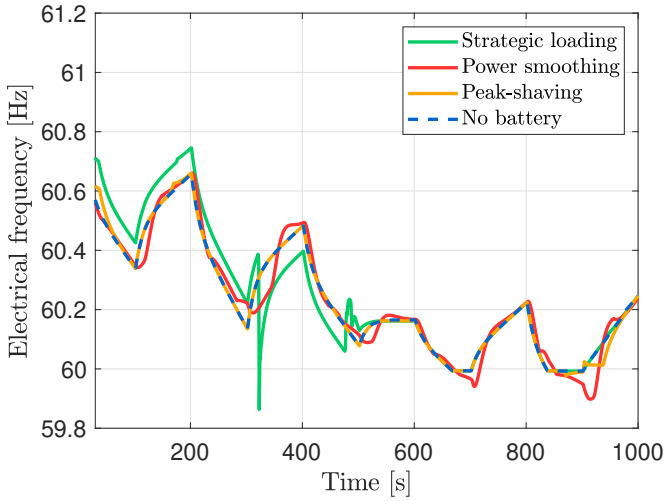

(a) Electrical frequency.

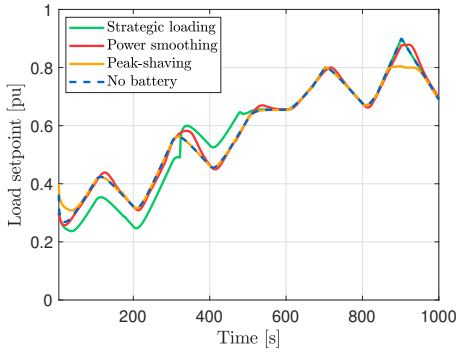

(b) Load setpoint.

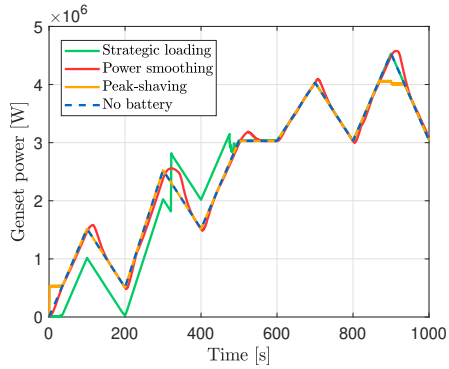

(c) Genset power.

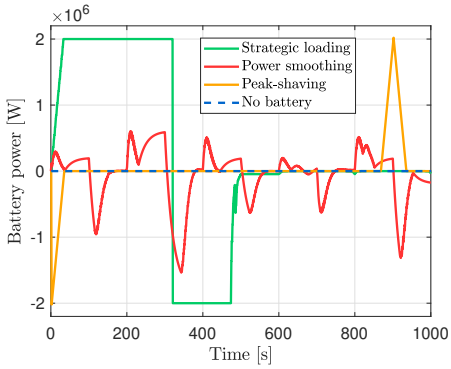

(d) Battery power.

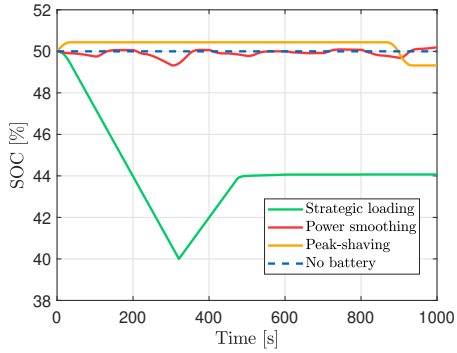

(e) Battery SoC.

Figure 5.4: Results for deterministic load profile.

Figure 5.4a shows the genset frequencies for the cases. The strategic loading frequency is a bit higher in the beginning and lower in the middle of the simulation compared to the no battery frequency. This is because the battery is first used for discharge (and gives a lower genset load, meaning higher frequency, due to droop control), before it starts charging (giving a higher genset load, thus a decrease in the frequency with droop control). The change between discharge and charge happens at around 300 seconds, and since the battery power is assumed to be delivered instantly, it leads to a fluctuation in the frequency, giving the frequency drop observed in the plot. After about 500 seconds, the strategic loading frequency stays the same as the no battery frequency, as the battery is not used, since the incoming load from the load profile is high, meaning that the gensets operate in a fuel efficient matter (discussed in Section 2.11.1), and there is no need to use the batteries to change the genset load. Further on, it can be seen that the power smoothing frequency is a bit smoother than the no battery frequency, since the battery is used to smooth out power fluctuations, and this is something that can be more economic for the gensets, since rapid load changes are avoided. The peak-shaving frequency differs from the no battery frequency in the beginning and in the end of the simulation, since peak-shaving is performed in the beginning, when the load from the load profile is low, and in the end, when the load is high.

In Figure 5.4b, the optimized load setpoints for the gensets are shown. The setpoints during strategic loading are lower than the no battery setpoints in the beginning, since the battery is discharged, and it therefore reduces the load to the gensets. Between 300-500 seconds, the setpoint is higher, as the battery is charged, thus increasing the genset load. After around 500 seconds, the strategic loading setpoints are the same as the no battery setpoints, since the battery power is close to zero. The power smoothing setpoints are again smoother than the no battery setpoints, as the battery smooths out the genset load. Also, the peak-shaving setpoints differ from the no battery setpoints in the beginning and end of the simulation, which is when peak-shaving is performed. The low load in the beginning is peak-shaved, and the battery is discharged, giving a higher load setpoint to the gensets, and the peak at around 900 seconds is used for charging of the battery, giving a lower load setpoint.

The genset power flow is shown in Figure 5.4c, where it is visible that the strategic loading uses the battery to change the genset power, first discharging the battery and then charging it, as well as not using the battery for high loads, as discussed before. In the power smoothing case, it can be seen that the genset load is smoothed out compared to the no battery case. For the peak-shaving, low loads are used for battery charging and high loads for discharging, as seen from the plot, where the lowest and highest loads are peak-shaved.

For the battery, the battery power is plotted in Figure 5.4d. It can be seen that the strategic loading first discharges the battery, until a lower SoC is reached, before it starts charging, until about 500 seconds, where the battery is not used, since the gensets operate at high load, which is fuel efficient, and battery power is not needed. The battery power in the power smoothing alternates between discharging and charging, as it smooths out power fluctuations, and for the peak-shaving case, the battery is charged in the beginning, and discharged in the end, on the lowest and highest peaks.

The battery SoC is shown in Figure 5.4e, with an initial SoC of 50%. The SoC in the strategic loading first decreases, as the battery is discharged, and when it reaches the minimum SoC set to 40%, the battery starts charging, and the SoC increases. After about 500 seconds, the SoC is constant, since the battery is not used. The power smoothing SoC varies between increasing and decreasing, as the battery is used for charging and discharging to smooth out the load. The SoC for peak-shaving increases in the beginning, when the battery is charged, and decreases at around 900 seconds, when it is discharged.

Note that in the power system configuration, there are *two* batteries, but in the plots, there is *one* plot for the battery power and SoC. This is because the two batteries have the same size, and as mentioned earlier, they will therefore behave similarly. Also, the genset plots show the *average* value of the four gensets, which all acted in a similar way, as the difference between the genset ratings is small.

The fuel consumption has been calculated for the different cases using the fuel consumption model described in Section 4.3.5, and the fuel consumption for the cases is shown in Table 5.8. In the table, the column ”Disconnection” describes if the gensets are disconnected or not during the simulation. The first four rows in the table are for the cases shown above (in Figure 5.4), when all gensets are connected at all times, while the plots for the last two rows in Table 5.8, when genset disconnection is performed, are shown in Appendix C. Genset disconnection is explained in Section 4.5, and the algorithm for genset disconnection is formulated in Equation (4.22).

From Table 5.8, it can be seen that the SPM indicates that neither peak-shaving or power smoothing is efficient for saving fuel, and they actually increase the fuel consumption for this load profile. Strategic loading on the other hand, saves approximately 7% fuel compared to not using the battery, for this load profile.

When engines are disconnected, this is also an efficient strategy for reducing the fuel consumption. Genset disconnection is only performed for strategic loading

Table 5.8: Fuel consumption for deterministic load profile.

Case	Disconnection	Fuel consumption [kg]	Reduction [%]
No battery	No	610.0	–
Peak-shaving	No	611.5	+0.25
Power smoothing	No	610.1	+0.02
Strategic loading	No	567.4	-6.98
No battery	Yes	511.9	-16.08
Strategic loading	Yes	501.8	-17.74

and without a battery, and not for peak-shaving or power smoothing, since they were not efficient strategies for saving fuel. From Table 5.8, disconnecting gensets alone (without using a battery) reduces the fuel consumption by 16.1%, and combining strategic loading and genset disconnection, a fuel saving of 17.7% can be obtained for this load profile. From the results, it seems like both strategic loading and genset disconnection are good options for saving fuel and emissions, and that combining these two strategies give the largest fuel reduction. Reasons to why genset disconnection saves fuel, are because the total genset power is reduced, and because the remaining gensets that are connected are allowed to operate at higher load, where they are more fuel efficient. As mentioned above, the plots for genset disconnection are not shown here, but in Appendix C, as they contained a lot of transient effects, but they will be discussed later in this chapter.

It should be mentioned that the final SoC for the strategic loading (44%) is significantly lower than the initial one (50%), which can be seen in Figure 5.4e. This means that the battery has discharged more power than it has charged, and therefore, a lower fuel consumption can be expected for strategic loading, since the total load to the gensets has been reduced. However, as will be seen in the next section, when the simulation time is much longer, strategic loading is indeed indicated as an efficient strategy for saving fuel.

5.5 Optimization for the Realistic Load Profile

The following section presents the optimization results for the realistic load profile from Figure 5.1b, for MPC optimization on the hybrid electric power system, using SPM as model, and with the cases as before, finding the optimal load setpoints to the gensets. The results for the realistic load profile are shown in Figure 5.5.

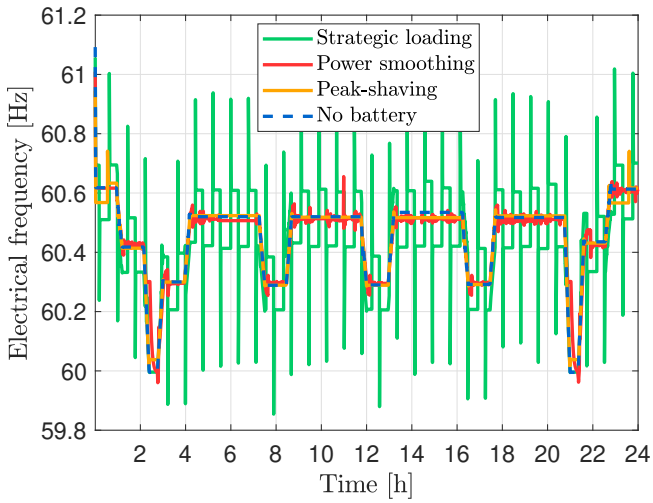

(a) Electrical frequency.

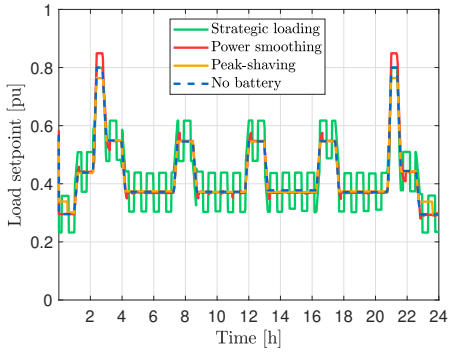

(b) Load setpoint.

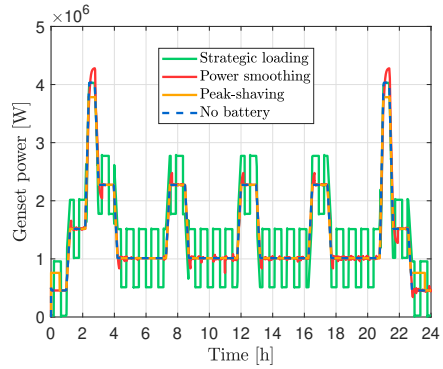

(c) Genset power.

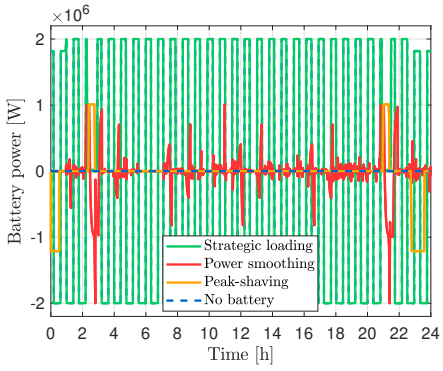

(d) Battery power.

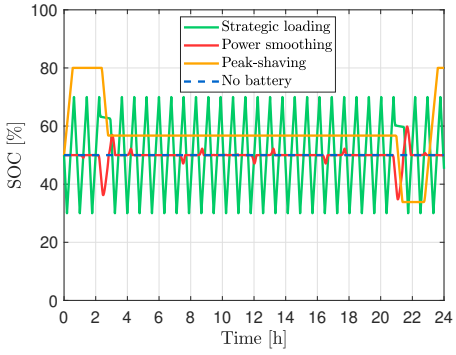

(e) Battery SoC.

Figure 5.5: Results for realistic load profile.

Figure 5.5a shows the frequency of the gensets. When performing strategic loading, it can be seen that the frequency is cyclically changing between a higher and a lower frequency than the no battery frequency, as the strategic loading performs cyclic charge and discharge of the ESD, which gives changes in the frequency. When the battery switches between charging/discharging, fluctuations are observed, as the battery power is assumed to instantly change the genset load. Further on, the frequency from power smoothing fluctuates more than the no battery frequency, as the battery is used actively in smoothing out the load and keeping an SoC reference. The peak-shaving frequency differs from the no battery frequency for high and low loads, which are at the beginning, at around 3 hours, 21 hours and in the end, where the frequency is lower at the low load peaks (since the battery is charged, and the genset load increases), and the frequency is higher at the high load peaks (since the battery is discharged, thus decreasing genset load). For the peak-shaving, the transient effects at around 1 hour and 23 hours happen because the battery stops charging, since it is fully charged, giving a fast change in the frequency.

From Figure 5.5b, it can be seen that the strategic loading gives changes in the optimized load setpoint for low loads (below 60% MCR, approximately), and does not change the setpoint for high loads (above 60% MCR, that happen around 3 and 21 hours), as discussed earlier, since the gensets already operate efficiently at high loads, and battery usage is not needed. Again, it is observed that the setpoints change cyclically, since the battery is used in charge/discharge cycles in the strategic loading. The load setpoint for power smoothing deviates slightly compared to not using the battery, as the battery is set to follow a reference by the low-pass filter (which the MPC is allowed to change). For instance, the load setpoints for the power smoothing are higher than without a battery at around 3 and 21 hours, since the battery is used for charging, giving a higher load. The load setpoint for the peak-shaving is higher than without the battery in the beginning and end (until it becomes the same, when the battery is fully charged), and at the peaks at 3 and 21 hours, the setpoint is lower, since the battery is discharged on these peaks, giving less genset load.

Figure 5.5c shows the genset power flow. In the strategic loading case, the genset power is cyclically changed by the battery, except for higher loads (above 60% MCR, more or less), where the gensets operate efficiently without a battery. The genset power from the power smoothing is different than without a battery, as the battery follows a reference from the low-pass filter and is adjusted by the MPC. For peak-shaving, the genset power peaks at the lower and higher loads are removed, as long as the SoC is within the limits of 20% and 80%. Therefore, the

peak-shaving at the lower peaks stops when the battery has reached its upper SoC limit, and at these times, a frequency fluctuation happens in the frequency plot in Figure 5.5a, since the battery power changes quickly to zero, giving an abrupt change in the genset load.

The battery power flow is shown in Figure 5.5d, where it can be seen that the strategic loading charges and discharges the battery cyclically, and that the battery flow is zero for high loads, occuring at around 3 hours and 21 hours. The battery flow for power smoothing is varying a lot between charging and discharging, since it receives a reference from the low-pass filter, and the MPC can decide to add or subtract battery power to stabilize the SoC. For the peak-shaving, it is evident from the plot that the battery is charged in the beginning (for the low peaks), and that it is discharged in the end (for the high peaks).

The battery SoC is seen in Figure 5.5e. It shows that the SoC for the strategic loading is varying between 30-70%, as the battery undergoes cyclic charging and discharging. The SoC changes between these values, except around 3 and 21 hours, when the battery is minimal, and the SoC is nearly constant. Furthermore, the SoC in power smoothing varies around 50%, as was expected, since the battery varies between charging and discharging, and the MPC tries to stabilize the SoC at 50%. For peak-shaving, the SoC first increases to its maximum value (80%) when it is charged, and decreases during two discharges, before increasing again when charged at the end.

The fuel consumption for the cases simulated with the realistic load profile was calculated, and the result is shown in Table 5.9. Again, the column ”Disconnection” indicates whether genset disconnection is performed or not. The plots in this section (Figure 5.5) were also performed *without* genset disconnection, so the fuel consumption of these cases is shown in the first four rows of Table 5.9. The plots for the cases with genset disconnection for the realistic load profile are shown in Appendix D, and the fuel consumption for these cases is shown in the last two rows of Table 5.9.

The results from Table 5.9 show that the SPM indicates that strategic loading is efficient for saving fuel, and that peak-shaving and power smoothing here also increase the fuel consumption slightly. Again, genset disconnection proves to be a very efficient strategy for this load profile, reducing the fuel consumption by 38.1% without battery, and by 38.5% with strategic loading. This is also consistent with the findings from Miyazaki (2017). It therefore seems like genset disconnection combined with strategic loading is a viable strategy for a hybrid electric power

Table 5.9: Fuel consumption for realistic load profile.

Case	Disconnection	Fuel consumption [kg]	Reduction [%]
No battery	No	45 910	–
Peak-shaving	No	46 380	+1.02
Power smoothing	No	45 990	+0.17
Strategic loading	No	43 480	-5.29
No battery	Yes	28 410	-38.12
Strategic loading	Yes	28 250	-38.47

system, saving slightly more fuel than without a battery. Now, since the simulation time is much longer than in the first simulation (24 hours compared to 1000 s previously), and since this load profile is based on a realistic vessel operation, one can with more certainty claim that strategic loading is a good battery strategy on a hybrid electric ship, and that genset disconnection also is an efficient method for reducing the fuel consumption. However, as seen from Figure 5.5, transient effects or spikes can occur with strategic loading, when the battery switches between charging and discharging. This was also observed in the genset disconnection cases, which now will be discussed.

5.6 Genset Disconnection Cases in Appendices C and D

As the plots for the genset disconnection cases contained a lot of transient effects, they were not included here in this chapter, but instead put in the appendix. The transients in the plots are to be expected, since the gensets were connected and disconnected immediately, and since synchronization to the grid was not performed. A short discussion of the plots for the deterministic load profile follows.

5.6.1 Genset Disconnection for the Deterministic Load Profile

Without Battery

Figure iv in Appendix C shows genset disconnection without battery, for the deterministic load profile. It can be seen that the frequency contains a lot of transient effects when disconnected gensets are connected to the grid, and that the SPM contains smaller spikes than Simscape. For disconnected gensets, the SPM frequency also goes quicker back to the reference frequency of 60 Hz than Simscape does, since disconnection of a genset makes the Simscape model unstable, and it takes some time for Simscape to stabilize. The load setpoints for the connected gensets are higher than without genset disconnection, which is beneficial and more fuel efficient for the genset operation (compare to Figure 5.4). Same goes for the genset power, which in general is much higher than without genset disconnection, making the gensets operate more efficiently. However, transient effects are also seen in the genset power.

With Strategic Loading

Figure v in Appendix C shows genset disconnection with strategic loading, for the deterministic load profile. Once again, the frequency and genset power contain a lot of transients, occurring when disconnected gensets are connected to the grid, or when large setpoint changes occur, either coming from the genset disconnection or from the instant battery power. The battery for the strategic loading is here only used for discharging, as the simulation time is too short for the battery to reach the lower SoC limit and start charging. The battery is actively discharging power when the load is low, and after about 500 seconds, the battery power is close to zero, since the genset load is high, making the gensets operate fuel efficiently. Here, the load setpoints are also higher than without genset disconnection (see Figure 5.4), meaning that when gensets are disconnected, connected gensets run more efficiently.

5.6.2 Genset Disconnection for the Realistic Load Profile

A short discussion of the genset disconnection plots for the realistic load profile follows below.

Without Battery

Figure vi in Appendix D shows genset disconnection without battery, for the realistic load profile. The frequency and genset power again have a lot of spikes when the load setpoints are changed rapidly, which in real life would be done gradually, by slowly ramping up the load to the genset and synchronizing it to the grid. However, from the plots, the load setpoints to the gensets are generally higher with genset disconnection compared to with all gensets connected (see Figure 5.5), making connected gensets operate much more efficiently when gensets are disconnected. From Figure vi (with genset disconnection), this is evident, where it can be seen that the lowest load setpoint for a connected genset is 0.5 pu, but it was around 0.3 pu for the simulation in Figure 5.5 (with all gensets connected), clearly showing that genset disconnection allows for more efficient energy usage.

With Strategic Loading

Figure vii in Appendix D shows genset disconnection with strategic loading, for the realistic load profile. Now, the frequency and genset power contain much more spikes, as the genset connection/disconnection is performed instantly, and since the battery is rapidly changing between charging/discharging cycles, causing transient effects. However, when using the battery for strategic loading, the battery makes the gensets operate longer at higher load than without a battery, which is beneficial from an efficiency standpoint. Genset disconnection also allows the connected gensets to operate at higher load, but as mentioned, the disconnection and connection must be performed more gradually and with synchronization to decrease the transient effects and increase the stability of the power system. It is seen that the battery again performs strategic loading for lower loads, but not for higher loads (above 60% MCR, roughly). Now, as the gensets operate more at higher loads (due to genset disconnection), the battery has more pauses where the battery power is close to zero (compare to Figure 5.5, where the battery is used much more), and at these pauses, the SoC is as expected changing much slower.

Chapter 6

Discussion

In this chapter, the results will be further discussed. This includes for instance discussing the SPM as a model for hybrid electric power systems, and comparing the different simulations from the case study to each other. Improvements to the thesis will also be investigated.

6.1 Performance of the SPM

The SPM performs well on a hybrid electric power system, as was seen in the verification study in Section 5.3. The SPM follows the verification model Simscape quite well, and the SPM also contains less fluctuations/transient effects than Simscape, especially when performing power smoothing and strategic loading. This can be beneficial for a controller, and it is proposed using the SPM as a control design model, meaning a simplified model that can be used for control purposes, as has been carried out in this thesis.

6.1.1 Reduction of the SPM frequencies

As observed from the verification study, the SPM frequencies were in general a bit higher than the frequencies in the verification model Simscape. The difference between SPM and Simscape is not big, but the SPM frequency could have been further reduced either by multiplying the load in the SPM equations with a factor bigger than 1, or by including losses like windage in the SPM equations to make the model more accurate, which will give more damping in the system, leading to a reduction in the estimated frequency.

6.1.2 Other Improvements of the SPM

The SPM can be further improved as a model by developing the SPM for reactive loads, and not only for active loads, as is the assumption for the current SPM. In addition, the bus voltages in the SPM are assumed to be constant. Constant voltage is suitable in steady state, but during transients, large voltage fluctuations can occur, and varying voltage should be included in these situations.

The transmission lines in the SPM are also assumed to be lossless. If the resistive losses are negligible, this assumption holds, but if not, power corresponding to the losses can be modeled as shunt loads drawing from the nodes (Dahl et al., 2017).

6.1.3 Improvements of the Battery Model

In the battery model, the voltage is assumed to be constant, and the temperature and resistance of the battery are neglected. Also, the SoC is calculated using the so-called Coulomb counting method, which in practical situations is sensitive to drift-off errors. Instead of the Coulomb counting method, the SoC estimation can be improved by using an observer, that estimates the SoC from measurements of the battery. The Extended Kalman Filter (EKF) is an example of such an observer, that can be used to estimate the SoC, as was done by Gulsvik (2017).

Battery degradation is also an important topic that is neglected in this thesis. This is especially relevant for strategic loading, as the battery goes through many charge/discharge cycles, and will after many cycles have a reduced battery capacity and a shortened battery lifetime. In the long simulation for the strategic loading, the battery is kept within an SoC of 30-70%, but in the literature, 20-80% is also frequently used. The limits 30-70% were chosen in order to ensure enough battery cycles in the simulation. See Simonsen (2019) for more information on battery degradation.

6.2 Stationary SFC Curve

As explained in Chapter 4, the SFC curve in the model is based on stationary values, and therefore it does not include the dynamics, since it only depends on the genset power P, similar to the curves in Figure 2.16. An improvement would be to implement an SFC curve depending on both genset speed ω and power P, as the one from Figure 2.17, to capture the engine dynamics, as the genset speed in the simulations is not constant.

6.3 Use of Different Batteries

The batteries used for peak-shaving and strategic loading would ideally be different. Peak-shaving is often performed with a *high-power* battery, as it is supposed to deliver the energy fast, but with strategic loading, an energy-dense battery, a *high-energy* battery, is desired, as the battery will be used a lot. In this thesis, this was neglected, and the battery size was the same for all the battery strategies.

In addition, the battery size should be chosen more carefully. The battery technology is in rapid development, so it is possible that there exist bigger batteries in the market (or will exist, in some years), that would probably make the strategic loading even more efficient (as it will be able to manipulate the genset load even more). It is also possible that a bigger battery will open up for one of the other battery strategies, like *zero-emission operation*, for a limited amount of time, as this requires a large ESD installed on the vessel. This will probably reduce the fuel consumption and emissions drastically, as the vessel will turn off all gensets and sail in a fully electric operation. MS Roald Amundsen, discussed in Chapter 1, is just one example of a hybrid electric ship that is able to sail in zero-emission operation for a shorter period of time, and this operation is typically used in exposed areas, which for instance can be in harbor or in world heritage fjords, where it is desired to reduce the noise or pollution from the vessel.

6.4 Include Varying Efficiency

The efficiencies for converters and transformers, and for battery discharging and charging are assumed constant for all loads. This is a simplification, and is something that should be improved on the model, by implementing a power-dependent efficiency. Also, implementing varying efficiency on the gensets should be taken into account, since the gensets are more efficient at higher loads.

6.5 Use a More Realistic Load Profile

The realistic load profile was as mentioned taken from Wu (2018), and it was assumed that the load was constant during each operation. It would perhaps be more ideal for the realistic simulation to have a load profile with more fluctuations and disturbances, as the loads for a real vessel will be more unpredictable. This can either be accomplished by using real vessel operational data, or the load profile in the thesis could have been disturbed with white noise, or with probable wave disturbances from irregular waves for an assumed sea-state.

6.6 Better Genset Disconnection

The genset disconnection in this thesis gives a lot of fluctuations and transients when the connection/disconnection of the gensets occur. This is because the procedure in this thesis is too simplified, and the genset is out of phase from the power system when it is connected, making the system unstable. For better performance and less transient effects, the load should be gradually ramped up or down (depending on connection or disconnection), and the genset must be synchronized to the grid before it is connected. However, some transient behavior when starting and stopping gensets can be expected, which normally will give extra emissions and increased fuel consumption during the transients.

When performing genset disconnection, MILP optimization can be performed, as done by Skjong et al. (2017), for instance. Constraints on the running hours and the number of starts/stops of each genset can also be implemented (Skjong et al., 2017), and a constraint on the ramping (how long time it takes to turn on or off a genset) can be included. See for instance Section 2.2.2 in Wärtsilä (2018) for recommended start-up times of diesel gensets, where it is stated that "a diesel generator typically reaches nominal speed in about 20-25 seconds after the start signal".

Even though the genset disconnection is very simplified in this thesis, it anyways demonstrates the importance of synchronization, by for instance regulating the genset frequency when connecting/disconnecting, and it is shown that the power system can become unstable if this is not performed.

6.7 Model Predictive Control

MPC requires that the weight matrices in the cost function are properly tuned, in order to obtain the desired performance between the objectives. In this thesis, there was a trade-off between reaching a reference frequency, a reference load setpoint and avoid too big changes in the load setpoint (in addition to reaching a reference SoC for the power smoothing case). These objectives could of course have been changed, using a different cost function, and the weights to each of these objectives could have been further tuned or adjusted.

When using MPC, it is important that the model used is a good model, that catches the dominant dynamics of the system. This thesis uses the SPM as model for the MPC, which through the verification study and from previous work done in

Bergen and Hill (1981), Hill and Bergen (1982), Dahl et al. (2017), Dahl et al. (2018) and Fiksdahl (2019) has proven to be a good model for power systems, and also a model that covers the frequency dynamics of a hybrid electric power system. Therefore, it is assumed that performing MPC with SPM as model is a robust solution for control of a hybrid electric ship.

6.8 Discussion of the Battery Strategies

The results have shown that strategic loading is indicated as an efficient battery strategy, and that peak-shaving and power smoothing is not as efficient for saving fuel, when assessing the fuel consumption of the cases. It has also been indicated that frequency transients can occur with strategic loading, when the battery changes between charging/discharging, and this is something that potentially can make the power system unstable.

From rules and regulations, small variations in the frequency are tolerated, but classification societies typically set a limit of $\pm 10\%$ deviation from the desired frequency. If this limit is exceeded, generators and some of the consumers will disconnect from the power grid, as is discussed in Veksler et al. (2012). In addition, too big variations in the loading also lead to higher NO_x emissions and more sooting, which is not desirable.

Going more into detail, according to DNV GL (2018), frequency variations in *AC installations* with a *fixed* nominal frequency shall be kept within $\pm 5\%$ of rated frequency under *steady* load, and within $\pm 10\%$ under *transient* load. In this thesis, the reference frequency is 60 Hz, meaning that the variation is allowed to be between 57-63 Hz in steady state and between 54-66 Hz in transient conditions.

Looking at the plots in Figures 5.4 and 5.5, it can be seen that for the short simulation (in Figure 5.4), the frequency is well within $\pm 5\%$ of 60 Hz for all the cases, also for the strategic loading. For the long simulation (in Figure 5.5), the frequency is again within the limits of 57-63 Hz, but there are more visible transients for the strategic loading, however not more than 61 Hz on the maximum.

6.9 Discussion of the Disconnection Cases

For the genset disconnection cases in Appendices C and D, the frequency fluctuates much more than before, as the system becomes unstable when disconnected gensets are connected to the grid.

For the short simulation without battery (in Figure iv), the frequency is within 57-63 Hz, except at the beginning, when transient effects would be expected, as it takes some time for the system to reach steady state. From the plot, it is seen that when turning on and off the gensets, transient effects in the frequency and power are observed at the times of connection/disconnection, as the load setpoint to the genset is changed instantly. As mentioned, synchronization and gradual ramping will probably improve this issue.

The same tendency is also seen in the short simulation with the battery performing strategic loading (in Figure v), but there are a lot more transient effects now, as both the genset scheduling *and* the battery usage lead to fluctuations in the frequency and genset power. Still, the frequency is kept within $\pm 5\%$ of 60 Hz, except at the beginning, when the system is initialized.

For the 24 hour simulation without battery (in Figure vi), the frequency actually exceeds 63 Hz at some times in the simulations, when the start/stop of the gensets make the system unstable. The fluctuation is just slightly more than 63 Hz and still within the $\pm 10\%$ class requirement for transient loads. It can be observed that the frequencies *for the SPM* are within 63 Hz, and it is the *Simscape power system* that fluctuates more. Even though a battery is not used in this simulation, it is possible to use an ESD, such as a battery, to control the frequency more actively, in order to reduce the transients. As an example, the battery can be discharged for too low frequencies (resulting in less load to the gensets, and thus an increase in the frequency), and charged for too high frequencies (thus lowering the frequency), as has been performed by Kim et al. (2014). Another example of using the battery to control the frequency is from Bø (2016), that demonstrated that a battery can make the power system more stable and increase the overall safety. When using the battery, Bø (2016) demonstrated that the power system had smaller frequency drops, and the author used the battery whenever the frequency dropped below 98.5% of the rated frequency.

When the battery is used for strategic loading in the long simulation (in Figure vii), the frequency and genset power contain a lot more transients, as was also observed in the short simulation. The frequency now exceeds the steady state limit of 63

Hz, with a maximum of 64 Hz, but it is still within the transient limits. The frequency transients occur in the beginning and end of the simulation, when only the smallest genset is connected to the grid, making the power system more vulnerable to instability, as the available genset capacity is minimal. The instability comes from quick and large changes in the load setpoint of the genset, when the battery changes between charging and discharging, and when gensets are turned on and off. Frequent start-up and shut-down of the gensets is something that may be harmful for the gensets, and is something that should be investigated further.

An assumption in this thesis is that two gensets must be switched on during DP operations, as a redundancy requirement (Wu, 2018). However, the battery can also be used for redundancy in the power system, such as using the battery as a spinning reserve, explained in Chapter 2. In this way, the battery can be used as a backup power, opening up for using only one genset during DP operations, which probably would reduce the emissions even more.

6.10 Comparison of Results from Fuel Consumption

Tables 5.8 and 5.9 indicate that strategic loading is a good battery strategy for reducing the fuel consumption on a hybrid electric ship, saving 7% fuel for the short, deterministic simulation and 5.3% fuel for the long, realistic simulation. Genset disconnection is also efficient for saving fuel, saving 16.1% and 38.1% fuel for the short and long simulation, respectively, and combining strategic loading and genset disconnection saves 17.7% and 38.5% fuel for the short and long simulation, respectively.

It is not certain that power smoothing or peak-shaving will increase the fuel consumption on a real vessel, even though the results from Tables 5.8 and 5.9 indicate this. Peak-shaving, for instance, is widely used in the industry to reduce the fuel consumption and to improve the safety of the vessel. It is therefore likely that the results would be different if another SFC curve were used, using an SFC curve based on the genset dynamics, taking both the genset power and speed into consideration, as has been discussed. It should also be mentioned that the load profiles in this thesis are simplified and not containing disturbances, which would be present in a real vessel operation. Hence, performing peak-shaving and power smoothing is not necessarily favorable for these somewhat static load conditions, but more ideal for loads with fluctuations. However, as the results indicate, it is important to be aware that peak-shaving or power smoothing not automatically reduce the fuel consumption in any given operation.

From the fuel consumption results in Tables 5.8 and 5.9, it is clear that genset disconnection reduces the fuel consumption remarkably, and that the genset disconnection is much more efficient for the long simulation (with genset disconnection giving 16.1% and 17.7% reduction for the short simulation, and 38.1% and 38.5% reduction for the long simulation, with and without battery, respectively). The reason why the genset disconnection saves more fuel in the longer simulation, is probably because the total genset load in general is much lower for the long simulation than in the short one. To exemplify this, the reader is advised to compare the two load profiles in Figure 5.1, where it can be seen that the load in the short, deterministic profile in Figure 5.1a is above 10 MW for about half of the simulation, while the load is above 10 MW only for about 2 of the 24 hours in the long, realistic profile in Figure 5.1b. Therefore, when the total load is in general lower in the long simulation, more gensets are allowed to disconnect for a longer time, reducing the total genset power, thus saving more fuel when performing genset disconnection for the realistic load profile.

It also seems like strategic loading is less efficient for the long simulation (changing from 7% reduction in the short simulation compared to 5.3% reduction in the long one, and also giving a smaller change when using strategic loading for genset disconnection in the long simulation). Again, this may be due to lower load in the long simulation. When the gensets run at low load for a long time, this is fuel inefficient, and for low loads, it can not be expected that the battery in the strategic loading manages to manipulate the genset load to the most efficient range, especially if the battery size is not big enough. In other words, the strategic loading may struggle to change the genset load to the optimal loading for low loads, and therefore, it can be expected that strategic loading will have less reduction of the fuel consumption in the long simulation.

6.11 Perform Laboratory Tests

Performing tests on a real hybrid electric power system would be a natural next step for this thesis, in order to further investigate and verify the theoretical advantages of a hybrid electric power system. It would also be very interesting to see if strategic loading is an efficient battery strategy compared to the other strategies, and to carry out testing of the SPM as a control design model. Miyazaki (2017), for instance, has performed laboratory tests in the NTNU Hybrid Power Systems Laboratory at the Department of Marine Technology.

Chapter 7

Conclusion

This master thesis has performed a thorough literature review on the SPM, MPC, and on hybrid electric power systems on ships, as was one of the objectives in the thesis. Another objective has been to define the PMS, BMS and EEMS, and the battery as an ESS, as well as describing how these systems work. In addition, the SPM has been extended with battery usage, and it is demonstrated through a verification study that the SPM is a robust model that can be used for control of hybrid electric power systems. Optimization problems for minimizing energy and emissions on the hybrid electric ship, using different battery strategies, have been formulated, and the solutions to these problems have been solved using MPC with SPM as the model.

The research question of this thesis has been: "*What battery strategy is the most efficient on a hybrid electric ship, according to the SPM?*". In accordance with the results from the case study, which uses the SPM as model, it is indicated that using the battery for strategic loading reduces the fuel consumption of the hybrid electric ship significantly. Neither peak-shaving or power smoothing are indicated as fuel efficient battery strategies, but it is suggested to use these strategies for fluctuating loads instead, which will improve the safety of the power system and be better for the gensets. Another method which was found very efficient for reducing the fuel consumption is genset disconnection, which is turning on and off gensets depending on the load. As an answer to the research question, it is therefore proposed to use genset disconnection in combination with strategic loading on the hybrid electric power plant, if the goal is to reduce the fuel consumption and emissions.

The thesis has contributed to the field by presenting and developing the SPM for battery storage, which is a new model for hybrid electric power systems, that can

be used for estimation of fuel consumption, analysis of genset frequency, genset power and optimization of load setpoint to the gensets, as well as calculation of the battery power and estimation of the battery SoC.

The simulations that are performed suggest that MPC, with SPM as optimization model, is suitable for control of hybrid electric ships, as the SPM catches the main physical properties of the power system, describing the frequency dynamics. The case study also highlights certain challenges related to the optimal control of the power system, demonstrating that strategic loading can lead to transient effects, and that genset disconnection can lead to instabilities in the power system, if synchronization and gradual ramping of the load are not performed. The SPM presented in this thesis may therefore be an important tool to understand how a battery changes the dynamics of the power system, and it can thus be used to predict the response of hybrid electric power systems.

In the years to come, hybrid ships, such as MS Roald Amundsen portrayed in Figure 1.1, will be even more widely used, as they drive the way to a more sustainable future for shipping. Hopefully this thesis has motivated using the SPM for modeling and optimization of such marine hybrid electric power systems.

7.1 Recommendations for Further Work

Several improvements to this thesis have already been proposed, and recommendations for further work include:

- Improve the SPM and make it more exact, by including losses, such as windage or losses in the transmission lines. Other improvements include development of the SPM for reactive loads, and implementation of varying bus voltages.
- Improve the battery model, for instance by including the resistance, temperature, varying voltage and battery degradation. The SoC estimation can also be done better, by using an observer, such as the Kalman filter.
- Use a non-stationary SFC curve that depends on both genset power and engine speed, as the engine speed is not constant in the simulations.
- Use different batteries for the battery strategies, for instance using a high-power battery for peak-shaving and a high-energy battery for strategic loading, to get a more fair comparison of the battery strategies.
- Include efficiency varying with power for the electrical components.

- Use real vessel operational data for the realistic load profile, or add disturbances to the load to make the simulations more realistic.
- Improve the genset disconnection algorithm, by synchronizing the gensets when connecting them to the grid, and by performing gradual ramping of the load, in order to reduce the transient effects. The algorithm can also be enhanced by making it optimization-based and not rule-based, by performing MILP optimization on the genset disconnection.
- Perform better tuning of the weight matrices in the cost function for the optimization, and consider to change the cost function.
- Analyze the effect on maintenance on the frequent start-up and shut-down of the gensets when performing genset disconnection.
- Calculate CO_2, NO_x or SO_x emissions for the simulations.
- Perform laboratory tests and verify the SPM as a control design model for a hybrid electric power system.

References

Akerbæk, E., 2018. Stemmer det at utslippene fra et containerskip tilsvarer 50 millioner biler? URL: https://www.faktisk.no/artikler/MA/stemmer-det-at-utslippene/-fra-et-containerskip-tilsvarer-50-millioner-biler.

Andrea, D., 2010. Battery Management Systems for Large Lithium-Ion Battery Packs. Artech House.

Bassam, A.M., Phillips, A.B., Turnock, S.R., Wilson, P.A., 2016. Sizing optimization of a fuel cell/battery hybrid system for a domestic ferry using a whole ship system simulator, in: 2016 International Conference on Electrical Systems for Aircraft, Railway, Ship Propulsion and Road Vehicles & International Transportation Electrification Conference (ESARS-ITEC), IEEE, Toulouse, France. pp. 1–6. doi:10.1109/ESARS-ITEC.2016.7841333.

Bergen, A., Hill, D., 1981. A Structure Preserving Model for Power System Stability Analysis. IEEE Transactions on Power Apparatus and Systems PAS-100, 25–35. doi:10.1109/TPAS.1981.316883.

Bondy, J., Murty, U., 2008. Graph Theory - Graduate Texts in Mathematics.

Borhan, H., Vahidi, A., Phillips, A.M., Kuang, M.L., Kolmanovsky, I.V., Di Cairano, S., 2012. MPC-Based Energy Management of a Power-Split Hybrid Electric Vehicle. IEEE Transactions on Control Systems Technology 20, 593–603. doi:10.1109/TCST.2011.2134852.

Bø, T.I., 2016. Scenario- and Optimization- Based Control of Marine Electric Power Systems (PhD thesis at NTNU, Department of Engineering Cybernetics) , 165.

Bø, T.I., Dahl, A.R., Johansen, T.A., Mathiesen, E., Miyazaki, M.R., Pedersen, E., Skjetne, R., Sørensen, A.J., Thorat, L., Yum, K.K., 2015. Marine Vessel and Power Plant System Simulator. IEEE Access 3, 2065–2079. doi:10.1109/ACCESS.2015.2496122.

Bø, T.I., Johansen, T.A., 2013. Scenario-based fault-tolerant model predictive control for diesel-electric marine power plant, in: 2013 MTS/IEEE OCEANS - Bergen, IEEE, Bergen. pp. 1–5. doi:10.1109/OCEANS-Bergen.2013.6607989.

Chartrand, G., 1977. Introductory Graph Theory. Courier Corporation. Google-Books-ID: rYuToT7vHbMC.

Dahl, A.R., Skjetne, R., Johansen, T.A., 2017. A Structure Preserving Power System Frequency Model for Dynamic Positioning Vessels, American Society of Mechanical Engineers Digital Collection. doi:10.1115/OMAE2017-61901.

Dahl, A.R., Thorat, L., Skjetne, R., 2018. Model Predictive Control of Marine Vessel Power System by Use of Structure Preserving Model. IFAC-PapersOnLine 51, 335 – 340. doi:https://doi.org/10.1016/j.ifacol.2018.09.501.

Dalaker, S., 2019. Regjeringa: Alle bilferjer skal gå på straum innan 2025. URL: https://www.nrk.no/sognogfjordane/regjeringa_-alle-bilferjer-skal-ga-pa-straum-innan-2025-1.14408153.

Dedes, E.K., Hudson, D.A., Turnock, S.R., 2012. Assessing the potential of hybrid energy technology to reduce exhaust emissions from global shipping. Energy Policy 40, 204–218. doi:10.1016/j.enpol.2011.09.046.

Desoer, C., Kuh, E., 1969. Basic Circuit Theory.

Dinh, T.Q., Bui, T.M.N., Marco, J., Watts, C., Yoon, J.I., 2018. Optimal Energy Management for Hybrid Electric Dynamic Positioning Vessels. IFAC-PapersOnLine 51, 98–103. doi:10.1016/j.ifacol.2018.09.476.

DNV GL, 2015. Ship rules for classification. Technical report, DNV GL.

DNV GL, 2018. RULES FOR CLASSIFICATION, Ships, Part 4: Systems and components, Chapter 8: Electrical installations.

Electronic Design, 2013. Understand Efficiency Ratings Before Choosing An AC-DC Supply (retrieved June

2020). URL: https://www.electronicdesign.com/power-management/article/21795830/understand/-efficiency-ratings-before-choosing-an-acdc-supply. library Catalog: www.electronicdesign.com.

Fiksdahl, O., 2019. Modeling a marine hybrid electric power plant by a structure-preserving model (Project Thesis at NTNU, Department of Marine Technology).

Fiksdahl, O., 2020. Model-based optimization for energy and emission management of a marine hybrid electric power system (Master thesis at NTNU, Department of Marine Technology).

Foss, B., Heirung, T.A.N., 2016. Merging Optimization and Control , 93.

Geertsma, R., Negenborn, R., Visser, K., Hopman, J., 2017. Design and control of hybrid power and propulsion systems for smart ships: A review of developments. Applied Energy 194, 30–54. doi:10.1016/j.apenergy.2017.02.060.

Ghimire, P., Park, D., Zadeh, M.K., Thorstensen, J., Pedersen, E., 2019. Shipboard Electric Power Conversion: System Architecture, Applications, Control, and Challenges [Technology Leaders]. IEEE Electrification Magazine 7, 6–20. doi:10.1109/MELE.2019.2943948.

Goebel, R., Sanfelice, R.G., Teel, A.R., 2012. Hybrid Dynamical Systems: Modeling, Stability, and Robustness. URL: https://press.princeton.edu/books/hardcover/9780691153896/hybrid-dynamical-systems.

Gonzalez-Castellanos, A., Pozo, D., Bischi, A., 2019. Detailed Li-ion battery characterization model for economic operation. International Journal of Electrical Power & Energy Systems 116, 105561. doi:10.1016/j.ijepes.2019.105561.

Gulsvik, K.A.K., 2017. Battery Management System for a low-cost ROV (Master thesis at NTNU, Department of Marine Technology) , 136.

Hansen, J.F., 2019. ABB ship electric propulsion: Guest lecture in TMR4240 - Marine Control Systems I (lecture 11).

Hill, D., Bergen, A., 1982. Stability analysis of multimachine power networks with linear frequency dependent loads. IEEE Transactions on Circuits and Systems 29, 840–848. doi:10.1109/TCS.1982.1085110.

Hovland, E.H., 2019. Algorithm for Efficiency Support in Marine Vessels (Master thesis at NTNU, Department of Electrical Engineering) , 134.

Hurtigruten, 2019. MS Roald Amundsen. URL: https://www.hurtigruten.no/skip/ms-roald-amundsen/.

Hyundai Heavy Industries, 2019. Low Load Operation Criteria - Engine Operation Project Guide.

IMO, 2008. MARPOL Annex VI, revised.

IMO, 2014. Third IMO GHG Study 2014 – Final Report: REDUCTION OF GHG EMISSIONS FROM SHIPS.

IMO, 2019a. Air Pollution, Energy Efficiency and Greenhouse Gas Emissions. URL: http://www.imo.org/en/OurWork/Environment/PollutionPrevention/AirPollution/Pages/Default.aspx.

IMO, 2019b. Nitrogen oxides (NOx) – Regulation 13. URL: http://www.imo.org/en/OurWork/Environment/PollutionPrevention/AirPollution/Pages/Nitrogen-oxides-(NOx)-%E2%80%93-Regulation-13.aspx.

IMO, 2019c. Sulphur oxides (SOx) – Regulation 14. URL: http://www.imo.org/en/OurWork/Environment/PollutionPrevention/AirPollution/Pages/Sulphur-oxides-(SOx)-%E2%80%93-Regulation-14.aspx.

Imsland, L.S., 2019. Lecture notes in TTK4135 - Optimization and Control.

Kalikatzarakis, M., Geertsma, R., Boonen, E., Visser, K., Negenborn, R., 2018. Ship energy management for hybrid propulsion and power supply with shore charging. Control Engineering Practice 76, 133–154. doi:10.1016/j.conengprac.2018.04.009.

Kim, K., Park, K., Roh, G., Chun, K., 2018. DC-grid system for ships: a study of benefits and technical considerations. Journal of International Maritime Safety, Environmental Affairs, and Shipping 2, 1–12. doi:10.1080/25725084.2018.1490239.

Kim, S.Y., Choe, S., Ko, S., Kim, S., Sul, S.K., 2014. Electric Propulsion Naval Ships with Energy Storage Modules through AFE Converters. Journal of Power Electronics 14, 402–412. URL: http://koreascience.or.kr/article/JAKO201409864555730.page, doi:10.6113/JPE.2014.14.2.402. publisher: The Korean Institute of Power Electronics.

Lund, K., 2020. Online optimization of a marine hybrid electric power plant using mixed integer linear programming (Master thesis at NTNU, Department of Marine Technology).

Madani, S., Schaltz, E., Knudsen Kær, S., 2019. An Electrical Equivalent Circuit Model of a Lithium Titanate Oxide Battery. Batteries 5, 31. doi:10.3390/batteries5010031.

MathWorks, 2020. Marine Full Electric Propulsion Power System (retrieved June 2020). URL: https://www.mathworks.com/help/physmod/sps/examples/marine-full-electric-propulsion-power-system.html.

MATLAB, 2019. Simscape - MATLAB & Simulink. URL: https://se.mathworks.com/products/simscape.html.

Mayne, D.Q., 2014. Model predictive control: Recent developments and future promise. Automatica 50, 2967–2986. doi:10.1016/j.automatica.2014.10.128.

Mayne, D.Q., Rawlings, J.B., Rao, C.V., Scokaert, P.O.M., 2000. Constrained model predictive control: Stability and optimality , 26.

Miyazaki, M.R., 2017. Modeling and control of hybrid marine power plants (PhD thesis at NTNU, Department of Marine Technology) , 176.

Miyazaki, M.R., Sørensen, A.J., Vartdal, B.J., 2016a. Hybrid marine power plants model validation with strategic loading. IFAC-PapersOnLine 49, 400–407. doi:10.1016/j.ifacol.2016.10.437.

Miyazaki, M.R., Sørensen, A.J., Vartdal, B.J., 2016b. Reduction of Fuel Consumption on Hybrid Marine Power Plants by Strategic Loading With Energy Storage Devices. IEEE Power and Energy Technology Systems Journal 3, 207–217. doi:10.1109/JPETS.2016.2621117.

Moura, S.J., Fathy, H.K., Callaway, D.S., Stein, J.L., 2011. A Stochastic Optimal Control Approach for Power Management in Plug-In Hybrid Electric Vehicles. IEEE Transactions on Control Systems Technology 19, 545–555. doi:10.1109/TCST.2010.2043736.

Nocedal, J., Wright, S.J., 2006. Numerical optimization. Springer series in operations research. 2nd ed ed., Springer, New York. OCLC: ocm68629100.

NTB, 2019. Regjeringen vil halvere utslippene fra skipsfart. URL: https://sysla.no/maritim/regjeringen-vil-halvere-utslippene/-fra-skipsfart/.

Oceana, 2019. Shipping Pollution. URL: https://eu.oceana.org/en/shipping-pollution-1.

Othman, M.B., Reddy, N.P., Ghimire, P., Zadeh, M.K., Anvari-Moghaddam, A., Guerrero, J.M., 2019. A Hybrid Power System Laboratory: Testing Electric and Hybrid Propulsion. IEEE Electrification Magazine 7, 89–97. doi:10.1109/MELE.2019.2943982.

P. Kundur, 1994. Power system stability and control. The EPRI power system engineering series, McGraw-Hill, New York.

Paran, S., Vu, T.V., Mezyani, T.E., Edrington, C.S., 2015. MPC-based power management in the shipboard power system, in: 2015 IEEE Electric Ship Technologies Symposium (ESTS), pp. 14–18. doi:10.1109/ESTS.2015.7157855. iSSN: null.

Park, H., Sun, J., Pekarek, S., Stone, P., Opila, D., Meyer, R., Kolmanovsky, I., DeCarlo, R., 2015. Real-Time Model Predictive Control for Shipboard Power Management Using the IPA-SQP Approach. IEEE Transactions on Control Systems Technology 23, 2129–2143. doi:10.1109/TCST.2015.2402233.

Pearce, F., 2009. How 16 ships create as much pollution as all the cars in the world. URL: https://www.dailymail.co.uk/sciencetech/article-1229857/How-16-ships-create-pollution-cars-world.html.

Rahmoun, A., Biechl, H., 2012. Modelling of Li-ion batteries using equivalent circuit diagrams .

Reddy, N.P., Pasdeloup, D., Zadeh, M.K., Skjetne, R., 2019a. An Intelligent Power and Energy Management System for Fuel Cell/Battery Hybrid Electric Vehicle Using Reinforcement Learning, in: 2019 IEEE Transportation Electrification Conference and Expo (ITEC), pp. 1–6. doi:10.1109/ITEC.2019.8790451. iSSN: 2377-5483.

Reddy, N.P., Zadeh, M.K., Thieme, C.A., Skjetne, R., Sorensen, A.J., Aanondsen, S.A., Breivik, M., Eide, E., 2019b. Zero-Emission Autonomous Ferries for Urban Water Transport: Cheaper, Cleaner Alternative to Bridges and Manned Vessels. IEEE Electrification Magazine 7, 32–45. doi:10.1109/MELE.2019.2943954.

Siemens, 2015. Reference List for Offshore Vessels.

Simonsen, E.B., 2019. Modeling and Optimization of a Hybrid Electric Ship Power System (Master thesis at NTNU, Department of Marine Technology) URL: https://ntnuopen.ntnu.no/ntnu-xmlui/handle/11250/2625268. accepted: 2019-10-29T15:01:00Z Publisher: NTNU.

Skjetne, R., 2012. Lecture notes in TMR4243 - Marine Control Systems II.

Skjong, E., Johansen, T.A., Molinas, M., Sørensen, A.J., 2017. Approaches to Economic Energy Management in Diesel–Electric Marine Vessels. IEEE Transactions on Transportation Electrification 3, 22–35. doi:10.1109/TTE.2017.2648178.

Stone, P., Opila, D.F., Park, H., Sun, J., Pekarek, S., DeCarlo, R., Westervelt, E., Brooks, J., Seenumani, G., 2015. Shipboard power management using constrained nonlinear model predictive control, in: 2015 IEEE Electric Ship Technologies Symposium (ESTS), pp. 1–7. doi:10.1109/ESTS.2015.7157853. iSSN: null.

Sørensen, A.J., 2019. Lecture notes in TMR4240 - Marine Control Systems.

Sørensen, A.J., Skjetne, R., Bø, T., Miyazaki, M.R., Johansen, T.A., Utne, B., Pedersen, E., 2017. Towards Safer, Smarter and Greener Ships Using Hybrid Marine Power Plants , 8.

Thorat, L., Skjetne, R., 2018. Optimal Online Configuration and Load-Sharing in a Redundant Electric Power System for an Offshore Vessel Using Mixed Integer Linear Programming, in: Volume 1: Offshore Technology, American Society of Mechanical Engineers, Madrid, Spain. p. V001T01A047. URL: https://asmedigitalcollection.asme.org/OMAE/proceedings/OMAE2018/51203/Madrid,%20Spain/277933, doi:10.1115/OMAE2018-77955.

V. Shipping, 2017. Efficiency Improvements to Main Engine Auxiliary Systems – VEUS-Shipping.com. URL: http://www.veus-shipping.com/2017/08/efficiency-improvements-to/-main-engine-auxiliary-systems/.

Veksler, A., Johansen, T.A., Skjetne, R., 2012. Transient power control in dynamic positioning - governor feedforward and dynamic thrust allocation. IFAC Proceedings Volumes 45, 158–163. URL: https://linkinghub.elsevier.com/retrieve/pii/S1474667016312216, doi:10.3182/20120919-3-IT-2046.00027.

Wu, Z., 2018. Comparison of Fuel Consumption on a Hybrid Marine Power Plant With Low-Power Versus High-Power Engines (Master thesis at NTNU, Department of Marine Technology), in: Volume 1: Offshore Technology, American Society of Mechanical Engineers, Madrid, Spain. p. V001T01A048. URL: https://asmedigitalcollection.asme.org/OMAE/proceedings/OMAE2018/51203/Madrid,%20Spain/277835, doi:10.1115/OMAE2018-77959.

Wärtsilä, 2018. Wärtsilä 26 - Product guide , 228,URL: https://www.wartsila.com/docs/default-source/product-files/engines/ms-engine/product-guide-o-e-w26.pdf?utm_source=engines&utm_medium=dieselengines&utm_term=w26&utm_content=productguide&utm_campaign=msleadscoring.

Yao, Y., Gao, W., Li, Y., 2014. Optimization of PHEV charging schedule for load peak shaving, in: 2014 IEEE Conference and Expo Transportation Electrification Asia-Pacific (ITEC Asia-Pacific), pp. 1–6. doi:10.1109/ITEC-AP.2014.6940718.

Zadeh, M., 2019. Lecture notes in TMR4290 - Marine Electric Power and Propulsion Systems.

Zahedi, B., Norum, L.E., Ludvigsen, K.B., 2014. Optimized efficiency of all-electric ships by dc hybrid power systems. Journal of Power Sources 255, 341–354. doi:10.1016/j.jpowsour.2014.01.031.

Ådnanes, A., 2003. Maritime Electrical Installations And Diesel Electric Propulsion - ABB AS Marine.

Appendix

A SPM parameters for Dahl et al. (2018)

Table i: Parameters used in Dahl et al. (2018).

Description	Parameter	Value	Unit
Load damping	D_1	0.0001	[s/rad]
	D_2	0.0001	[s/rad]
Mechanical starting time	M_1	0.7833	[s]
	M_2	3.3667	[s]
Rated power	S_1	5	[MVA]
	S_2	30	[MVA]
Line reactance	X_1	0.0189	[pu]
	X_2	7	[pu]
	X_3	1.1667	[pu]

B Hybrid Electric Power Systems in Simscape

B.1 Configuration for Peak-Shaving

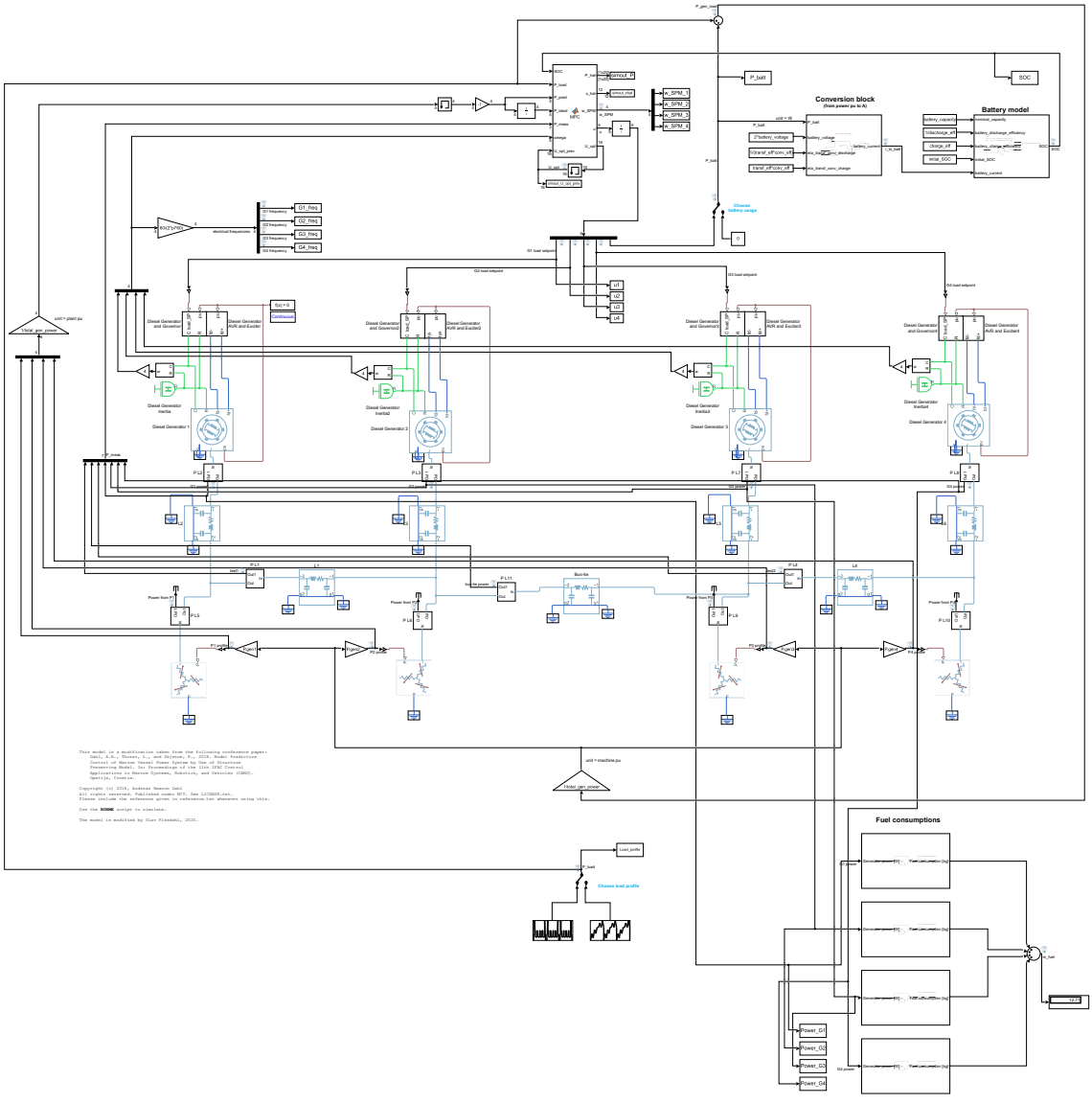

Figure i: Peak-shaving power system in Simscape.

B.2 Configuration for Power Smoothing

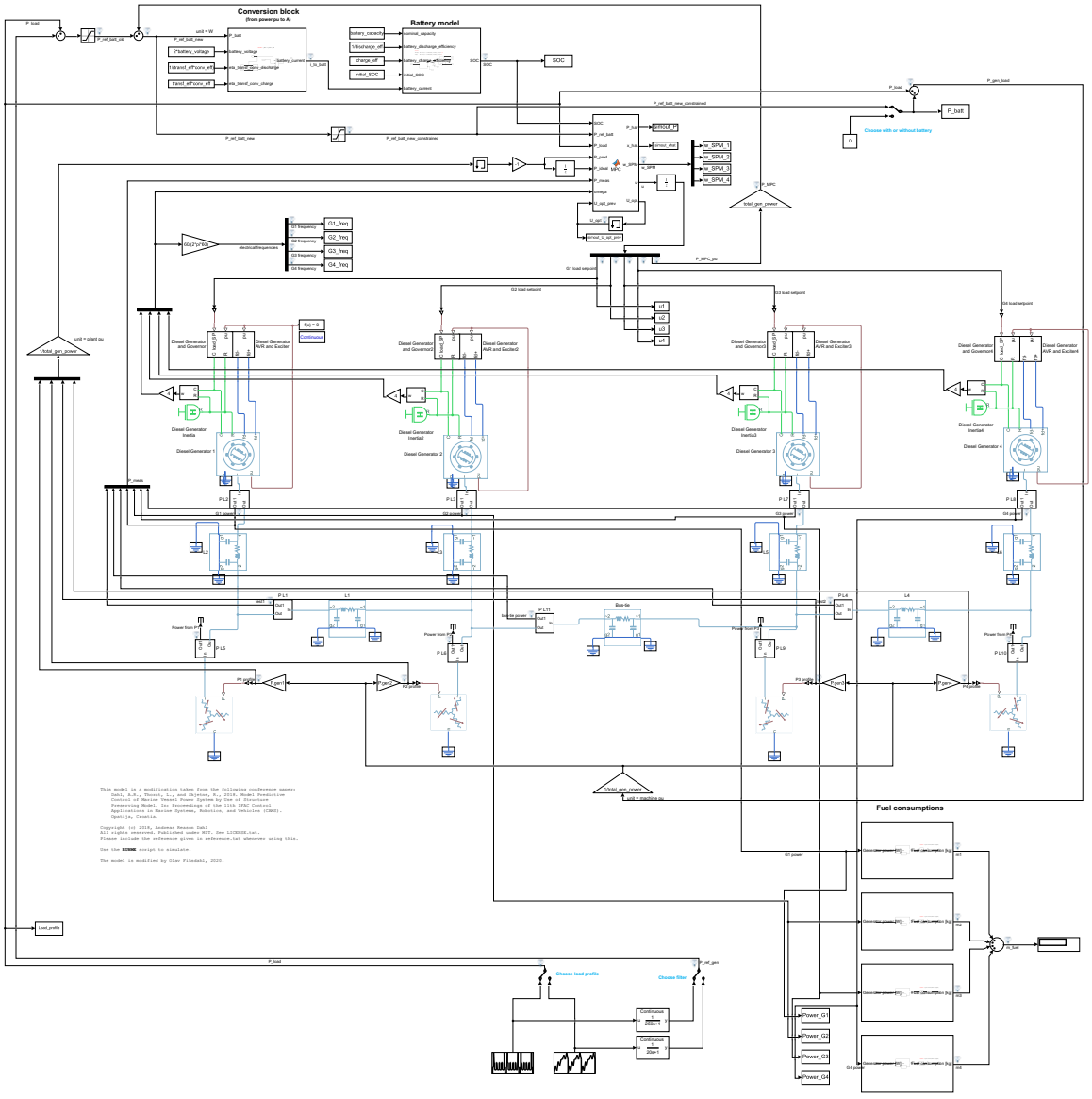

Figure ii: Power smoothing power system in Simscape.

B.3 Configuration for Strategic Loading

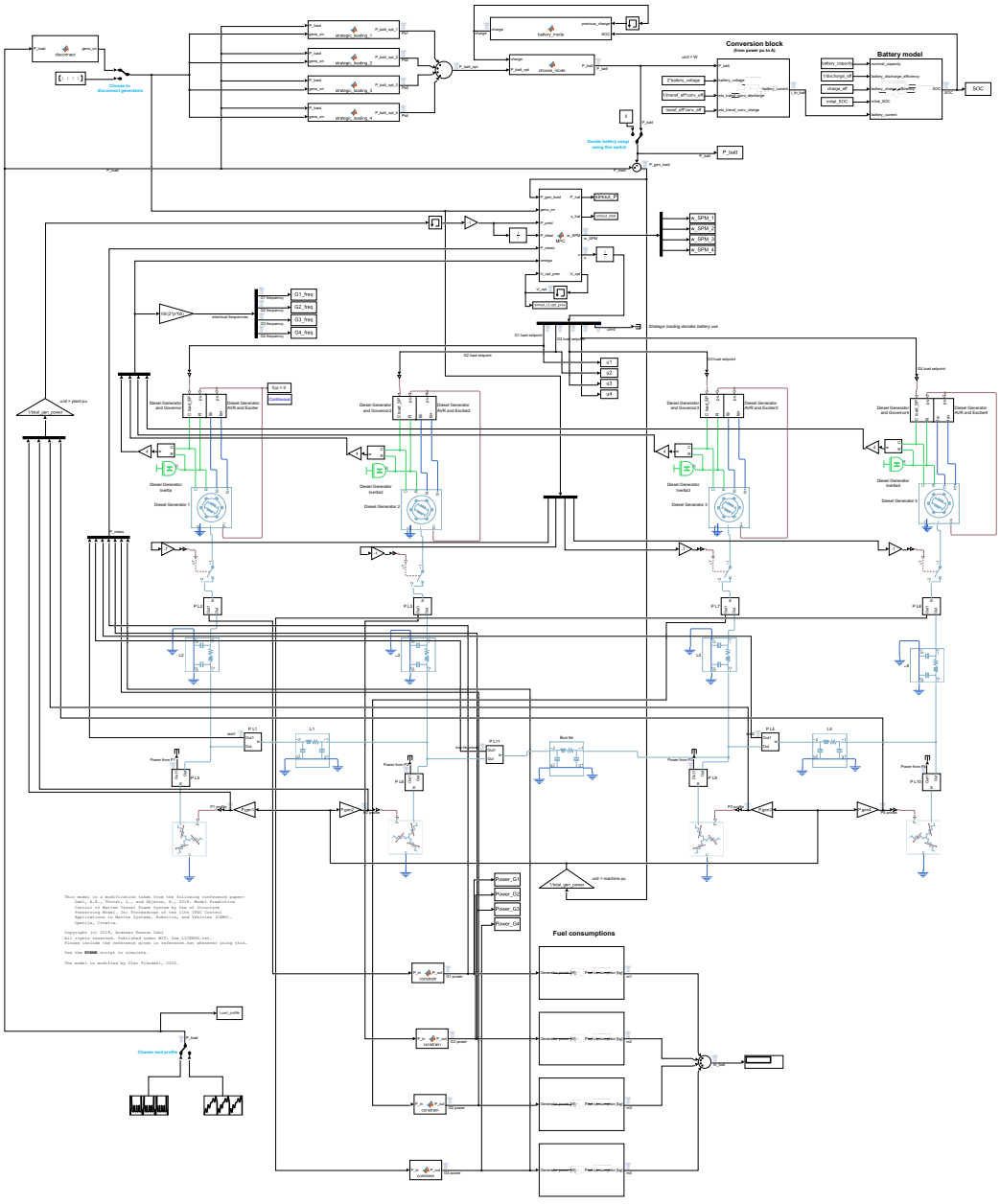

Figure iii: Strategic loading power system in Simscape.

C Disconnection Cases for Deterministic Load Profile

C.1 No Battery + Disconnection

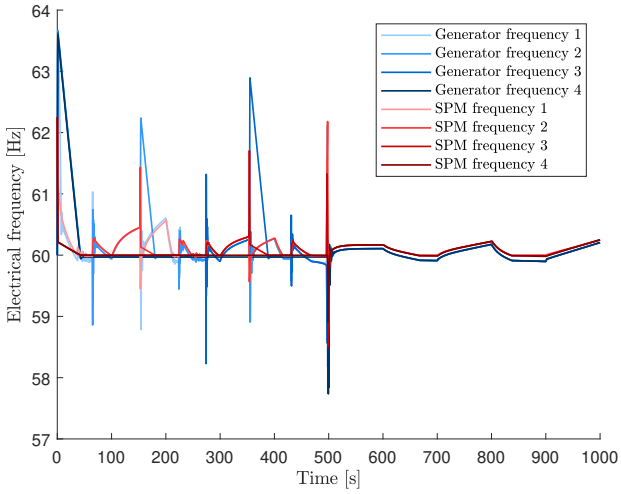

(a) Electrical frequency. Blue is for Simscape, and red is for the SPM.

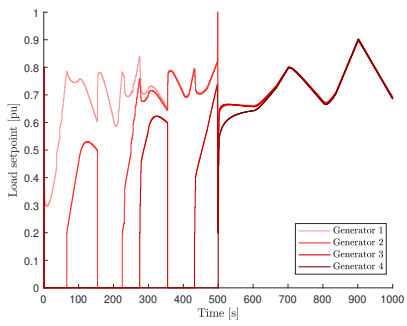

(b) Load setpoint.

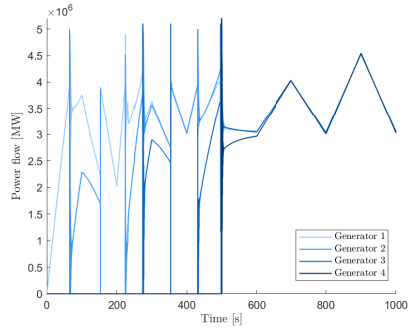

(c) Genset power.

Figure iv: Results for no battery + genset disconnection on deterministic load profile.

C.2 Strategic Loading + Disconnection

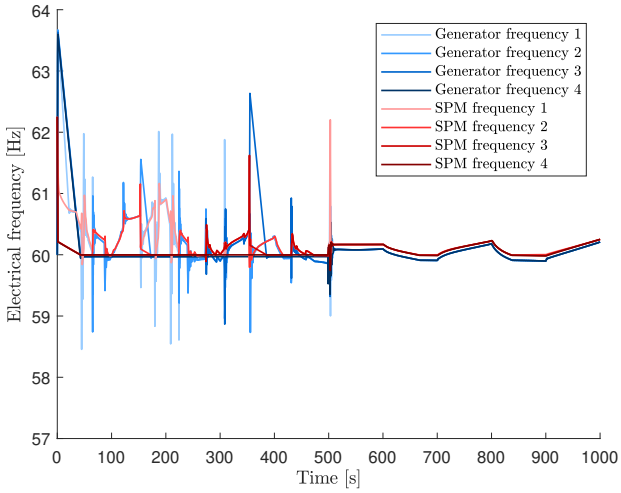

(a) Electrical frequency. Blue is for Simscape, and red is for the SPM.

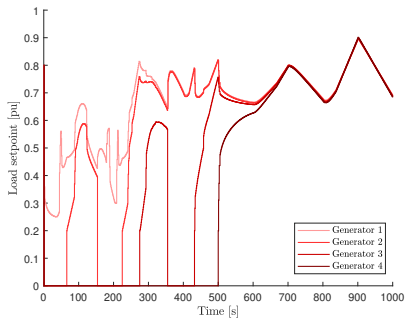

(b) Load setpoint.

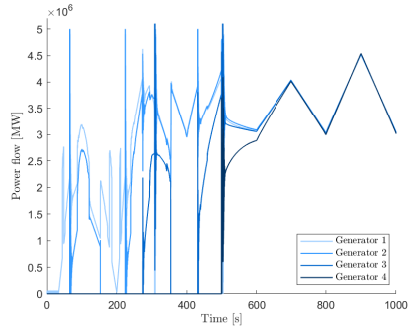

(c) Genset power.

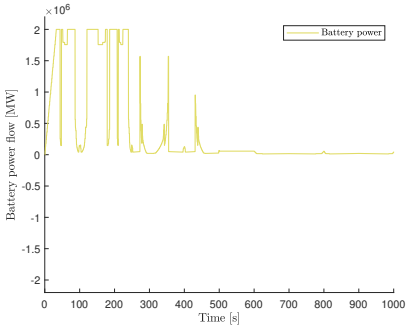

(d) Battery power.

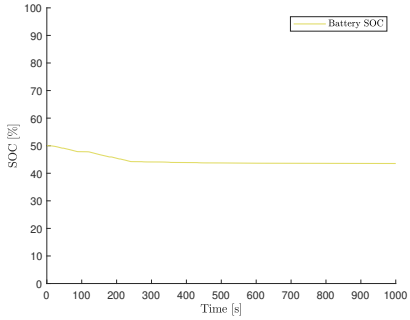

(e) Battery SoC.

Figure v: Results for strategic loading + genset disconnection on deterministic load profile.

D Disconnection Cases for Realistic Load Profile

D.1 No Battery + Disconnection

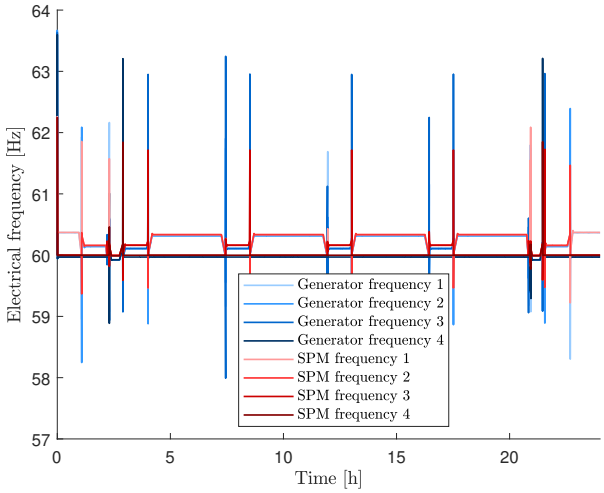

(a) Electrical frequency. Blue is for Simscape, and red is for the SPM.

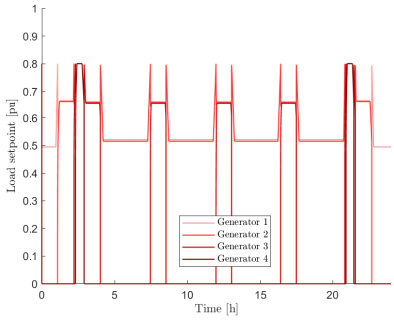

(b) Load setpoint.

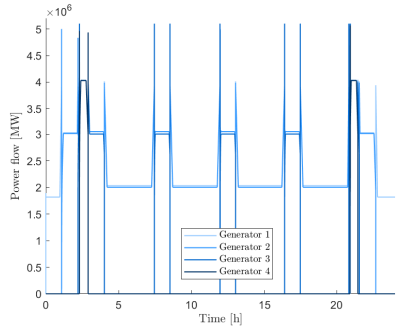

(c) Genset power.

Figure vi: Results for no battery + genset disconnection on realistic load profile.

D.2 Strategic Loading + Disconnection

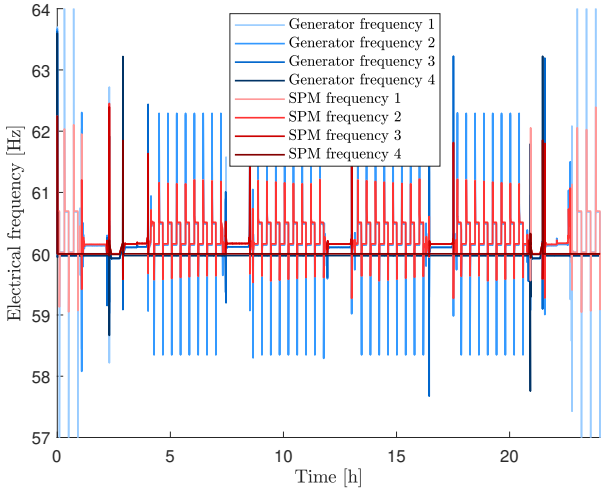

(a) Electrical frequency. Blue is for Simscape, and red is for the SPM.

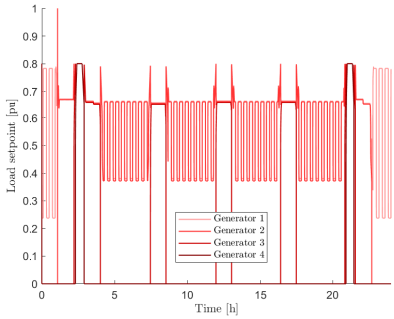

(b) Load setpoint.

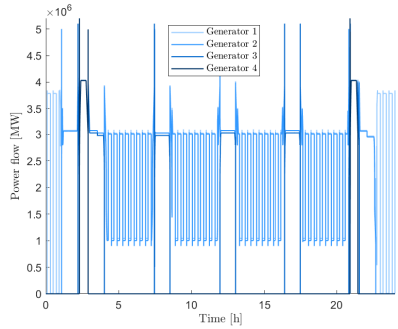

(c) Genset power.

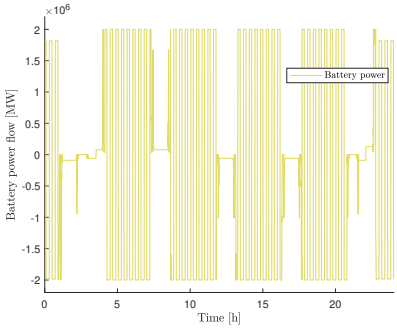

(d) Battery power.

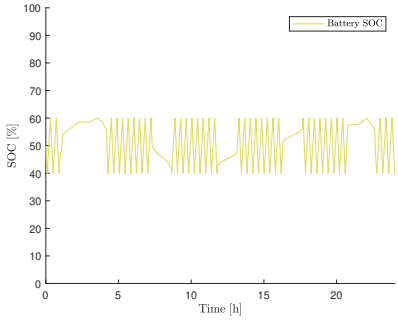

(e) Battery SoC.

Figure vii: Results for strategic loading + genset disconnection on realistic load profile.

Olav Fiksdahl

NTNU
Norwegian University of
Science and Technology